Complex Vector Synchronous Frame PI Current Regulator Development in Discrete-time Domain

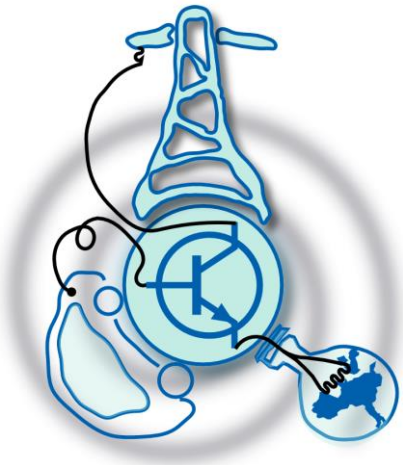

Submitted to the Department of Electrical Engineering, Electronics, Computers and Systems in partial fulfilment of the requirements for the degree of Erasmus Mundus Masters Course in Sustainable Transportation and Electrical Power Systems at the

UNIVERSIDAD DE OVIEDO

September 2018

Author……

Fatima Razzaq

Certified by……

Dr. Fabio Giulii Caponi

Associate Professor

Thesis Supervisor

Complex Vector Synchronous Frame PI Current Regulator Development in Discrete-time Domain

by

Fatima Razzaq

Submitted to the Department of Electrical Engineering, Electronics, Computers and Systems on August 31st, 2018, in partial fulfilment of the requirements for the degree of Erasmus Mundus Masters Course in Sustainable Transportation and Electrical Power Systems

Abstract

In this thesis, mathematical model for synchronous machines is developed in stationary and synchronous reference frame. Two type of vector controllers named synchronous frame PI current regulator with cross-coupling decoupling and complex vector synchronous frame PI current regulator are developed in discrete-time domain. Tuning of current controllers is also detailed in continuous as well as discrete-time domain. It is shown that complex vector type controller shows better performance and it is less sensitive to electrical parameter variation. Speed estimation algorithms are also studied which use incremental encoder output directly or indirectly. Comparative study regarding pulse width modulation strategies, is also made.
It is also discussed how motor electrical parameters can be determined, if not available. A high voltage digital motor control and power factor correction kit by Texas Instruments is used as part of experimental setup. PSIM provided tool, SimCoder, is used to program the controller.

Thesis Supervisor: Dr. Fabio Giulii Capponi
Title: Associate Professor

Acknowledgements

This thesis work has been carried out at La Sapienza University of Rome as part of Erasmus Mundus Masters Course (EMMC) in Sustainable Transportation and Electrical Power Systems (STEPS) and hosted by Universidad de Oviedo.

First of all, I would like to thank all the teachers, I had in my life. I was very lucky to have good teachers throughout my academic career. During this Master's degree program, I had the chance to study from some teachers, whose teaching style revamped my interest in engineering studies and research.

I would like to express my utmost gratitude to my thesis supervisors Dr. Fabio Giulii Capponi and Dr. Giulio De Donato for giving me a chance to work under their supervision. Their continuous support, suggestions and encouragement made me learn a lot during this thesis work. Without any doubt, one can hardly get such cooperative teachers.

I would like to thank all my STEPS fellows for making this time memorable for me. I also owe thanks to my fellows, I had in lab, during this thesis work for their valuable suggestions and help.

I would also like to thank my parents who are my real strength, who always stood by me, who always encouraged me and who supported me beyond their capacities and duties. Finally, I would like to thank my siblings for their continuous support and love.

Table of Contents

List of Figures

List of Tables

List of Abbreviations

AC	Alternating current
DC	Direct current
EMF	Electromotive force
EV	Electric vehicle
FOC	Field oriented control
HEV	Hybrid electric vehicle
HVCntrl+PFC kit	High voltage digital motor control and power factor correction kit
IM	Induction machine
IPMSM	Interior permanent-magnet synchronous motor
PI	Proportional integral
PM	Permanent magnet
SPWM	Sinusoidal pulse width modulation
SVPWM	Space vector pulse width modulation
SRM	Switched reluctance machine
ZOH	Zero-order-hold

Keywords

Complex vector Current Controller, Vector Tracking Observer, SimCoder, Incremental Encoder, Space Vector Pulse Width Modulation

List of Symbols

αβ	Stationary or stator coordinates
E	Back-EMF voltage
f_{BW}	Bandwidth in hertz
f_{sw}	Switching frequency
i_d	d-axis component of the stator current
i_q	q-axis component of the stator current
J	Total moment of inertia for a system
L_s	Stator winding inductance
L_d	Direct-axis inductance
L_q	Quadrature-axis inductance
P	Number of pole pairs
R/R_s	Stator phase winding resistance
t	Time variable
T	Electromagnetic torque
T_L	Load torque
T_{SW}	Switching/sampling period
V_{DC}	DC-link voltage
v_d	d-axis component of the stator voltage
v_q	q-axis component of the stator voltage
λ	Flux linkage
λ_{pm}	Permanent-magnet flux linkage

θ_e	Electrical angle of rotor
θ_m/θ_r	Mechanical angle of rotor
ω_e	Electrical angular speed
ω_m/ω_r	Mechanical angular speed

1. Introduction

Nowadays applications in which the control of the torque, the speed or the position of an electrical machine working at high speed, is needed, are very common. Specially, automotive industry is shifting rapidly from gasoline to electric vehicles. This paradigm change brought drive control field more in demand.
The main purpose of the thesis is to develop complex vector current controller for IPMSM based servo drive. Understanding complete hardware system and techniques deployed to control this hardware, is necessary, to perform the task. This chapter will briefly describe structure of different type of electric machines. And why IPMSM is a good option for traction applications. Encoder state-of-the-art technology is also discussed which is integral part of this drive control system. Conventional and novel modulation techniques are studied briefly for voltage source inverter. Vector control scheme will also be discussed in general context to compare with scalar control scheme.

1.1 State-of-the-Art Review

1.1.1 Electrical Machines

Electric machines are the most significant part of electric vehicles. For energy efficiency, comfort and safety, effective control techniques are developed and tested for different kind of machines. Control strategy depends highly upon the structure of the machine. Selection of machine depends on application and cost. For traction purpose different types of machines are considered over the years. Important types of rotating machines are shown in figure 1.1.1.1 to present an overview.
DC motors have been used in automotive industry for long time because of simple control mechanism, relatively low manufacturing cost and technological maturity. But these benefits come with bulky construction, low efficiency, less reliable operation and need for frequent maintenance. Sparking at brushes makes it unsafe in specific environments. For example, for automotive use especially at high speeds.

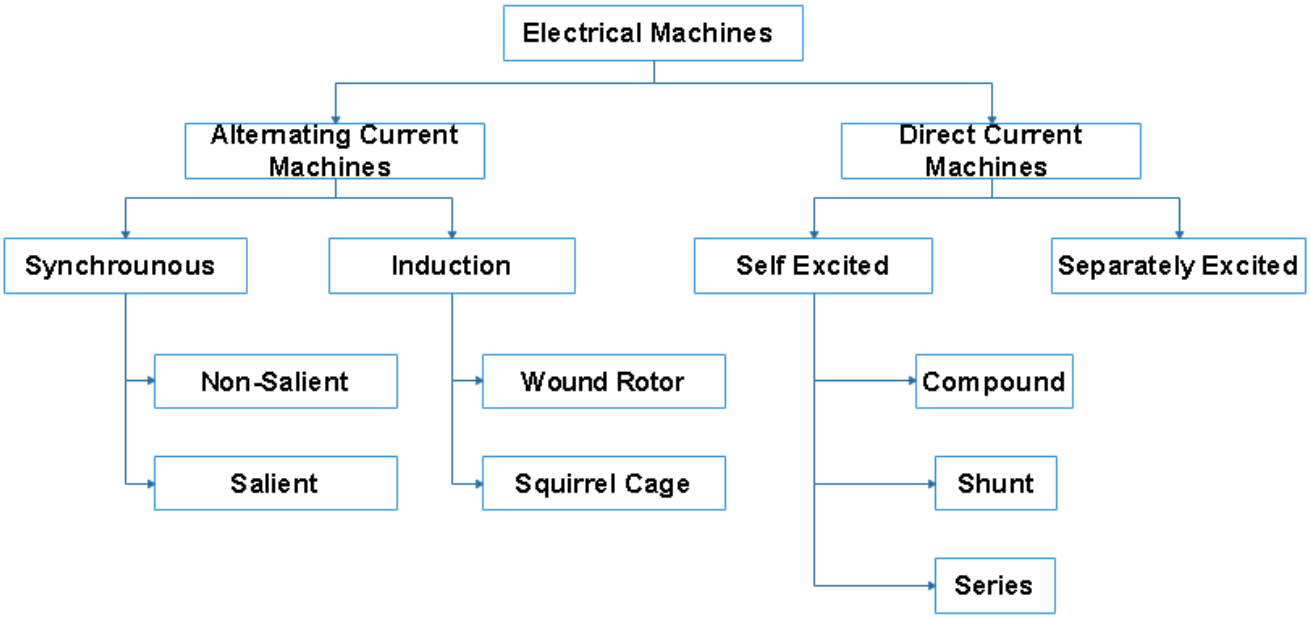

Figure 2.1.1.1: Types of Rotating Electrical Machines

Induction motors have penetrated much for industrial as well as automotive application because of its low cost, ruggedness and low maintenance requirement. Squirrel cage rotor motor is preferred over wound rotor motor. Large constant power region makes use of induction motor more favorable as it is demand for automotive application. Control of Induction machine is quite complex because rotor and stator windings are not fixed orthogonal with respect to each other. Rotor field is induced by stator field, complicating the torque control even more [1]. However Field Oriented Control gives satisfactory results. Nonetheless high losses, poor power factor, high weight, large volume and the limitations regarding overload have made the synchronous especially permanent magnet drives more suitable choice during past few years.

Permanent magnet machines are highly accepted choice for electric vehicles. PM excitation makes the machine compact and light for given power rating. Removing rotor winding improves power efficiency and thermodynamic effects of the machine. Field oriented control of permanent magnet machine is easier than that for induction motor. Permanent magnet is buried inside rotor material (IPMSM) or attached on its surface (SPM) making the machine rotor type salient or non-salient respectively.

SPM suffers with mechanical stress and possibility to demagnetization of magnet decreasing reliability at high loads and speeds. However, for PM machines losses are mainly iron losses in stator so employing a cooling system can resolve this issue.

IPMSM has more robust structure and magnet buried inside the rotor material keeps it from temperature and thus demagnetization effects so IPMSM offers more reliable solution for tracking applications allowing to make use of reluctance torque along with many other benefits. Field weakening capability of IPMSM is better owing to higher inductance value, which is very important for high speed applications.

High price of magnet is urging the researchers to develop novel designs of machines and their efficient control strategies. Synchronous Reluctance Machine (SRM) is good candidate in this regard. They have salient rotor structure without any winding and magnet so electromechanical torque is reluctance torque only. Direct-Drive systems have made scientists to look towards Axial Flux Permanent Magnet (AFPM) machines also. For both SRM and AFPM, technology is not mature yet. Novel control techniques are being developed for both. Still there is long way to make them compete radial PM machines.
Basic structures of above mentioned electrical machines are shown below in figure 1.1.1.2.

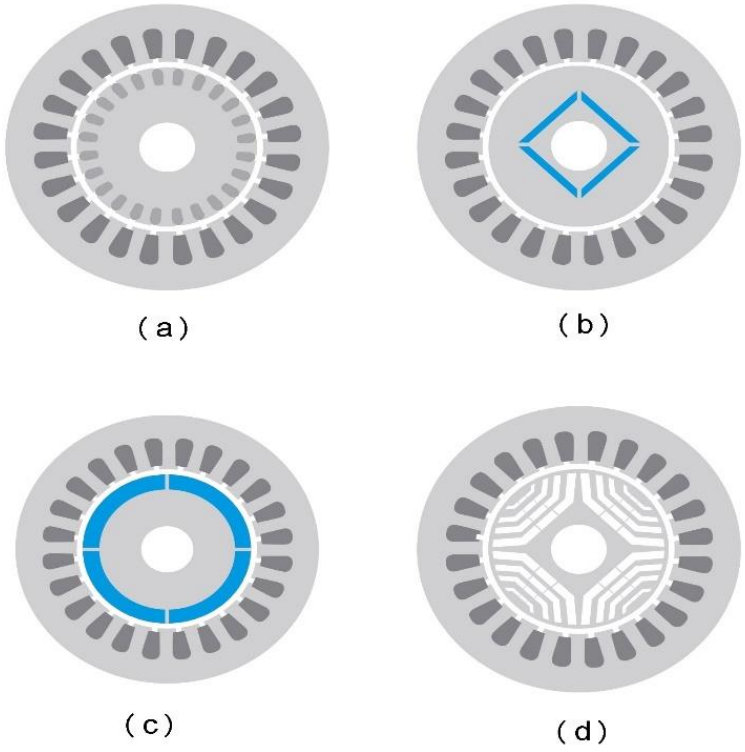

Figure 1.1.1.2: Basic Structure of Various Electrical Machines (a) Induction Machine (b) Internal Permanent Magnet Synchronous Machine (c) Surface Permanent Magnet Synchronous Machine (d) Reluctance Machine

In context to above discussion, it can be concluded that IPMSM is a good option for traction applications. It is reliable and safe. Successive discussion will focus specially on IPMSM.

1.1.2 Optical Encoders

For Field Oriented Control (FOC), it is compulsory to be aware of shaft position throughout the operation. Shaft encoders can be used for this purpose which are digital transducers for measuring angular displacements and velocities. Choice of encoder depends upon application requirements, cost of the system, size, weight and ease of installation and maintenance.

Performance of the transducer is measured in terms of resolution, accuracy, linearity, reliability and life. Accuracy specifies how faithfully output gives input (position indication). Resolution is the measure of the minimum change in input which will be reflected in output. While linearity describes how constant is the ratio between input and output. Not one of these performance characteristics is enough to make choice for the transducer [2].

Optical shaft encoders are classified mainly into two categories depending on the nature and method of interpretation of the output: Incremental and absolute encoders [3]. Disk structure of both types of encoders is shown in figure 1.1.2.1.

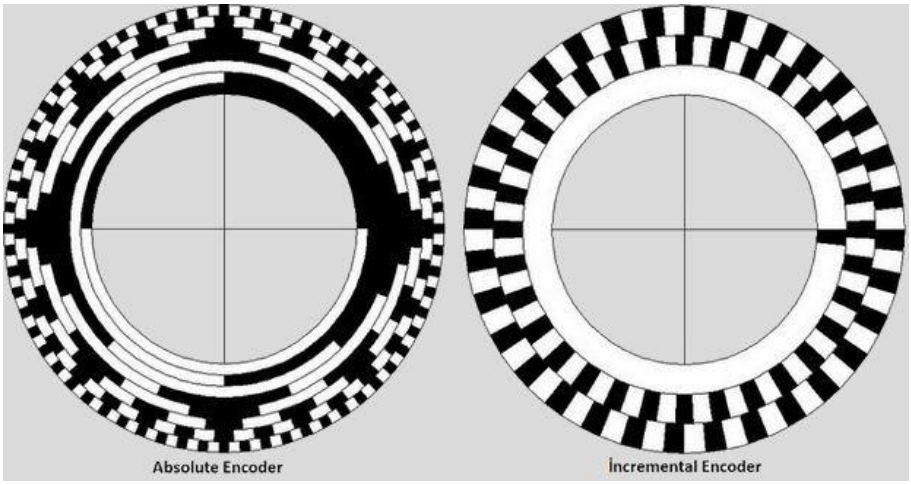

Figure 1.1.2.1: Absolute and Incremental Encoder Disk Structure

An absolute encoder has many pulse tracks on its disk. When disk rotates, several pulse trains are generated which are equal to number of tracks. Resolution of encoder depends upon number of tracks. Pulse signal can have two magnitudes 0 or 1 depending opaque or transparent portion of disk is read. So disk pattern is organized in such a way that consecutive positions lead to sequel of binary numbers or gray code. Outermost disk corresponds to Least Significant bit (LSB) while inner most disk is for Most Significant Bit (MSB). In case of power loss, absolute encoder based system is not affected. As with the recovery of power, encoder will start reading the exact position again.

Absolute encoders are generally more expensive. Incremental encoder provides a relatively cheap solution. It is equipped with two pulse tracks displaced 90 degree from each other to determine direction of rotation. Usually clockwise direction is defined as signal 'A' going positive before signal 'B'. Resolution depends upon number of slots on a track. Encoder falling and rising edges are detected and two tracks are there so reading is updated four times during one pair of slot passage. If track on incremental encoder has 2500 lines, it can provide maximum pulse count (N_p) of 10,000. So the resolution will be given by; $^{2\pi}/_{N_p}$; where $N_p = 4N$ and N corresponds to number of lines on A or B track.

Mostly encoders are equipped with a third track having just one slot called zero or index position mark.

Contrary to absolute encoder, it doesn't provide exact position instead it gives relative position with respect to some initial point. Zero pulse occurs once in full mechanical rotation. This mark is useful to determine the absolute position of shaft. During the rotation readings might be missed causing error. Zero pulse resets the reading in the start of every rotation and helps avoid integrating errors. Pulse signals from incremental encoder disk are shown in figure 1.1.2.2 assuming positive direction of rotation.

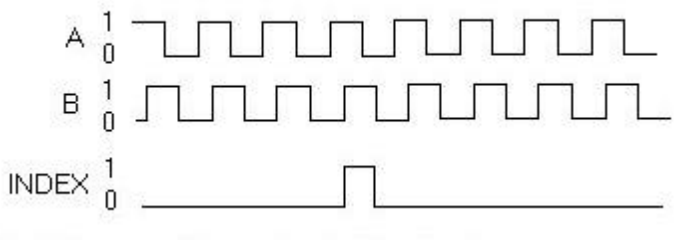

Figure 1.1.2.2: Incremental encoder disk track patterns

Diagram shows signals from A and B track, which are displaced 90 degrees and index or zero pulse.

Careful consideration must be made regarding electrical angle. As the angle calculated from encoder is mechanical angle but for field-oriented control implementation electrical angle is needed.

1.1.2.1 Detecting Offset Angle of Rotor Shaft with Respect to Encoder Zero Signal

As incremental encoder is used for position tracking so absolute position of shaft is not known directly. Zero-mark on third track is to determine absolute position. At the time of installation, it can be made sure that zero position mark of transducer is aligned with q-axis of permanent magnet machine. But during mass productions it is quite hard to follow this practice. So for the available motor, angle between rotor quadrature axis and zero position mark is to be calculated once. This angle is termed as offset angle.

Back EMF is aligned along Q-axis. θ_e is the electrical angle between Q-axis of the rotor and phase-a of conventional three phase system. So back EMF will appear as follows on all three axes. (1.1.2.1.1)

$$e_a = E\cos\theta_e$$

$$e_b = E\cos(\theta_e - \frac{2\pi}{3}) \qquad (1.1.2.1.1)$$

$$e_c = E\cos(\theta_e + \frac{2\pi}{3})$$

It shows clearly that e_a will be at its peak when angle will be zero or when zero position mark will occur as shown in figure 1.1.2.1.1.

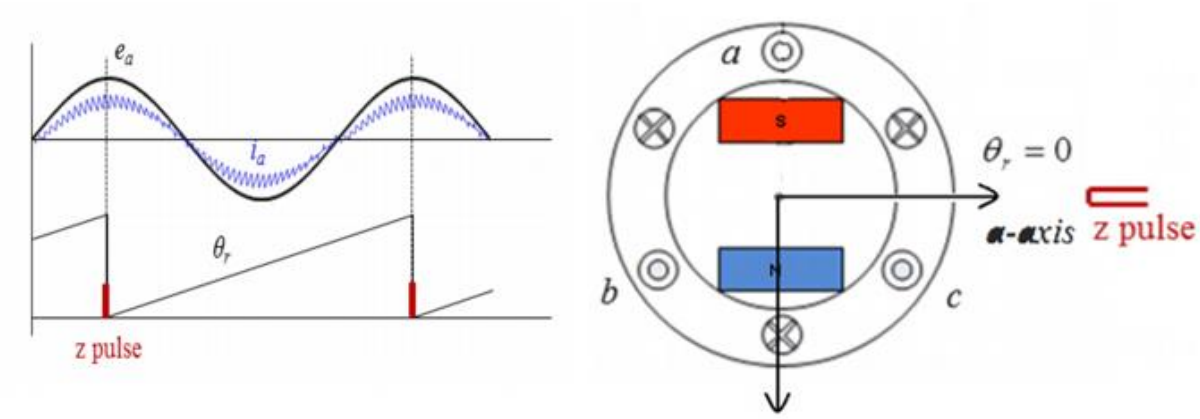

Figure1.1.2.1.1: Z-pulse Position and Back-EMF when Offset Angle is Zero

As mentioned earlier, this is ideal case. Actually, quadrature axis and encoder zero pulse are not aligned so offset angle exists and needs to be calculated. Back-EMF waves and encoder zero pulse can be plotted together and observed that z-pulse and peak of back-EMF of phase-a do not occur at the same point. This situation is shown in Figure 1.1.2.1.2. Expected and actual encoder readings are shown. Angle difference between actual z-pulse and expected z-pulse is offset angle.

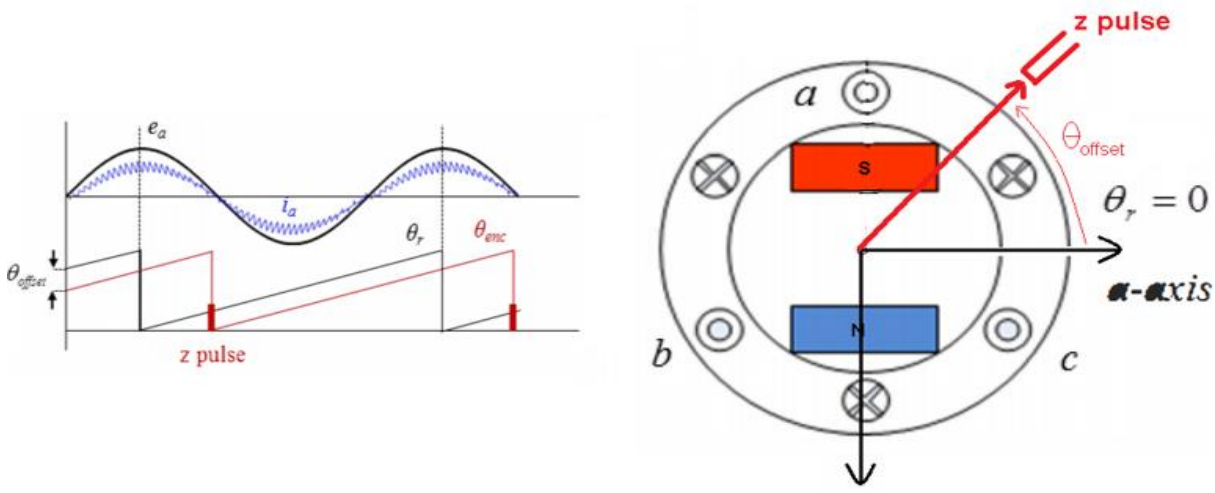

Figure 1.1.2.1.2: Z-pulse Position and Back-EMF when Offset Angle is not Zero

1.1.3 Inverter Control Techniques

A typical electric drive system consists of electric motor and a power converter which serves as interface between motor and AC mains. Converter comprises of rectifier, DC-link and three phase inverter. Increased safety, better power efficiency and vehicle's ability to follow demanded speed curve quickly emphasizes the need to study and develop new inverter control strategies which are relatively robust and could provide high performance.

Mentioning motor control is nothing but controlling switching of all six switches in the inverter. Current controller gives voltage as output to be fed to inverter as reference making it voltage source inverter (VSI) [4] and thus we will be having control over output voltage. For this thesis work, VSI is assumed as a linear device having unity gain. Harmonics induced because of switching of gates, are ignored and assumed that VSI gives only fundamental harmonic at its output terminals. Pulse width modulation technique is most used technique for inverter control. A quick review is given for popular modulation techniques used in advanced drives to realize the concept.

1.1.3.1 Sinusoidal Pulse width modulation (SPWM)

Sinusoidal pulse width modulation technique (SPWM) has been used widely for inverter control owing to its simple implementation and good results. For the sake of simplicity, one single phase inverter is shown in figure 1.1.3.1.1 or alternatively it can be referred to as one leg of three phase inverter. Three phase inverter will work the same way except that three sinusoidal signals distanced 120 degrees from each other will be used as reference.

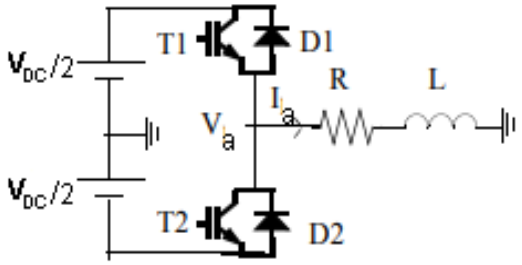

Figure 1.1.3.1.1: Basic Topology of Single-phase Inverter with RL Load

Switches of VSI can be turned on and off as per requirement. Both switches of the leg can't be in conducting mode at the same time so dead time will be introduced at switching moments but ignored here as this is not the focus of the discussion. Switching upper switch on and off results in square wave. Switching pulses are generated by comparing reference signal (modulating wave) with a high frequency carrier wave. Triangular and saw tooth waves are generally used as carrier. In figure 1.1.3.1.2, modulation wave, carrier wave and resultant phase voltage on the basis of gating pulses are shown.

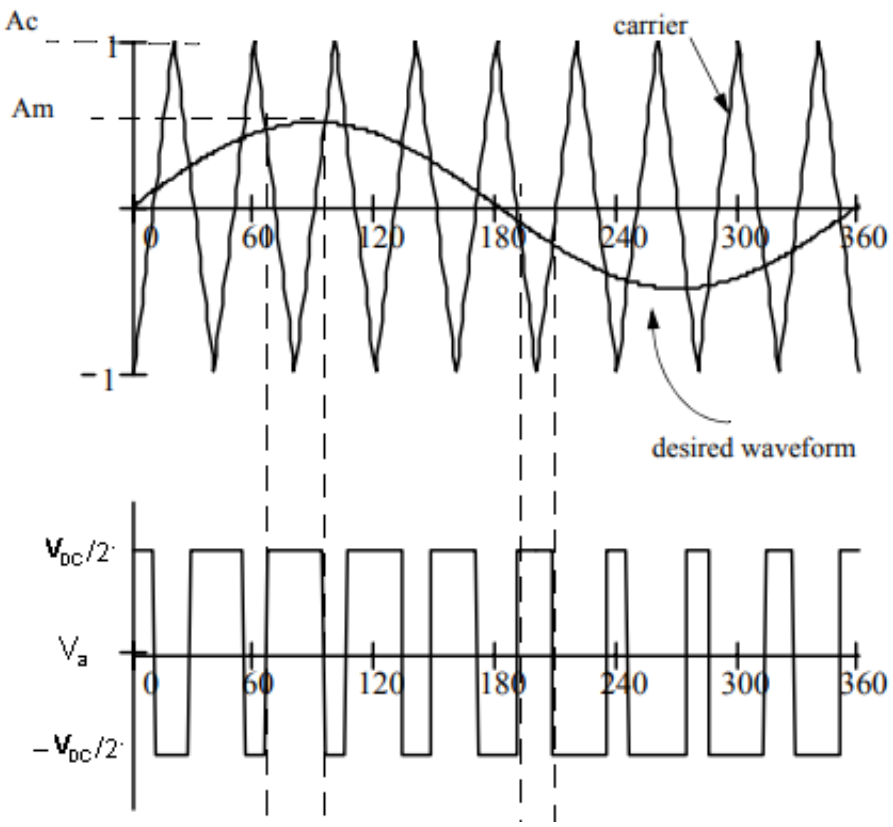

Figure 1.1.3.1.2: SPWM Comparison Signal with Triangular Carrier wave and Unfiltered SPWM Output Wave

It is shown very clearly if reference signal amplitude will be higher than carrier wave amplitude then upper switch will conduct. Otherwise lower switch will conduct.

The ratio of modulation signal amplitude $A_m$to carrier wave amplitude A_c is called modulation index. Modulation index controls the amplitude of output applied voltage.

$$m_a = \frac{A_m}{A_c} \qquad (1.1.3.1.1)$$

Likewise, frequency modulation ratio (m_f) plays important role in harmonic content control. Fast switching can improve the harmonic profile substantially. Careful adjustment of m_f will help eliminate lower order harmonics which will be at the cost of higher order harmonics but can be ignored as inductive nature of load will help filter out those harmonics [4].

$$m_f = \frac{f_c}{f_m} \qquad (1.1.3.1.2)$$

Here f_c is carrier wave frequency and f_m is fundamental harmonic frequency of reference signal. For some reference signal and carrier wave, Instantaneous line to center voltage is shown in figure 1.1.31.2. Mean value of this instantaneous voltage will replace the smooth

demand curve when operated at sufficiently high frequency ratio m_f. Advanced solid state devices can operate at very high switching frequencies fulfilling the purpose.

1.1.3.2 Space vector pulse width modulation (SVPWM)

SVPWM is one of the most recent trends for pulse generation. It is considered better approach as it provides better fundamental output voltage, flexibility to utilize pre-defined switching states for calculated time to minimize switching losses and low current ripple [5]. Specialty about the technique is, at some instant only one leg will switch its state. As this modulation technique is used in experimental implementations so it will be discussed in little more detail.

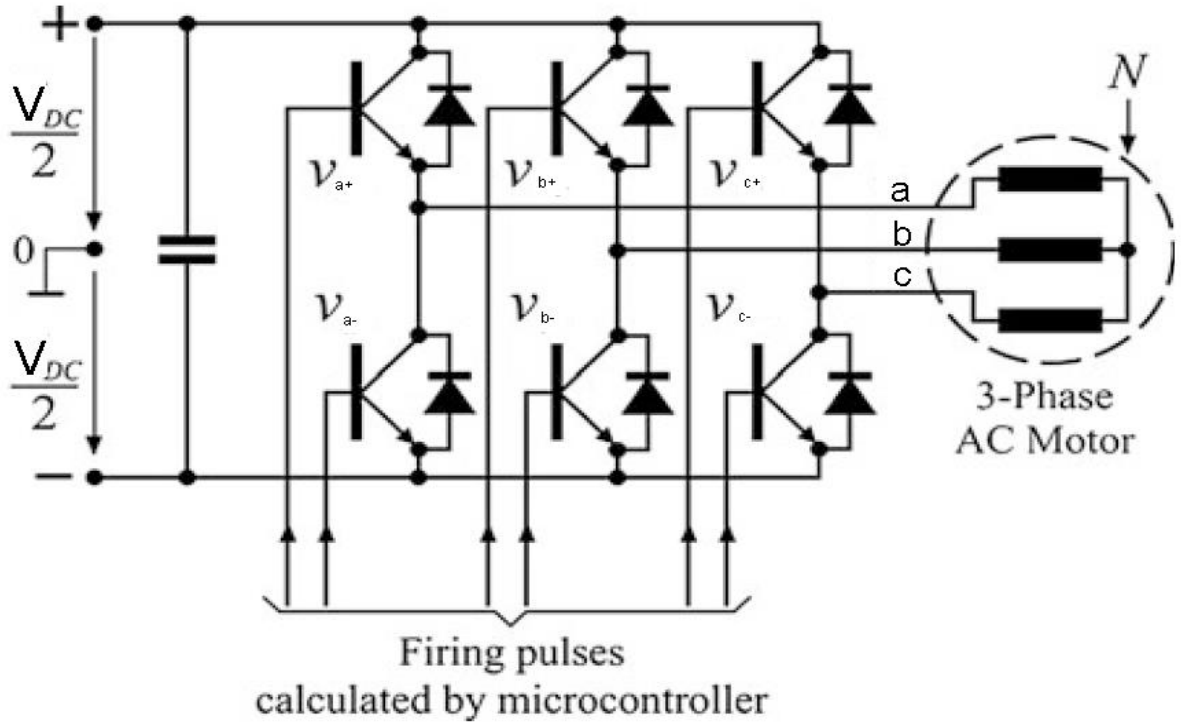

Figure 1.1.3.2.1: Basic Topology of a VSI-fed Three-Phase Motor

Figure 1.1.3.2.1 shows the circuit of an inverter feeding a three phase motor with windings a, b and c. Three pair of semiconductor switches are used to apply three phase voltages with amplitude, frequency and phase angle defined by firing pulses generated by microcontroller. Some winding logical position could be 0 or 1 depending whether lower switch is conducting or upper one respectively. Thus for three windings there are eight possible logical states $(u_0, u_1 \dots u_7)$ shown in table 1.1.3.2.1.

	u_0	u_1	u_2	u_3	u_4	u_5	u_6	u_7
a	0	1	1	0	0	0	1	1
b	0	0	1	1	1	0	0	1
c	0	0	0	0	1	1	1	1

Table 1.1.3.2.1: Standard Voltage Vectors and Respective Logic States

Two of these states are termed as zero vectors when all lower switches are conducting (u_0) or all upper switches are conducting (u_7). Rest six states are positioned in stator-fixed αβ coordinates to divide vector space into six equal sectors$S_1 - S_6$, four quadrants are indicated by$Q_1 - Q_4$. Figure 1.1.3.2.2 (a) shows all eight possible voltage vectors, placed in respective sector and quadrant.

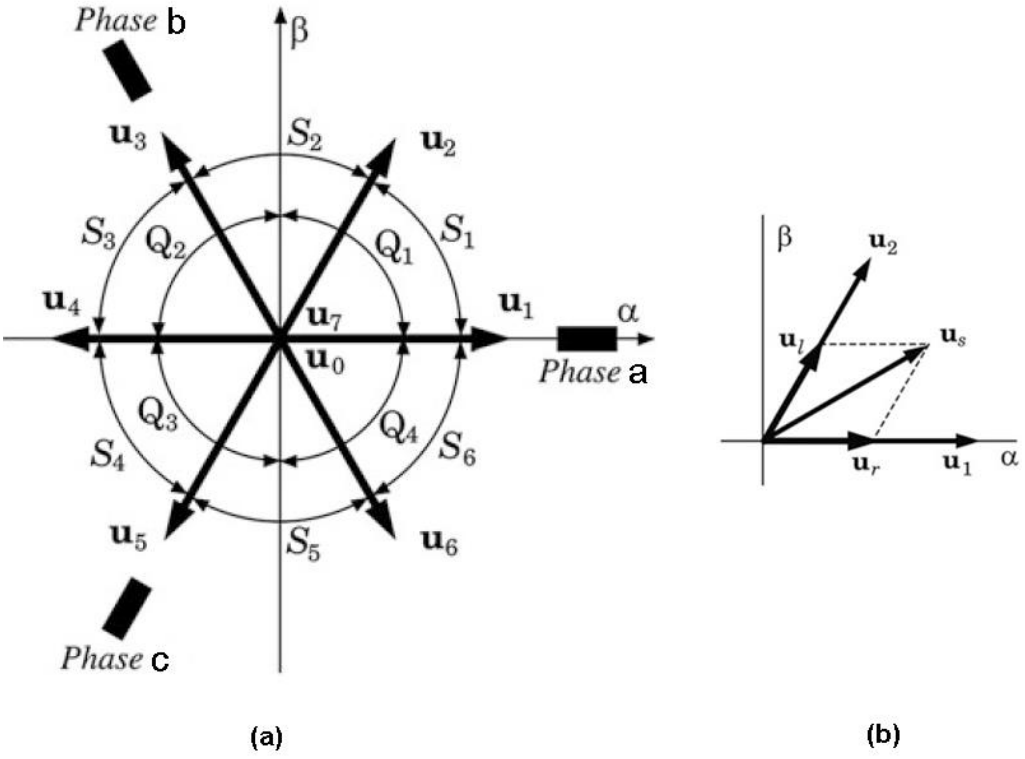

Figure 1.1.3.2.2: (a) Standard Voltage Vectors (b) Realization of an Arbitrary Voltage Vector from two Boundary Vectors

1.1.3.2.1 Principle of Space Vector Modulation

Space vector modulation implementation [22] needs reference frame transformation to determine sector. Magnitude of vector is used to calculate the timings of three adjacent states to result averaged required output. The procedure is illustrated using one example.

Let's say at some instant $\boldsymbol{u_s}$ is the vector to be realized which is located in first sector S_1. $\boldsymbol{u_s}$ can be obtained from vectorial sum of $\boldsymbol{u_l}$ and $\boldsymbol{u_r}$ and its maximum modulus can be $\frac{2}{3}V_{DC}$ when it will be pointed towards any of the hexagonal corner . And magnitude adjustment is to be made using zero vectors (u_0 and u_7). One complete pulse period T_p is available to realize the desired vector. This scenario is shown in figure 1.1.3.2.2 (b).

$\boldsymbol{u_l}$ and $\boldsymbol{u_r}$ are realized by using switching state logic of u_2 and u_1 respectively as given in table 1.1.3.2.1. u_2 will be applied for T_l time and u_1 will be applied for T_r time span. These time spans are given below.

$$T_r = T_p \frac{|\boldsymbol{u_r}|}{|\boldsymbol{u_s}|_{max}} ; T_l = T_p \frac{|\boldsymbol{u_l}|}{|\boldsymbol{u_s}|_{max}}$$

Time left in pulse period $T_p - (T_l + T_r)$ will be for zero vectors (u_0 and u_7). So required output vector $\boldsymbol{u_s}$ is realized as follows. (1.1.3.2.1.1)

$$u_s = u_r + u_l + u_0 \,(or\, u_7) \; = \frac{T_r}{T_p} u_1 + \frac{T_l}{T_p} u_2 + \frac{T_p - (T_l + T_r)}{T_p} u_0 \qquad (1.1.3.2.1.1)$$

Likewise output vector situated anywhere in the space can be realized using adjacent three logical state vectors according to procedure detailed in [22].

1.1.3.3 Modulation Range limits for SPWM and SVPWM

Theoretically, maximum amplitude modulation index m_a is 1. But in higher modulation index values, inverter losses its ability to fully control output voltage waveform. Such modulation region will be termed as over-modulation region or inverter's non-linear modulation region. So reachable modulation index needs to be determined such that we are always operating in the linear region. This limit is defined by peak value of fundamental harmonic of inverter output voltage (V_{1max}) and peak of fundamental harmonic of output voltage when in six-step operation($\frac{2}{\pi} V_{DC}$).

In case of sinusoidal Pulse Width Modulator, peak of fundamental harmonic voltage is $\frac{V_{DC}}{2}$. While for Space Vector Pulse Width Modulator, peak of fundamental harmonic voltage is $\frac{V_{DC}}{\sqrt{3}}$. So maximum limit of modulation index for linear region is given as;

$$m_{\max\_SPWM} = 0.785 \qquad (1.1.3.3.1)$$

$$m_{\max\_SVPWM} = 0.907 \qquad (1.1.3.3.2)$$

In [6], a comparative study is made between SPWM and SVPWM with rigorous analysis on modulation limits.

1.2 Scalar vs Vector Control

High performance drive applications demand fast torque response. For good steady state response and excellent transient behavior, different control strategies are studied over past few decades including scalar and vector control technique. These two being the mostly used techniques, will be discussed here briefly.

1.2.1 Scalar Control

In scalar control or alternatively Volts/Hz control scheme, speed of motor is controlled by adjusting the stator voltages and frequency such that air gap flux is maintained at desired level. If we ignore stator voltage drop, the stator terminal voltage can be expressed as:

$$V_s \propto \varphi * f_e$$

Where φ is airgap flux and f_e is synchronous frequency. So airgap flux can be made constant by keeping the ratio of applied voltage and frequency constant and torque becomes independent of supply frequency. As the speed increases, the stator voltages must, therefore, be proportionally increased in order to keep the constant ratio of V_s to f_e. Voltage boost is introduced at low speeds to counteract the larger state of stator resistance [7].
Another advantage is that V/f is the only control method which allows for multiple motors to be run off of a single VFD. When running multiple motors, all motors will start and stop at the same time, as well as follow the same speed reference. But in case of any problem, there is no way to determine if motor shaft is actually rotating. As a solution, this control strategy can be modified to make the speed response better by monitoring feedback signals and adjusting voltages accordingly. This modified control system is named as V/f with encoder control system [8].

1.2.2 Vector Control

Vector control (VC) scheme was introduced in 1970s to provide a way to control AC machines like separately excited DC machines. It was a major breakthrough for control realization of high speed drives. In vector control instantaneous positions of flux, voltage and current space vectors are controlled, ideally giving correct orientation both in steady state and transient condition [7]. Three to two phase transformation (qd transformation) is the key step of this control technique. Newly established variables are mutually orthogonal and thus pose no net interaction between each other. It gives ease to relate control variables directly with torque. VC separates current into field (d-axis) and torque (q-axis) producing components. Synchronous frame transformation results constant valued controllable parameters as shown in figure 1.2.2.1.

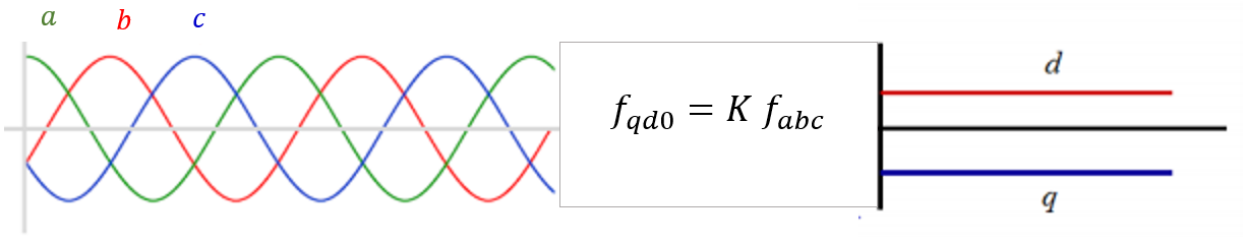

Figure 1.2.2.1: Stator Fixed abc and qd-Reference Frame Waveforms

For stator-fixed three phase system, controllers need to track sinusoidal signals, which is almost impossible and steady state error is always there. On the other hand for vector control, Once field is established and can be held constant then q-axis current is the parameter to be

controlled for desired torque response [7] and this is the reason behind VC being the fast control system relatively.

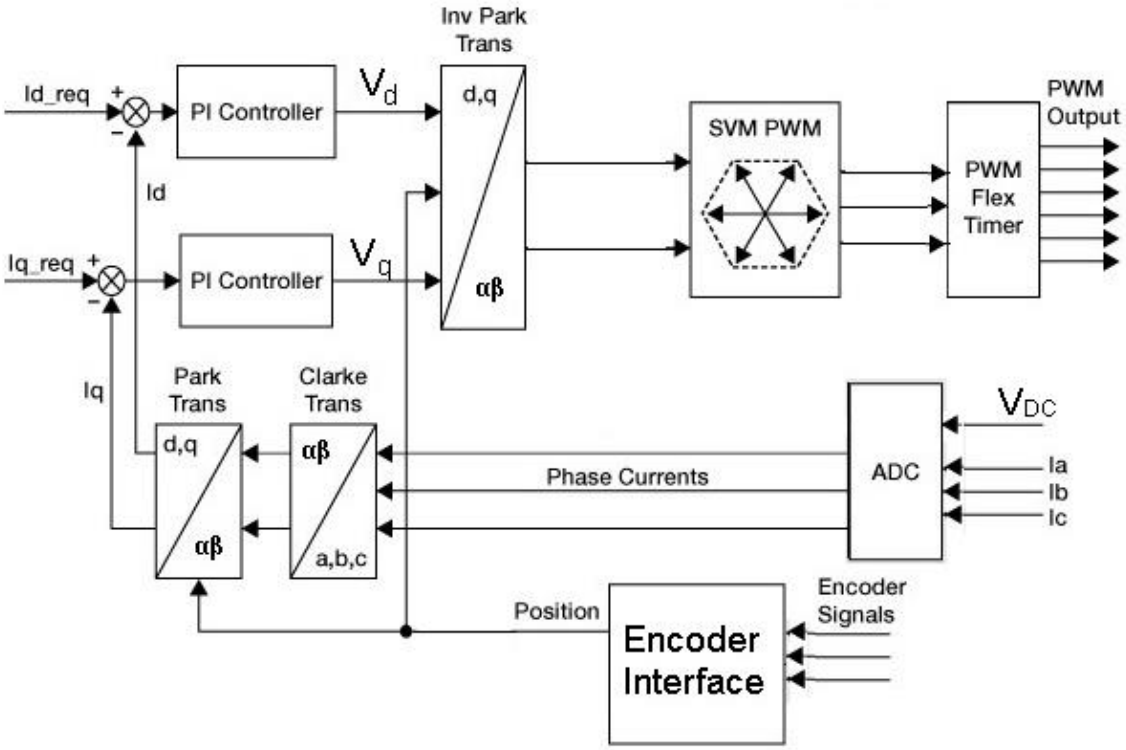

Figure 1.2.2.2: Basic Topology of Field Oriented Control equipped with Incremental Encoder

Basic Vector control topology is shown in figure 1.2.2.2. Here, all three line currents are measured and fed-back, but minimum two current sensors are required to measure two line currents. The measured three phase currents are transformed into synchronous reference frame components. For this transformation encoder signals are used to determine position of the rotor. Two current regulators are implemented in synchronous reference frame contrary to three current regulators, needed to control the motor in stator-fixed abc reference frame. Though this advantage is on the cost of enhanced computations.

For efficient controller development, it is necessary to understand machine topology well. Machine structure determines how d-axis and q-axis parameters will be controlled to get Maximum Torque per Ampere (MTPA) and how rotor position will be determined. Like for IPMSM, reluctance torque can be made use of, by controlling d-axis current as per equation 2.3.2.1.

2. Theoretical Model Development of IPMSM

Development and understanding of mathematical model of an electrical machine is necessary for either type of control implementation. This section will detail the process of getting the mathematical model of internal permanent magnet motor in three phase coordinates and then conversion into synchronous reference frame for vector control implementation. Though, the model developed, is equally valid for all type of synchronous machines. But IPMSM will be taken as reference. Basic structural model of IPMSM is shown in figure 2.1 to depict magnet placement in the rotor causing its salient nature specifically. Direction of rotor flux and rotor axis is also indicated.

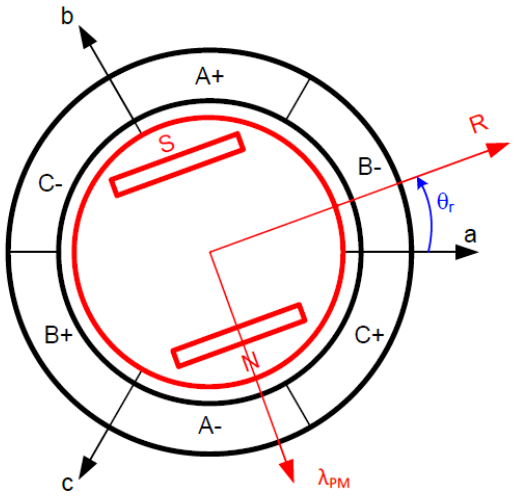

Figure 2.1: Basic structure of IPMSM

2.1 IPMSM Model Development in Three Phase Coordinates

2.1.1 Voltage and Flux Equations

Phase voltage of each winding of machine is the sum of armature –resistance voltage drop $R_a i_a$ and the induced voltage [9]. Induced voltage is caused by time varying flux with respect to specific winding. For all three phases voltage is given as;

$$v_a = R_a i_a + \frac{d\lambda_a}{dt}$$

$$v_b = R_b i_b + \frac{d\lambda_b}{dt}$$

$$v_c = R_c i_c + \frac{d\lambda_c}{dt}$$

Armature winding resistances of all three windings are equal so$R_s = R_a = R_b = R_c$. As windings are wound symmetrically so flux linkage also poses a symmetric behavior. Thus, voltage equation can be written as

$$v_{abc} = R_s i_{abc} + \frac{d\lambda_{abc}}{dt} \qquad (2.1.1.1)$$

Flux linkage of a winding is caused by current in its own winding (self-inductance), other phase windings (mutual inductance) and rotor flux. Flux linkages in terms of phases a, b, c and rotor flux can be expressed as follows

$$\lambda_{abc} = L_{abc} i_{abc} + \lambda_{pm,abc} \qquad (2.1.1.2)$$

λ_{pm} is the magnitude of flux linkage caused by permanent magnet embedded in the rotor structure. As mentioned, L_{abc} will contain self and mutual inductances. It can be expressed as follows mathematically.

$$L_{abc} = \begin{bmatrix} L_{aa} & L_{ab} & L_{ac} \\ L_{ba} & L_{bb} & L_{bc} \\ L_{ca} & L_{cb} & L_{cc} \end{bmatrix} \qquad (2.1.1.3)$$

Diagonal elements of matrix are self-inductances while all other elements are mutual inductances. As windings are symmetric so flux linkage behavior is also symmetric or $L_{ab} = L_{ba}$, $L_{ac} = L_{ca}$, $L_{bc} = L_{cb}$.

Self-inductance comprises of magnetizing (L_m) and leakage inductance (L_l)

$$L_{aa} = L_{bb} = L_{cc} = L_l + L_m$$

As rotor structure presents saliency so magnetizing inductance (L_m) varies with rotor position. Magnetizing inductance shows co-sinusoidal behavior when plotted against electrical angle ($\theta_e = P\theta_r$), P being the number of pole pairs of machine. Variation of L_m with electrical angle is shown in figure 2.1.1.1.

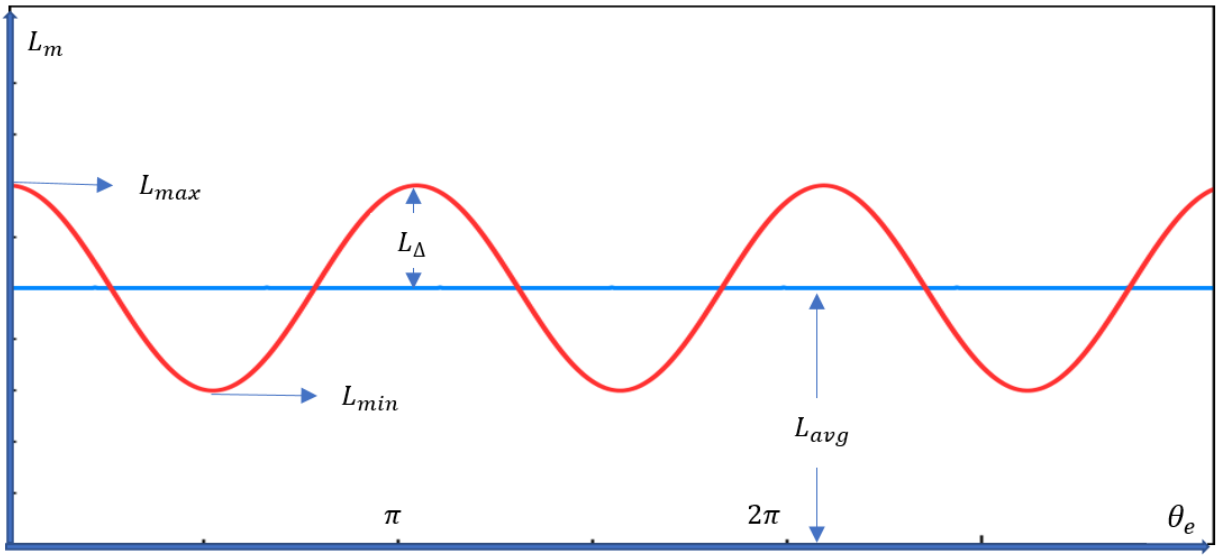

Figure 2.1.1.1: Magnetizing Inductance as a Function of Electrical Angle

L_{max} and L_{min} are maximum and minimum magnetizing inductances respectively.

L_{avg} is average magnetizing inductance given by $\frac{L_{max}+L_{min}}{2}$.

L_Δ gives variation in inductance from average inductance value which is calculated as $\frac{L_{max}-L_{min}}{2}$.

Either north or south pole is facing respective winding, effect on magnetizing inductance will be same. Figure 2.1.1.1 shows this fact. As magnetizing inductance variation curve has double frequency that that of electrical frequency.

In context to this discussion, equation 2.1.1.3 can be written as function of rotor electrical angle as follows:

$$L_{abc}(\theta_e) = \begin{bmatrix} L_l + L_{avg} + L_\Delta \cos 2\theta_e & -\frac{1}{2}L_{avg} + L_\Delta \cos 2(\theta_e - \frac{\pi}{3}) & -\frac{1}{2}L_{avg} + L_\Delta \cos 2(\theta_e + \frac{\pi}{3}) \\ -\frac{1}{2}L_{avg} + L_\Delta \cos 2(\theta_e - \frac{\pi}{3}) & L_l + L_{avg} + L_\Delta \cos 2(\theta_e - \frac{2\pi}{3}) & -\frac{1}{2}L_{avg} + L_\Delta \cos 2(\theta_e + \pi) \\ -\frac{1}{2}L_{avg} + L_\Delta \cos 2(\theta_e + \frac{\pi}{3}) & -\frac{1}{2}L_{avg} + L_\Delta \cos 2(\theta_e + \pi) & L_l + L_{avg} + L_\Delta \cos 2(\theta_e + \frac{2\pi}{3}) \end{bmatrix} \quad (2.1.1.4)$$

In equation 2.1.1.2, $\lambda_{pm,abc}$ is also a function of rotor electrical angle, which can be expressed as follows.

$$\lambda_{pm,abc}(\theta_e) = \lambda_{pm} \begin{bmatrix} \sin(\theta_e) \\ \sin(\theta_e - \frac{2\pi}{3}) \\ \sin\left(\theta_e + \frac{2\pi}{3}\right) \end{bmatrix} \quad (2.1.1.5)$$

2.1.2 Torque Equation

Power input in machine is known in terms of voltage and current.

$$i_{abc}{}^{T} v_{abc} = i_{abc}{}^{T} R_s i_{abc} + i_{abc}{}^{T} \frac{d\lambda_{abc}}{dt}$$

$$i_{abc}{}^{T} v_{abc} = i_{abc}{}^{T} R_s i_{abc} + i_{abc}{}^{T} * \frac{\partial}{\partial t}\lambda_{abc} + i_{abc}{}^{T} * \frac{\partial}{\partial \theta_e}\lambda_{abc} * \frac{\partial \theta_e}{\partial t}$$

Here, first term corresponds to losses in armature windings. Second term is related to energy stored in magnetic circuit while third term is used to calculate electromagnetic torque.

$$T * \omega_r = T.\frac{\omega_e}{P} = i_{abc}{}^{T} * \frac{\partial}{\partial \theta_e}\lambda_{abc} * \frac{\partial \theta_e}{\partial t}$$

$$T = P.\, i_{abc}{}^{T} * \frac{\partial}{\partial \theta_e}\lambda_{abc} \qquad (2.1.2.1)$$

2.2 Introduction to Coordinate Transformation

In stator-fixed three phase machine model, we get magnetizing inductances, which are position dependent. Permanent magnet flux linkage behavior with armature windings is also complex. These time dependent variables, when used in control implementation, make it almost impossible to get zero steady state error for high speed drives. Transient behavior is even worse. This problem is resolved by transforming system parameters and implementing control algorithm in rotating reference frame.

Coordinate transformation can be done in several ways but here only dq0 (Clarke + Park) transformation will be described. Transformation will lead to three (abc) to two phase (qd) transformation, one aligned with the field-winding axis called direct-axis component, and one in quadrature with the field-winding axis called quadrature-axis component as shown in figure 2.2.1.

Angle (θ) between quadrature axis of transformed reference frame and phase-a of abc reference frame is given by

$$\theta(t) = \int_0^t \omega(\tau) d\tau + \theta(0)$$

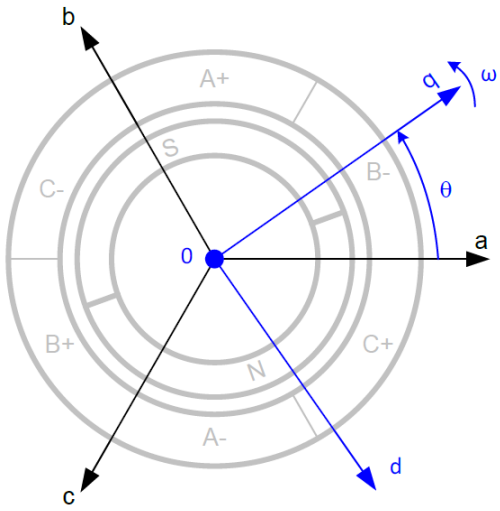

Figure 2.2.1: Transformed axis for PM drive

Here $\theta(0)$ is the angle between two frames at t=0. If speed ω of dq reference frame is such that $\omega = \omega_e$, transformed reference frame will be called synchronous reference frame. The usefulness of this concept stems from the fact that although each of the stator phases sees a time-varying inductance due to the saliency of the rotor, the transformed quantities rotate with the rotor and hence see constant magnetic paths [9]. Subsequent discussion will be made for synchronously rotating reference frame only.

The transformation from three phase to two phase coordinate system is established using transformation matrix K.

$$f_{qd0} = \begin{bmatrix} f_q \\ f_d \\ f_0 \end{bmatrix} = K * f_{abc} = K * \begin{bmatrix} f_a \\ f_b \\ f_c \end{bmatrix} \qquad (2.2.1)$$

$$K = k \begin{bmatrix} \cos(\theta_e) & \cos(\theta_e - \frac{2\pi}{3}) & \cos(\theta_e - \frac{4\pi}{3}) \\ \sin(\theta_e) & \sin(\theta_e - \frac{2\pi}{3}) & \sin(\theta_e - \frac{4\pi}{3}) \\ h & h & h \end{bmatrix}$$

The "0" component always represents homopolar components which will be ignored in the case of balanced three phase system. There are two choices for selection of constant values k and h.

1. k=2/3 and h=1/2 will result in amplitude conservative transformation. However, power conservation needs to be imposed this way

$$p_{abc}(t) = v_a i_a + v_b i_b + v_c i_c$$

$$p_{qd0}{}'(t) = v_q i_q + v_d i_d + v_0 i_0$$

$$p_{qd0}(t) = \frac{3}{2}(v_q i_q + v_d i_d + v_0 i_0) = p_{abc}(t) \qquad (2.2.2)$$

2. $k = \sqrt{\frac{2}{3}}$ and $h = \sqrt{\frac{1}{2}}$ will result in transformation which is conservative with respect to power.

$$p_{qd0}(t) = v_q i_q + v_d i_d + v_0 i_0 = p_{abc}(t)$$

2.3 IPMSM Model Development in Synchronous Reference Frame

As explained above, for synchronous reference frame transformation, speed of axis will be chosen to be synchronous speed. Direct axis will be chosen along the field axis of rotor and quadrature axis will be aligned with rotor axis. Angle θ_e must be known at any instant which can be calculated using estimation methods or encoder reading mounted on rotor shaft. For our case, incremental encoder is used to know rotor instantaneous position.

2.3.1 Voltage and Flux Equations

In synchronous reference frame, voltage equation is written as

$$v_{qdo} = R_{qdo} * i_{qdo} + \frac{d\lambda_{qdo}}{dt} + \omega_e * \lambda_{dq} \qquad (2.3.1.1)$$

In comparison with equation 2.1.1.1, a new term $\omega_e * \lambda_{dq}$ is added which is function of speed and causes coupling between two newly established d and q coordinates.

Using equation 2.2.1, different parameters [2] in equation 2.3.1.1 can be written as follows.

$$R_{qdo} = K\, R_s\, K^{-1} = R_s \qquad (2.3.1.2)$$

$$\lambda_{dq} = \begin{bmatrix} \lambda_d \\ -\lambda_q \\ 0 \end{bmatrix} \qquad (2.3.1.3)$$

Flux equation can be expressed as follows.

$$\lambda_{qdo} = \lambda_{pm,qdo} + L_{qdo} i_{qdo} \qquad (2.3.1.4)$$

As qd0 reference frame is chosen such that direct axis is aligned with rotor flux axis so permanent magnet flux along q-axis does not exist.

$$\lambda_{pm,qdo} = \begin{bmatrix} 0 \\ \lambda_{pm} \\ 0 \end{bmatrix} \qquad (2.3.1.5)$$

λ_{pm} is flux linkage caused by permanent magnet.

Now equation 2.3.1.3 can also be modified to result;

$$\lambda_{dq} = \begin{bmatrix} \lambda_d \\ -\lambda_q \\ 0 \end{bmatrix} = \begin{bmatrix} \lambda_{pm} + L_d i_d \\ -L_q i_q \\ 0 \end{bmatrix} \quad (2.3.1.6)$$

Inductance matrix can be written as follows

$$L_{qdo} = K\, L_{abc}\, K^{-1} = \begin{bmatrix} L_q & 0 & 0 \\ 0 & L_d & 0 \\ 0 & 0 & L_0 \end{bmatrix}$$

D and q-axis inductances are given as;

$$L_q = L_l + \frac{3}{2} L_{avg} + L_\Delta \quad (2.3.1.7)$$

$$L_d = L_l + \frac{3}{2} L_{avg} - L_\Delta \quad (2.3.1.8)$$

$$L_0 = L_l \quad (2.3.1.9)$$

In the case of SMPM machine, q-axis inductance- L_q and d-axis inductance- L_d will be equal. Finally, d-axis and q-axis voltage equation can be written explicitly using equations 2.3.1.1 and 2.3.1.6

$$v_q = R_s * i_q + \frac{d(L_q i_q)}{dt} + \omega_e(\lambda_{pm} + L_d i_d) \quad (2.3.1.10)$$

$$v_d = R_s * i_d + \frac{d(L_d i_d)}{dt} - \omega_e(L_q i_q) \quad (2.3.1.11)$$

2.3.2 Torque Equation

Power formula is used to derive torque equation 2.1.2.1 in three phase reference frame. Same strategy will be opted here. As mentioned above in section 2.2, regarding choice of constants for axis transformation, power balance will be assured by manipulating with appropriate constants in equation.

Power input inclusive of losses is given by;

$$\frac{3}{2} {i_{qd0}}^T v_{qd0} = \frac{3}{2} {i_{qd0}}^T \left(R_{qdo} * i_{qdo} + \frac{d\lambda_{qdo}}{dt} + \omega_e * \lambda_{dq}\right)$$

$$\frac{3}{2} {i_{qd0}}^T v_{qd0} = \frac{3}{2} {i_{qd0}}^T R_{qdo} * i_{qdo} + \frac{3}{2} {i_{qd0}}^T \frac{d\lambda_{qdo}}{dt} + \frac{3}{2} {i_{qd0}}^T \omega_e * \lambda_{dq}$$

Exactly like the case of three phase system reference frame, first term represents joule losses, second one corresponds to stored magnetic energy and the third one will cause torque output.

$$T * \omega_r = T.\frac{\omega_e}{P} = \frac{3}{2} {i_{qd0}}^T \omega_e * \lambda_{dq}$$

$$T = \frac{3}{2} P * {i_{qd0}}^T * \lambda_{dq}$$

Using equation 2.3.1.6

$$T = \frac{3}{2} P(i_q \lambda_{pm} + (L_d - L_q) i_d i_q) \qquad (2.3.2.1)$$

This torque expression has two terms. First term is proportional to permanent magnet flux and corresponds to synchronous torque. Second term depends on proportion of anisotropy and relates to reluctance torque. For IPMSM $L_d < L_q$, as equation 2.3.1.7 and 2.3.1.8 depict. So direct axis current is injected in negative direction to keep reluctance torque positive. In case of SPM, second term is cancelled out as SPM is non-salient machine. While in case of synchronous reluctance machine, first term is eliminated because rotor doesn't have magnets but just a salient structure.

3. Design of Current Control Loop

Current control loop is the innermost loop in all servo drives, so it operates on the highest bandwidth amongst all. Current control loop is also referred to as torque control loop because torque demand is fulfilled by respective current demand, though indirectly. To reduce the order of closed current control loop, so dynamics of the system could be studied clearly, zero of controller is placed such as it cancels pole of the plant. But plant exists in continuous time domain and controller implementation is realized in discrete time domain. If switching frequency is high then this effect can be ignored and zero placement can be made according to continuous time functions as it is easy to analyze motor dynamics. This chapter will contain controller design details for both continuous as well as discrete time system considerations.

In section 1.1.3, it is mentioned that VSI is used as power converter, switching harmonics will be neglected and assumed that only fundamental harmonic of voltage is produced. Losses occurring across the switches are also neglected. However, voltage compensation because of dead-time will be considered which is introduced to avoid shootthrough in inverter legs.

3.1 Analysis and Tuning of Current Controller

3.1.1 Analysis and Tuning of Current Controller in s-domain

A classical PI regulator [2] is developed in synchronous reference frame. Controller gains are determined on the basis of plant parameters and bandwidth of the loop. Maximum bandwidth of current controller depends on the achievable switching frequency of the inverter switches.

Regulator parameters are determined like a simple RL load. A system based on RL load is shown with current regulator in figure 3.1.1.1.

Controller function C(s) and plant function P(s) can be written as;

$$C(s) = K_p + \frac{K_i}{s} = \frac{K_p s + K_i}{s} = K_i \frac{\frac{K_p s}{K_i} + 1}{s} \qquad (3.1.1.1)$$

$$P(s) = \frac{1}{sL + R} = \frac{\frac{1}{R}}{\frac{sL}{R} + 1} \qquad (3.1.1.2)$$

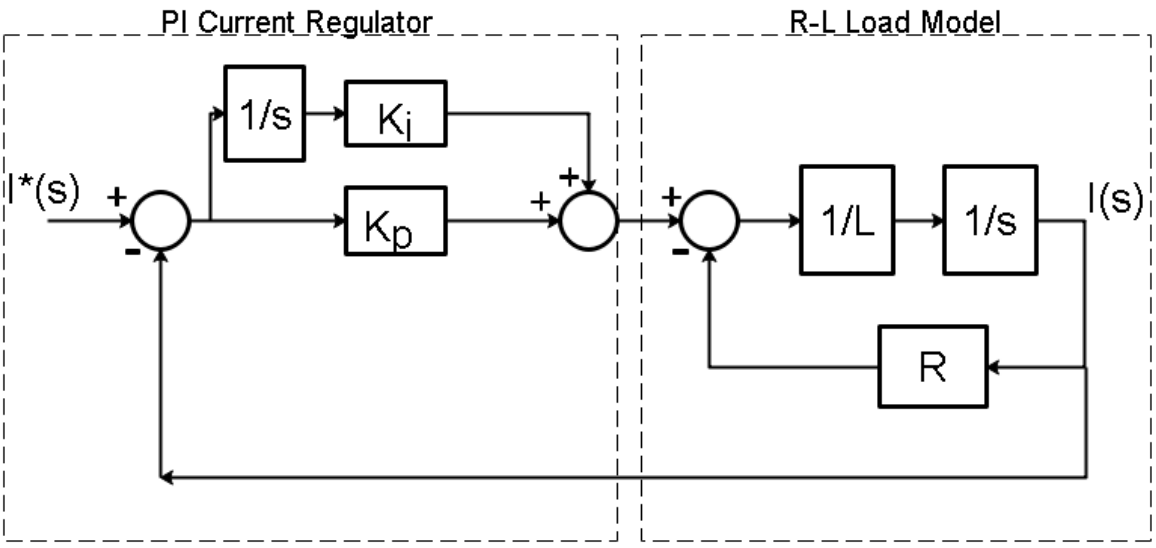

Figure 3.1.1.1: Synchronous Frame PI Current Regulator with RL Load Model in s-domain

From equation 3.1.1.1 and 3.1.1.2, it can be seen that if controller zero is chosen according to equation 3.1.1.3, then current controller open loop transfer function (OLTF) will be given as per equation 3.1.1.4.

$$\frac{K_i}{K_p} = \frac{R}{L} \tag{3.1.1.3}$$

$$OLTFi(s) = \frac{K_i}{sR} \tag{3.1.1.4}$$

And closed loop transfer function (CLTF) can be expressed as;

$$CLTFi(s) = \frac{OLTFi(s)}{1 + OLTFi(s)} = \frac{\frac{K_i}{sR}}{1 + \frac{K_i}{sR}} = \frac{1}{1 + \frac{sR}{K_i}} \tag{3.1.1.5}$$

Closed loop of current controller is expected to act like a low-pass filter to give first order output response with unity gain. So closed loop bandwidth of the controller, f_{BW_i}, can be related with gains as follows;

$$\omega_{BW\_i} = 2 * \pi * f_{BW\_i} = \frac{K_i}{R} \tag{3.1.1.6}$$

From equations 3.1.1.3 and 3.1.1.6, controller gains can be given as follows;

$$K_i = 2 * \pi * f_{BW\_i} * R \qquad and \qquad K_p = \frac{L}{R} K_i \tag{3.1.1.7}$$

If gains will be chosen according to equation 3.1.1.7, then root locus for the system would be presented as follows.

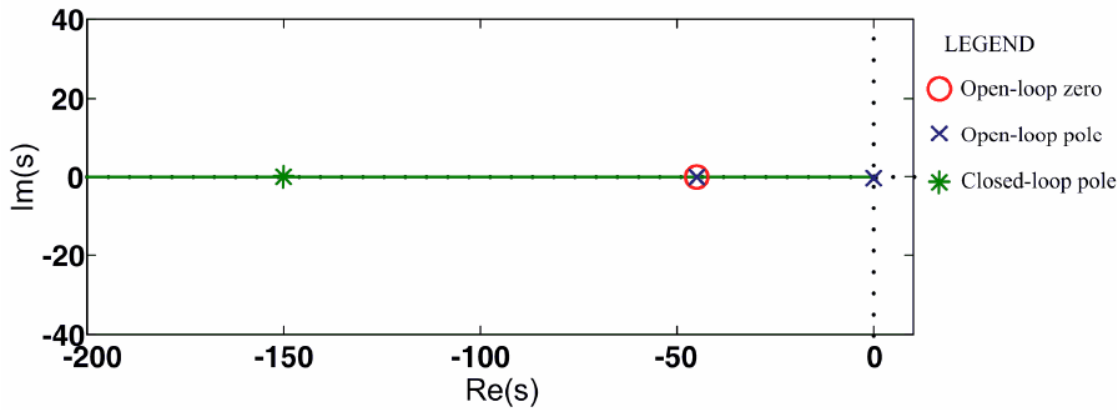

Figure 3.1.1.2: Root Locus of Regulated RL Load with Zero-pole Cancellation at 150Hz Bandwidth in s-domain

Figure 3.1.1.2 elaborates placement of open-loop zero over open-loop pole. Closed-loop pole is placed on real axis depending on chosen bandwidth. If current demand would be DC then integrator term of the controller will ensure zero steady state error. For gain calculation, motor electrical parameters estimated in section 6.1 are used.

3.1.2 Analysis and Tuning of Current Controller in Z-domain

As mentioned earlier, actual physical system is running in continuous time domain while controller gives signal in discrete time domain according to switching frequency set for pulse width modulator. Moreover, there are delays associated with power conversion unit which are not modelled while tuning the controller. This will hinder obtaining desired closed loop bandwidth. To design synchronous frame PI regulator in discrete domain, plant will be represented in z-domain according to concept presented in figure 3.1.2.1.

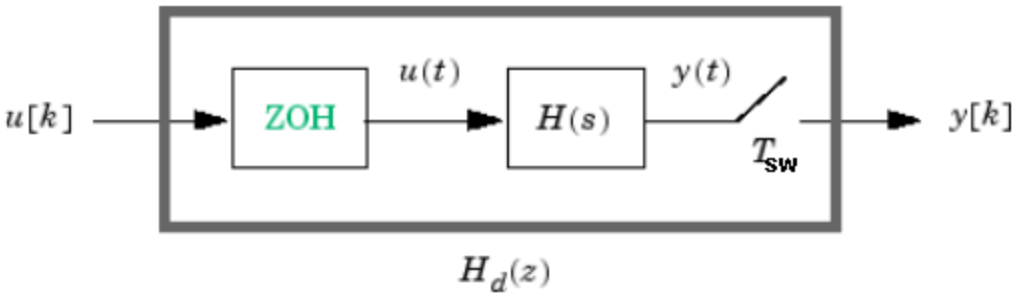

Figure 3.1.2.1: Zero-Order Hold Discretization of a Linear System

So discrete domain function [19] is obtained from continuous domain function in series with a ZOH function[1]. Plant z-domain transfer function is derived as follows.

[1] Zero Order Hold (ZOH) block holds its input for one time period as follows;

$$P(z) = (1 - z^{-1})\, Z\left\{\frac{P(s)}{s}\right\}$$

$$P(z) = \frac{(1 - z^{-1})}{R}\, Z\left\{\frac{1}{s(^{sL}/_{R} + 1)}\right\} = \frac{1}{R}\left(\frac{1 - e^{-R/L T_{sw}}}{z - e^{-R/L T_{sw}}}\right) \qquad (3.1.2.1)$$

$T_{sw}$is PWM switching frequency. ADC is also receiving its samples at the same frequency in this case because ADC is synchronized with PWM. Controller z-domain transfer function can also be derived in the similar manner but here it is just expressed as follows;

$$C(z) = K_p + K_i T_{sw} \frac{z}{z - 1} \qquad (3.1.2.2)$$

Discrete domain plant with current regulator is shown in figure 3.1.2.2.

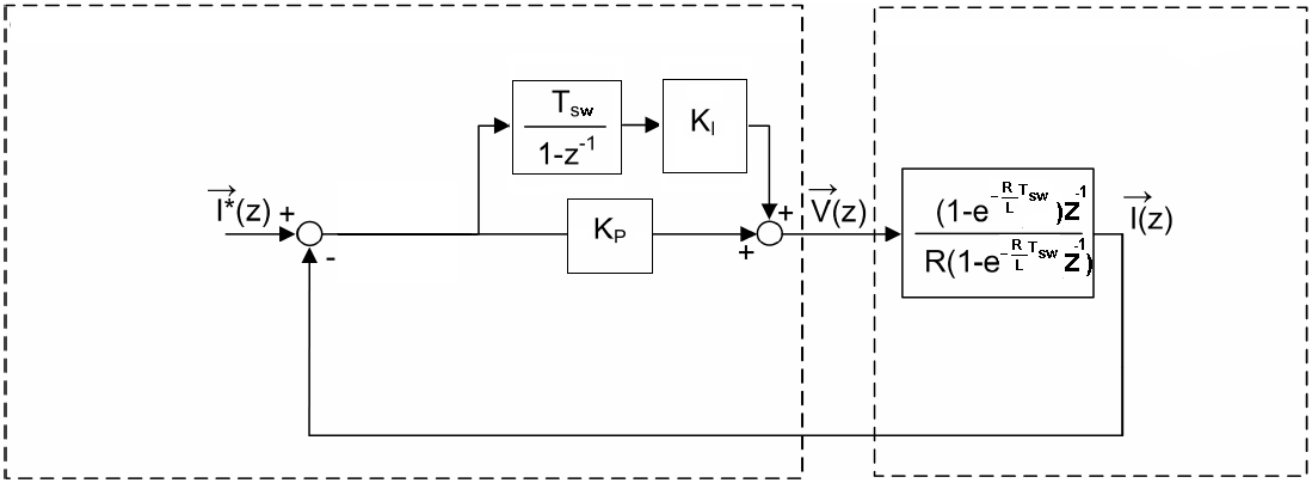

Figure 3.1.2.2: Synchronous Frame PI Current Regulator with RL Load Model in z-domain

Open loop transfer function of the system can be written as;

$$OLTFi(z) = (K_p + K_i T_{sw} \frac{z}{z - 1}) * \frac{1}{R}\left(\frac{1 - e^{-R/L T_{sw}}}{z - e^{-R/L T_{sw}}}\right)$$

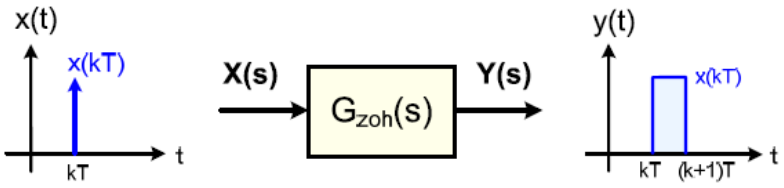

ZOH transfer function is given as$\frac{1-z^{-1}}{s}$ [19].

$$= \frac{(K_p + K_i T_{sw})(1 - e^{-R/L T_{sw}})}{R(z-1)} \left(z - \frac{K_p}{K_p + K_i T_{sw}}\right)\left(\frac{1}{z - e^{-R/L T_{sw}}}\right) \quad (3.1.2.3)$$

To cancel plant pole with controller zero, zero will be selected such as

$$\frac{K_p}{K_p + K_i T_{sw}} = e^{-R/L T_{sw}} \quad (3.1.2.4)$$

Let's say $K = \frac{(K_p + K_i T_{sw})(1 - e^{-R/L T_{sw}})}{R}$. Open loop transfer function, with zero-pole cancellation, becomes $\frac{K}{z-1}$.

Closed loop transfer function can be written as;

$$CLTFi(z) = \frac{OLTFi(z)}{1 + OLTFi(z)} = \frac{K}{z - (1 - K)} \quad (3.1.2.5)$$

To achieve desired closed loop bandwidth f_{BW_i}, closed loop pole should be placed such that

$$1 - K = e^{-2\pi T_{sw} * f_{BW_i}} \quad (3.1.2.6)$$

By solving equations 3.1.2.4 and 3.1.2.6, gain parameters for digital controller can be calculated.

$$K_p = R(e^{-R/L T_{sw}}) \left(\frac{1 - e^{-2\pi T_{sw} * f_{BW_i}}}{1 - e^{-R/L T_{sw}}}\right) \quad (3.1.2.7)$$

$$K_i = \frac{R}{T_{sw}}(1 - e^{-2\pi T_{sw} * f_{BW_i}}) \quad (3.1.2.8)$$

Root locus in z-domain is replica of s-domain root locus on unit circle and in case of exact zero-pole cancellation, it can be given as shown in figure 3.1.2.3.

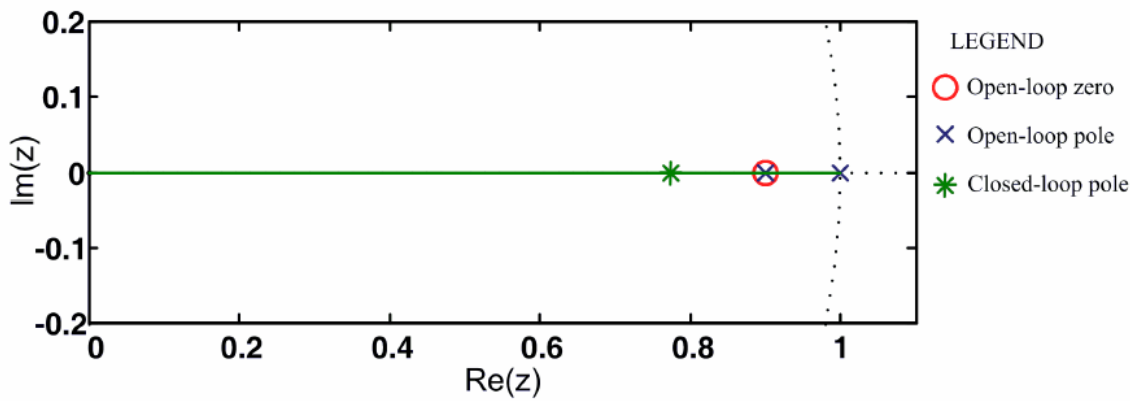

Figure 3.1.2.3: Root Locus of Regulated RL Load with Zero-pole Cancellation in z-domain

3.2 Current Controllers for Synchronous Machine

While designing current controller for a high speed drive, different parameters are considered like its ability for reference tracking and dynamic stiffness. Moreover it is important to know how a controller can keep its performance with changes in hardware parameters and speed. It is already discussed in section 1.2.2 that synchronous reference frame regulators receive controller input as DC quantity so good performance is achieved over a wide frequency range with PI type regulator. Various types of controllers are developed in synchronous reference frame. Cross-coupling decoupling type and complex vector type controller [20] are amongst the popular ones and very easy to implement. Here, both types will be discussed.

3.2.1 Cross-Coupling Decoupling Synchronous Frame PI Current Regulator

Controller tuning for three phase motor is similar to one described in section 3.1.1 and 3.1.2 because motor is just three-phase RL load. For better performance, there are some changes to be considered. This comparative analysis is made on the basis of mathematical model of system under consideration. Section 2.3 describes how an IPMSM is modelled in synchronous reference frame. According to equations 2.3.1.10 and 2.3.1.11, q and d axis voltages for IPMSM are given as follows;

$$v_q = R_s * i_q + \frac{d(L_q i_q)}{dt} + \omega_e(\lambda_{pm} + L_d i_d)$$

$$v_d = R_s * i_d + \frac{d(L_d i_d)}{dt} - \omega_e\left(L_q i_q\right)$$

These equations denote that there are speed dependent terms introduced in model while making reference frame transformations. These terms cause plant pole to move with speed but while designing controller in section 3.1.1 and 3.1.2, poles are assumed at a fixed point. To get expected response, these terms must be compensated for while designing the controller. In other words, system should be designed such as controller zero and plant pole remain at same position at all speeds. Plant pole position is given by $-\frac{R}{L} - j\omega_e$ in synchronous reference frame. By adding compensation terms, pole is moved back to $-\frac{R}{L}$ in synchronous reference frame. In stationary reference frame, it moved from $-\frac{R}{L}$ to $-\frac{R}{L} + j\omega_e$ [20]. This concept is elaborated in figure 3.2.1.1 where complex vector root locus of cross-coupling decoupling synchronous frame PI current regulator is shown in stationary reference frame for different synchronous frequencies.

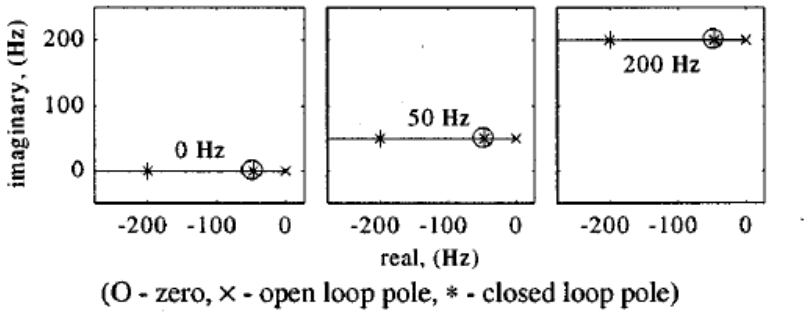

Figure 3.2.1.1: Complex Vector Root Locus of an RL Load with Cross-coupling Decoupling Synchronous Frame PI Regulator Shown in Stationary Reference Frame (f_e=0, 50 and 200Hz)

Synchronous frame PI regulator with compensated terms and motor model is shown in figure 3.2.1.2. As the terms $\omega_e(L_q i_q)$ and $\omega_e(L_d i_d)$ arise from cross coupling between two coordinates, so compensation is termed as cross-coupling decoupling. On the other hand, $\omega_e \lambda_{pm}$ corresponds to back-EMF compensation which arises because of permanent magnet flux.

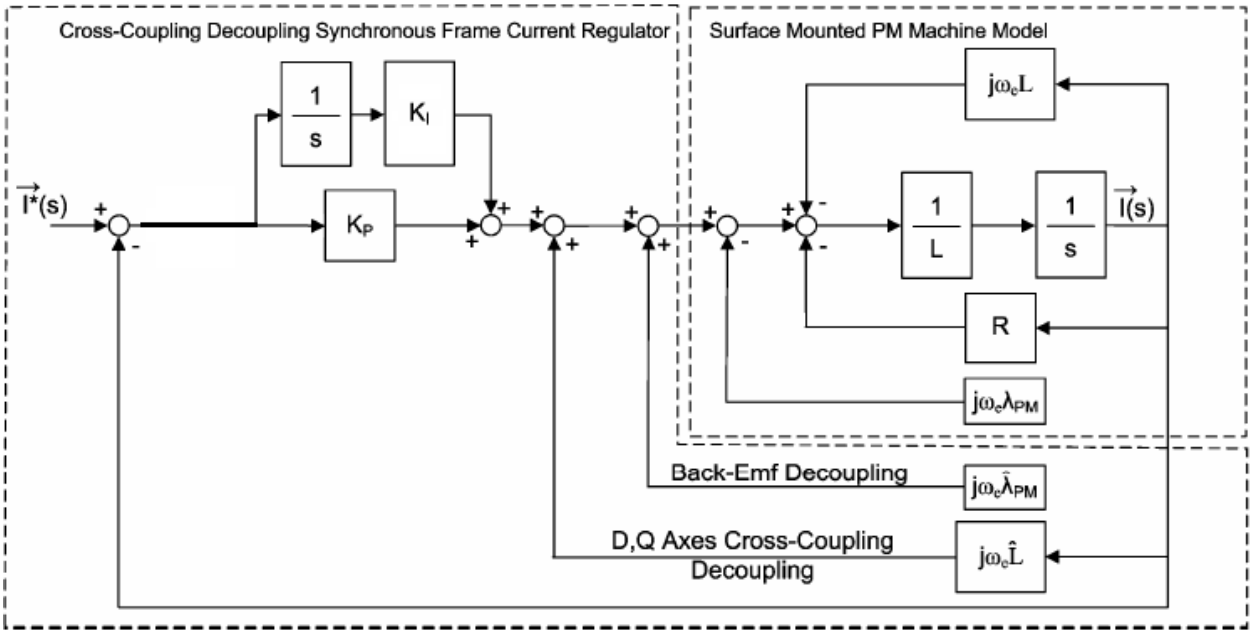

Figure 3.2.1.2: Synchronous Frame PI Current Regulator with Cross-coupling Decoupling for an RL Load

If these decoupling terms compensate exactly for cross coupling then model will be reduced to figure 3.1.1.1 for s-domain and figure 3.1.2.2 for z-domain. But usually this is not the case, as motor electrical parameters used to make compensations, are approximated values obtained by running some experiments. Moreover, actual parameters are prone to changes depending on environmental conditions and operating point.

3.2.2 Complex Vector Synchronous Frame PI Current Regulator

In section 3.2.1, cross-coupling decoupling type controller is developed. Using this technique, plant pole is made to stay on real axis in synchronous reference frame. It is also mentioned that decoupling terms don't compensate for cross-coupling exactly. Because these terms use estimated values of electrical parameters of motor. Another type of controller can be developed such as controller zero moves with plant pole as speed changes. In other words, zero of the controller is complex. This type of controller is called Complex vector controller [20]. As motor parameter estimates are not used to change controller zero placement, better response than that of cross-coupling decupling controller will be expected in actual scenarios. Figure 3.2.2.1 shows the schematic of complex vector PI current regulator in synchronous reference frame.

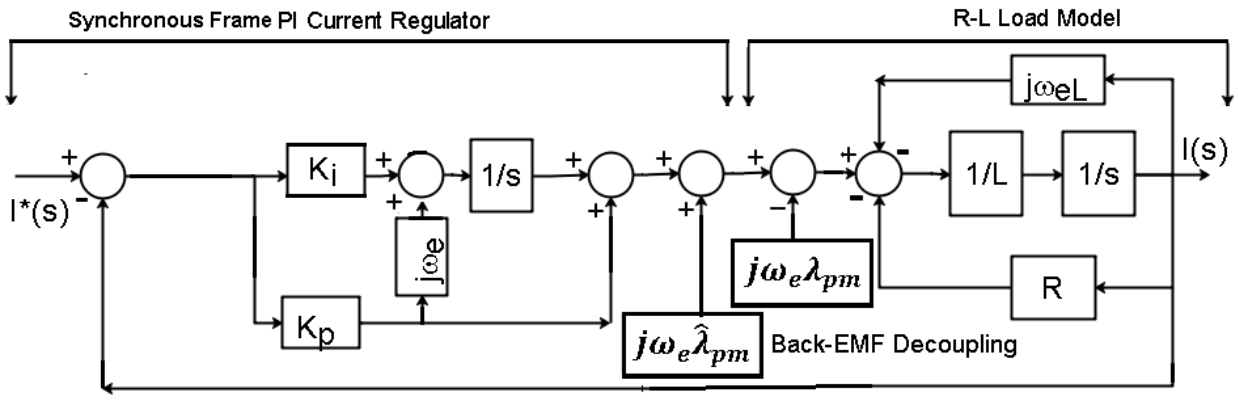

Figure 3.2.2.1: Complex Vector Synchronous Frame PI Current Regulator for an RL Load

Controller tuning done in section 3.1.1 and 3.1.2 remains valid for complex vector controller in s-domain and z-domain respectively. It is obvious from figure 3.2.2.1 that modification in controller is made without using any estimated electrical parameters of motor. So transient response of controller is expected to improve. It must be noted that back-EMF compensation is made exactly the way, it is made for cross-coupling decoupling type controller.

This type of controller ensures zero pole cancellation by moving zero of controller from $-\frac{R}{L}$ to $-\frac{R}{L}-j\omega_e$ in synchronous reference frame or $-\frac{R}{L}+j\omega_e$ to $-\frac{R}{L}$ in stationary reference frame. Complex vector root locus of complex vector synchronous frame PI current regulator for an RL load is shown in figure 3.2.2.2 in stationary reference frame for different synchronous frequencies.

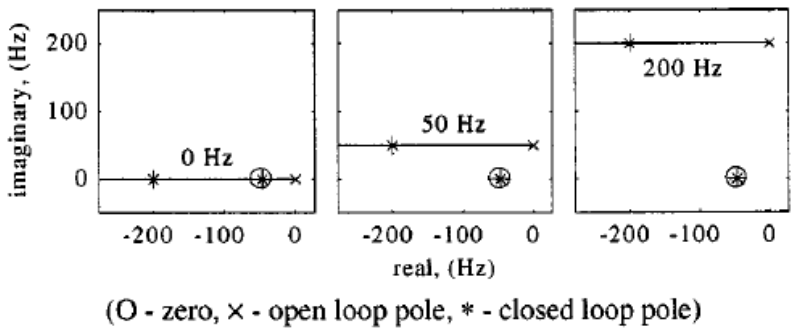

Figure 3.2.2.2: Complex Vector Root Locus of an RL Load with Complex Vector Synchronous Frame PI Regulator Shown in Stationary Reference Frame (f_e=0, 50 and 200Hz)

3.3 Inverter Non-Linear Behavior

3.3.1 Saturation and Anti-windup Algorithm Development

In the development of current controller, inverter is assumed to have unity gain which supplies demanded voltage fundamental harmonic without any distortion in amplitude and phase. But voltage that can be applied at winding terminals, depends upon DC-link voltage and limitations imposed by inverter and motor design. PWM technique also plays its role as explained in section 1.1.3.3.

Modulation index increases with controller output voltage demand. Over a certain modulation range, power converter has full control over its voltage output and this range is linear modulation range. For different PWM techniques, linear modulation region limits are also discussed in section 1.1.3.3. When demanded voltage is high enough to cause modulation index higher than the ones mentioned in equation 1.1.3.3.1 and 1.1.3.3.2 for SPWM and SVPWM respectively, operation region is called non-linear operation region. It is made sure that the inverter never works in the non-linear region so voltage demand is saturated on the basis of current DC-link voltage.

Saturating controller output voltage will in turn cause current errors and thus integrator term windup. Even after controller output voltage might have come under acceptable range, integrator term will take time to exit this saturation state. So for better response anti-windup algorithm is developed for integrator term so that controller output leaves saturation quickly after current error reduces to zero. Saturation and anti-windup algorithm for both cross-coupling decoupling and complex vector controllers is presented here.

3.3.1.1 Saturation and Anti-windup Algorithm for Cross-coupling Decoupling Synchronous Frame PI Current Regulator

Cross-coupling decoupling synchronous frame PI current regulator developed in section 3.2.1 is used. But before feeding voltage command to inverter, it is saturated on the basis of instantaneous DC bus voltage. And difference between regulator output voltage and motor command voltage is fed-back to integrator term. This topology is referred to as back-calculation scheme. It must be noted that saturation is applied after addition of compensation voltages.

Figure 3.3.1.1.1 shows complete model of synchronous frame PI current regulator with cross-coupling decoupling and anti-windup algorithm [23].

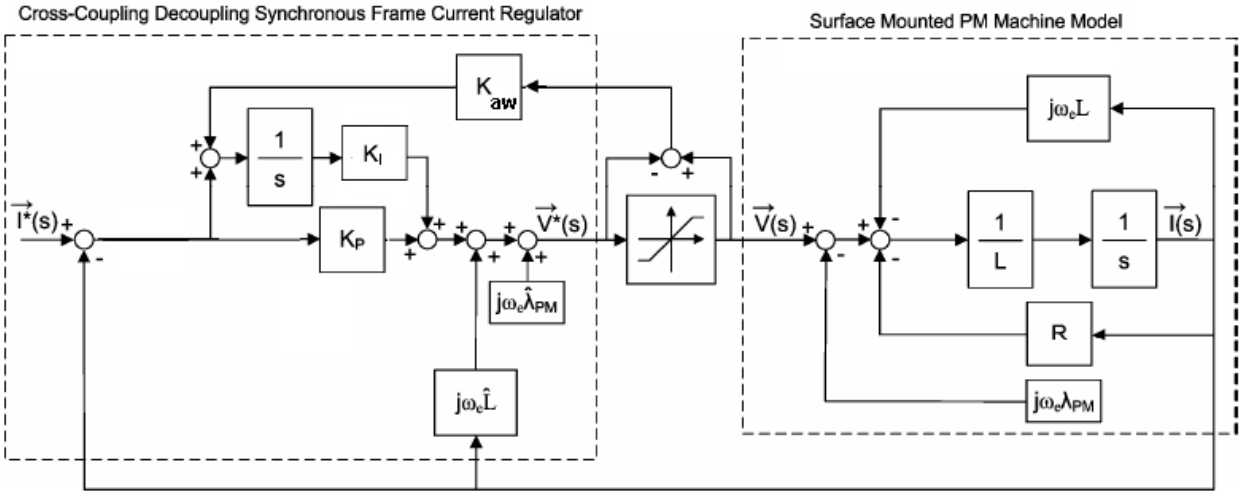

Figure 3.3.1.1.1: Synchronous Frame PI Current Regulator with Cross-coupling Decoupling and anti-windup scheme

For this scheme anti-windup gain is given by;

$$K_{aw} = \frac{1}{K_p} \qquad (3.3.1.1.1)$$

3.3.1.2 Saturation and Anti-windup Algorithm for Complex Vector Synchronous Frame PI Current Regulator

Anti-windup algorithm is almost same for complex vector synchronous frame PI current regulator. Figure 3.3.1.2.1 shown complex vector regulator along with anti-windup algorithm.

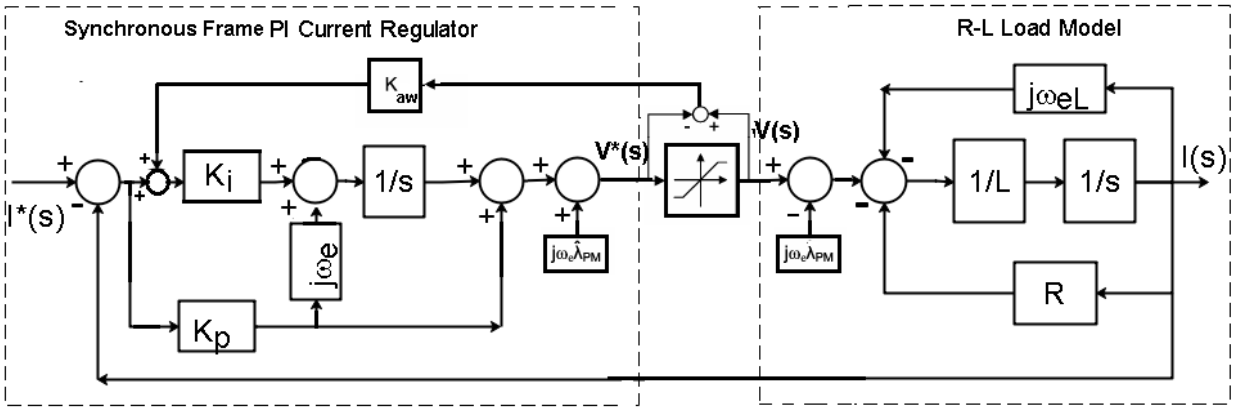

Figure 3.3.1.2.1: Synchronous Frame PI Current Regulator with Cross-coupling Decoupling and anti-windup scheme

Major difference comes here in calculation of anti-windup gain value [23], which is given by equation 3.3.1.2.1.

$$K_{aw} = \frac{1}{K_p} + \frac{j\omega_e}{K_i} \qquad (3.3.1.2.1)$$

3.3.2 Dead-time Compensation

As mentioned above, it is assumed that VSI is unity gain inverter but voltage saturation is a phenomenon which causes reduction of applied voltage and thus lower than expected speed or torque response in non-linear operation region of inverter. Apart from that, there are factors which hinder VSI to be unity gain converter even in linear region. Dead-time being one of those is discussed here and how its affect is compensated, is shown. It is also termed as volt-sec compensation.

A blanking time is introduced intentionally to avoid shootthrough of the DC-link. This blanking time will ensure that both switches in a leg will never be conducting at the same time. Figure 3.3.2.1 explains the idea where a-phase leg of inverter is shown switching from on-period to off-period for positive current.

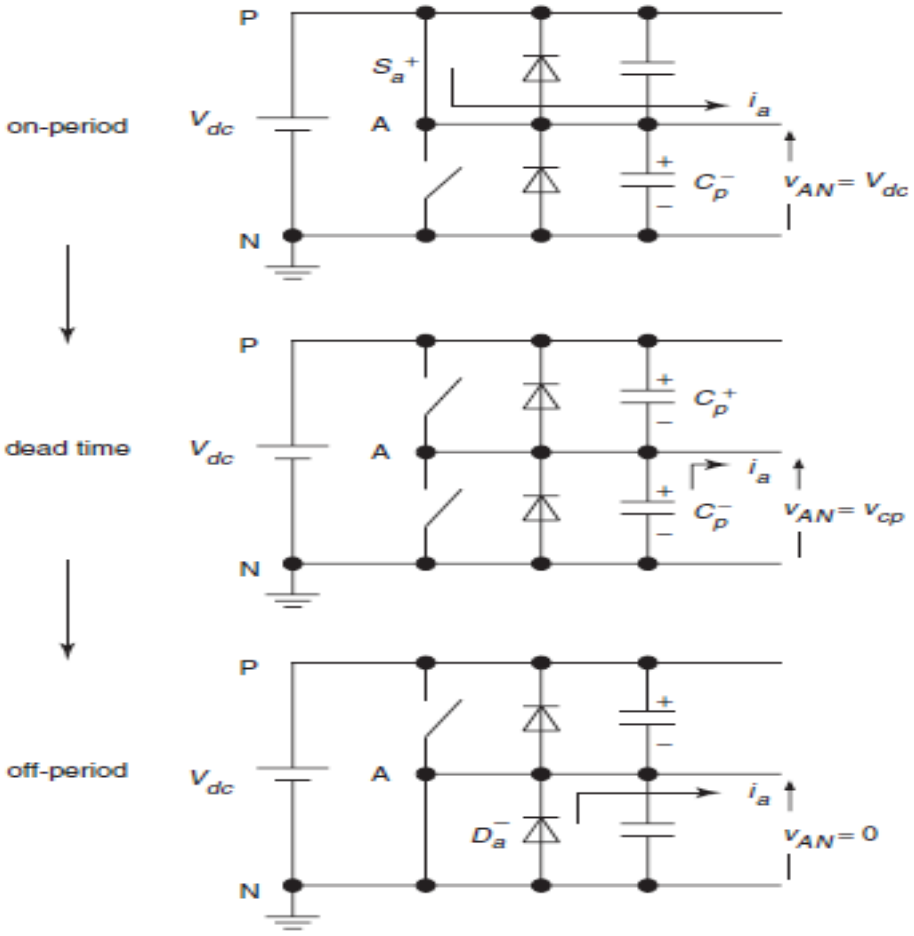

Figure 3.3.2.1: Transition of Phase-a leg from on to off Period for Positive Current

Parasitic capacitance is compulsory to be considered while taking inverter non-linear behavior into consideration. When upper switch is conducting, lower parasitic capacitor gets charged. During dead-time, lower parasitic capacitor gets discharged to make phase current flow and upper starts getting charged. So for this reason, during dead-time phase voltage is shown$V_{AN} = v_{cp}$, which is terminal voltage of lower parasitic capacitor [10].

For safe operation, introduction of dead-time is necessary but this causes waveform distortion and fundamental voltage drop. This voltage distortion increases with switching frequency. Consequently, resultant current supply will effect torque response of machine. Unsmooth operation of motor will cause noise and vibration. In context to this discussion, it can be said that volt-second compensation is necessary for improved performance. Dead-time compensation techniques rely on two basic parameters: magnitude of the volt-second lost during each PWM cycle and direction of current [11]. For each phase it is calculated as per equation 3.3.2.1.

$$\Delta V_{dt_a} = -\frac{T_{dt}}{T_{sw}} V_{DC} sign(i_a) \qquad (3.3.2.1)$$

Here V_{DC} is the DC-Link voltage, i_a is the phase-a current and T_{dt} is the dead-time introduced in PWM implementation. For all three phases, volt-sec compensation is calculated and added in respective phase voltage. This technique is most simple one but does not compensate for the distortions effectively because of inclusion of phase current sign. Parasitic capacitor causes clamping of current at zero crossing, so sign of phase current might be wrong and thus compensation might be fed wrong causing even worse behavior. This effect is studied in [10] and a way is introduced where compensation voltages are transformed into synchronous reference frame voltages and peak of d-axis compensation voltage is compared with peak of expected d-axis compensation voltage. If found higher, then phase current with minimal magnitude is detected and its sign is reversed from the originally determined sign. This correction of sign involves intensive calculations.

In [12], a technique is introduced to avoid involvement of sign of current for dead-time compensation. This strategy determines inverter output frequency in synchronous reference frame, angle of current vector from stationary reference frame to know the instantaneous sector (1-6) of reference current vector. Once sector is determined, compensation voltages are calculated in αβ reference frame as follows.

$$V_{\alpha}{}^{*} = \frac{4}{3} V_f cos\left[\frac{\pi}{3} Trunc\left(\frac{\left(\omega_e t + \theta^{*} + \frac{\pi}{6}\right)}{\frac{\pi}{3}}\right) - \omega_e t\right] \qquad (3.3.2.2)$$

$$V_{\beta}{}^{*} = \frac{4}{3} V_f sin\left[\frac{\pi}{3} Trunc\left(\frac{\left(\omega_e t + \theta^{*} + \frac{\pi}{6}\right)}{\frac{\pi}{3}}\right) - \omega_e t\right] \qquad (3.3.2.3)$$

Here, $V_f = \frac{T_{dt}}{T_{sw}} V_{DC}$, $\theta^{*} = \tan^{-1}\frac{I_q{}^{*}}{I_d{}^{*}}$ and ω_e is electrical angular frequency of synchronous reference frame. α and β denote transformed stationary reference frame coordinates. These voltages might be transformed into synchronous reference frame coordinates to make compensation or compensated directly if software already contains some stage dealing in stationary reference frame coordinates. Compensation voltages will look like the ones shown in figure 3.3.2.2, in synchronous reference frame coordinates.

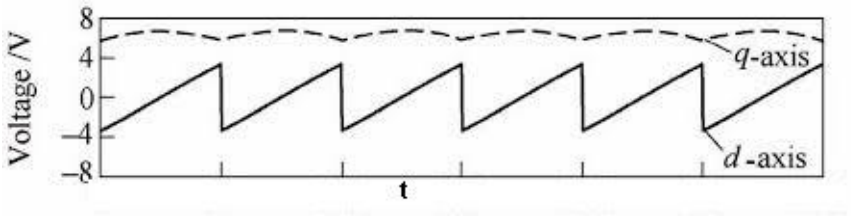

Figure 3.3.2.2: Compensating Signals for Proposed Dead-time Compensation Technique

Figure 3.3.2.3 theoretically proves that how volt-sec compensation, if made correctly, results in improved performance theoretically when represented in normal three phase coordinates.

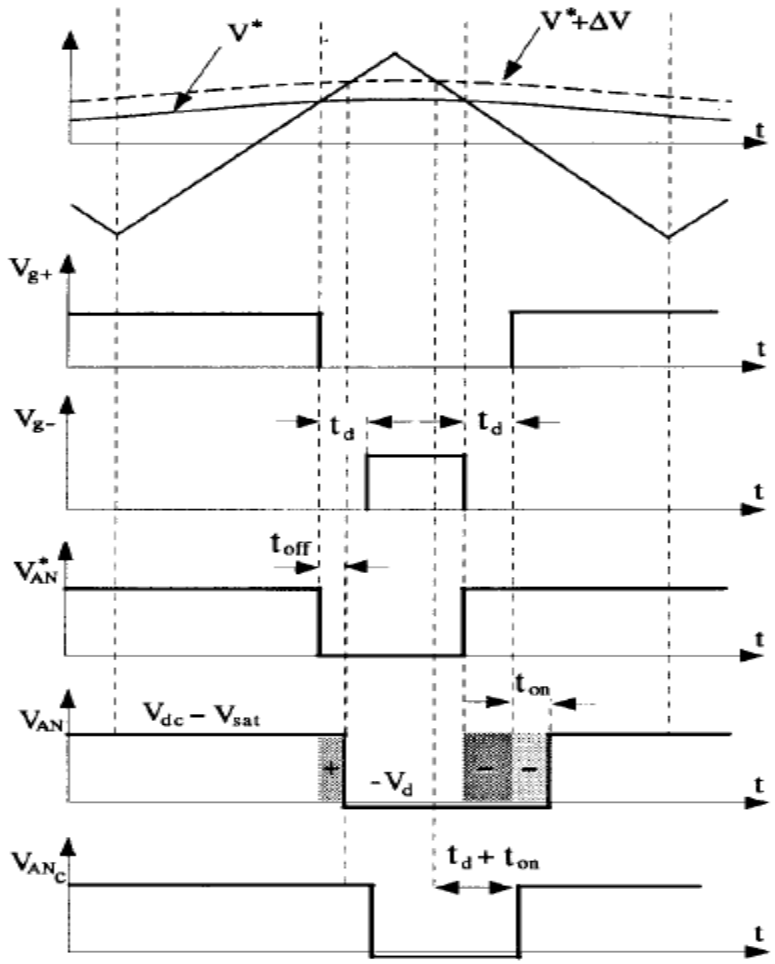

Figure 3.3.2.3: PWM voltage waveforms for positive current. From the top: reference voltages and carrier signal, gate voltage top device, gate voltage bottom device, commanded pole voltage before compensation, actual pole voltage before compensation, and actual pole voltage after compensation.

In figure 3.3.2.3, idealized waveforms of the PWM carrier signal and reference voltages, gating signals $V_g{}^+$ and $V_g{}^-$, ideal output voltage $V_{AN}{}^*$, actual voltage V_{AN} and actual voltage $V_{AN\,C}$ after dead-time compensation is shown. Turn-on and turn-off time of switches is also considered to draw actual voltage waveforms.

4. Speed Estimation Algorithms using Incremental Encoder

For closed loop speed and position control, it is desired to know velocity and position of the rotor of machine at each sampling instant. Generally position transducers are mounted on the rotor shaft which don't produce a velocity estimation. Addition of a separate speed transducer is costly and mechanically difficult. So signal processing and estimation techniques are used to calculate instantaneous velocity which is used as feedback signal for velocity control loop as well as for back-EMF compensation, cross-coupling decoupling and/or complex vector controller development in synchronous reference frame. In this chapter, different speed estimation algorithms are discussed and drawbacks associated with each technique are stated.

The least complicated method to estimate velocity is by measuring frequency of encoder pulses. In a defined time window, pulses are counted and discrete incremental ratio results speed estimation [15].

$$\omega_m = \frac{d\theta_m}{dt} = \frac{\Delta\theta_m}{T_{def}} = \frac{2\pi * \Delta N}{N_p * T_{def}} \left(\frac{rad}{s}\right) \qquad (4.1)$$

Here N_p is maximum pulse count in one rotation, T_{def} is defined time-window and ΔN is the number of pulses counted in the respective time-window. Lack of synchronization between time-window and encoder pulses will result significant errors [15]. Specially, at low speeds the result will have big oscillations showing unstable behavior. An alternative solution to reduce this measurement error is to select period measurement instead of frequency measurement. As name indicates, periods of a high frequency signals are counted within one or more encoder pulses. So

$$\omega_m = \frac{d\theta_m}{dt} = \frac{\Delta\theta_m}{n * T_{hf}} = \frac{2\pi}{N_p * n * T_{hf}} \left(\frac{rad}{s}\right) \qquad (4.2)$$

Here n is number of pulses of high frequency signal counted in only one period of encoder signal. Time period of this high frequency signal is given by T_{hf}. At very low speeds number of high frequency pulses might be quite high which can cause saturation of digital timer employed for measurement. Moreover, updated speed might not be available at each sampling period [15].

4.1 Luenberger Observer

Another technique, which is used very widely, is luenberger observer. This is closed loop observer which uses angle measurement from incremental encoder and applied/load torque feedback, if necessary. This observer results in position and velocity measurement.

Estimated position is compared with measured position to get controller input. Closed loop operation reduces sensitivity introduced because of measured parameters and noise. To apply this state estimation, mechanical model of the machine is developed. If model is given as;

$$T - T_L = J\frac{d\omega_m}{dt} + B\omega_m \qquad (4.1.1)$$

T and T_L are applied electromagnetic and load torque of the machine respectively. J and B being the total inertia and friction of the system and ω_m is the mechanical speed. The equation can be written in equivalent electrical parameters as well by manipulating mechanical variables with number of pole pairs appropriately. Inertia of the whole system is calculated experimentally and will be denoted as$\hat{J}$. It comprises inertia of motor under consideration, machine acting as load and connecting shaft. Friction is negligible so it is ignored to simplify the model and ease understanding. But it will be taken into account while tuning the controller so that order of the transfer function could be reduced. Estimated speed, position and all other parameters will be denoted as capped variables. Thus, closed loop observer structure is given in figure 4.1.1. This observer model is based on mechanical model concept presented in equation 4.1.1.

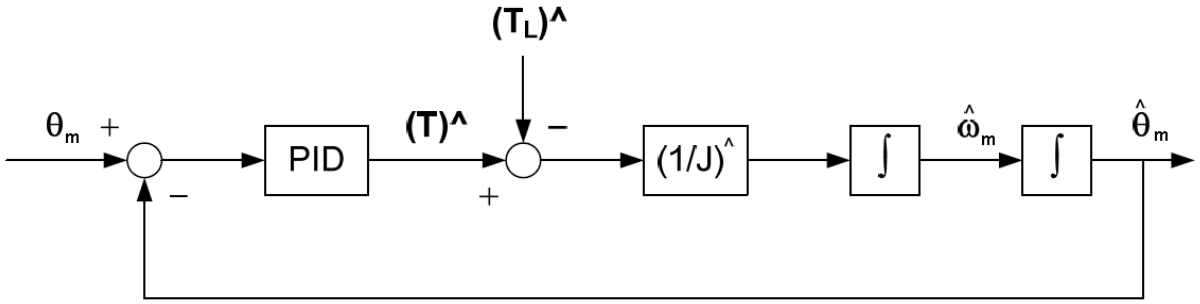

Figure 4.1.1: Block Diagram of a Closed-Loop Luenbeger Observer

PID controller gives electromagnetic torque as output. After manipulation with load torque and inertia of the system as per equation 4.1.1, speed is obtained. It is easy to get position from speed just by using integration function. This observer structure is getting load torque estimation $\hat{T}_L$ as feedforward which is quite hard to estimate. On the other hand, applied torque is easy to estimate from equation 2.3.2.1, either by using commanded currents or actual currents, when current regulator is able to keep current error zero. So a modified structure of observer will be as per figure 4.1.2.

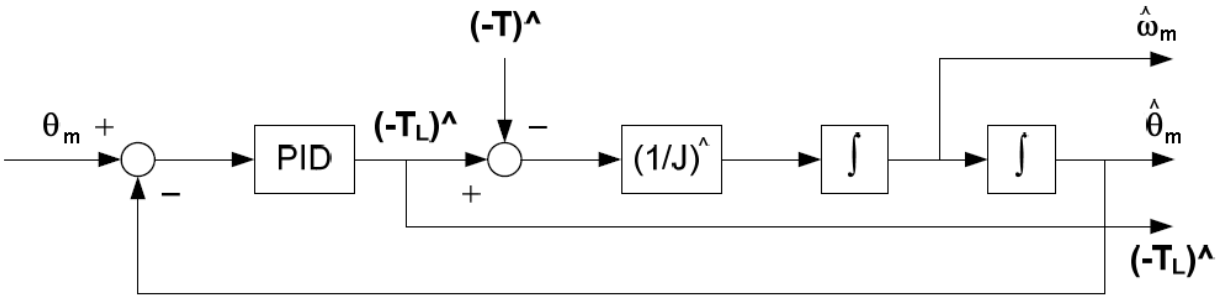

Figure 4.1.2: Block Diagram of a Modified Closed-Loop Luenbeger Observer

Signs of torques must be taken care of, to satisfy mechanical model equation. Load torque estimate is also available through this observer. The effect of the feedforward torque input to the observer is to guarantee that the observer will accelerate just like the motor when torque is applied. Thus, the velocity estimate from the observer does not require past position in order to adjust for the commanded acceleration made to actual system [17]. In other words, there will be no time lag in tracking the position input. This observer has good accuracy, resolution and bandwidth.

This kind of speed observer works very fine and tracks angle given from encoder. But for incremental encoder, assuming shaft is rotating with constant speed, counter value resets each cycle. So speed estimate will see very high negative or positive values each mechanical rotation for positive and negative motion direction respectively. As speed estimation is to be used for compensations in current controller, these unwanted glitches will cause problem because both q-axis and d-axis voltages will see overshoot and disrupt the normal operation. It refers that angle command to observer needs to be manipulated in some way so that speed estimation doesn't contain any unwanted content.

As compared to the conventional linear luenberger observer with scalar feedback, a vector tracking observer (VTO) can help resolve the problem. Apart from input signal, structure of the observer is maintained including tuning of the controller. Modified vector tracking observer is based on Phase Locked Loop (PLL) and shows no unwanted content in estimated speed. Though, estimated speed waveform might have very little oscillations as estimated mechanical parameters, used to develop controller, will not be exactly equal to actual parameters. First, idea of PLL will be presented leading to final observer structure and then tuning of observer in continuous as well as discrete-time domain.

4.2 Phase Locked Loop (PLL)

PLL [16] is a non-linear feedback system that tracks the phase of input signal. The basic PLL configuration contains three parts named phase detector (PD), Time-invariat linear loop filter and Voltage-controlled oscillator (VCO). Basic structure is shown in figure 4.2.1.

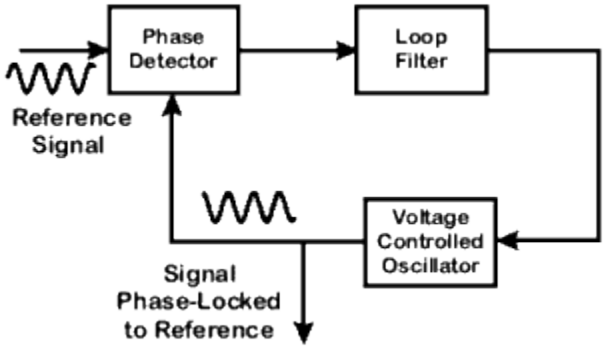

Figure 4.2.1: Basic Structure of Phase Locked Loop

Phase detector is the source of non-linearity in the PLL. It is usually an analog multiplier which produces an error signal that is proportional to the phase error or the difference between the phases of the input and output signals of the phase locked loop. Loop filter is low-pass filter which determines the dynamics of the loop by suppressing noise and unwanted PD outputs. Voltage-controlled oscillator generates a sinusoidal signal whose instantaneous frequency is dependent upon filter's output. A nonzero output voltage must be provided to VCO so it could tune its output frequency like that of input signal frequency, in case of phase error between two signals. Thus, PLL tracks the phase of input signal with some phase error. Which can be kept low by tuning the controller well and appropriate feed forward compensation as made for Luenberger tracking observer explained in section 4.1.

To elaborate the concept, let's say that θ_m is rotor position read through encoder and $\hat{\theta}_m$ is the variable storing position information obtained from observer. Phase detector will make cross product of sines and cosines of both position signals to determine error.

$$\sin(\theta_m - \hat{\theta}_m) = \sin\theta_m \cos\hat{\theta}_m - \cos\theta_m \sin\hat{\theta}_m \qquad (4.2.1)$$

If $\hat{\theta}_m \rightarrow \theta_m$, then $\sin(\theta_m - \hat{\theta}_m) \rightarrow (\theta_m - \hat{\theta}_m)$ and phase detector will be able to provide position error signal well. In case, the assumption $(\theta_m - \hat{\theta}_m) \rightarrow 0$ is invalid, within a full rotation, system will converge as demonstrated in figure 4.2.2.

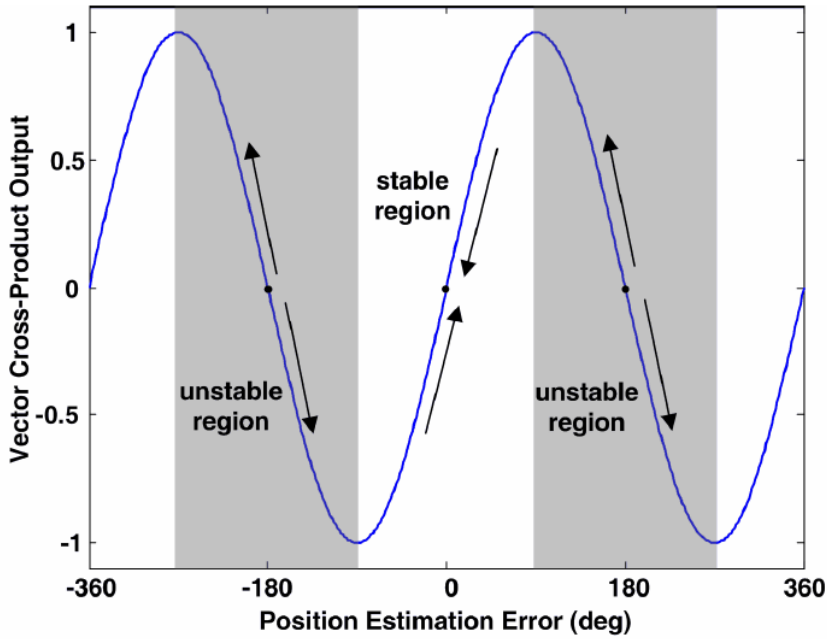

Figure 4.2.2: Vector Cross Product Output as a Function of Estimation Error and indicating Stability of PLL

Once the idea of PLL is clear, Vector tracking observer (VTO) can be built which will typically work on the same principle as that of PLL.

4.3 Vector Tracking Observer (VTO)

Structure of vector tracking observer is shown in figure 4.3.1. It consists of a phase detector like PLL which gives error signal to controller, tuned on the basis of dynamics controlled by mechanical system equation 4.1.1. Because a sinusoidal wave is to be tracked so a steady state error is most likely to exist. Addition of feedforward term and differential term to output can improve the behavior substantially as explained in Section 4.1. Addition of enhanced derivative term will make observer track the input position signal better, meanwhile it will introduce strong oscillations in speed estimation (enhanced speed estimate). While the speed before addition of enhanced derivative term will contain less noise, termed as unenhanced speed estimate.

Anyhow, the reason to move from linear, scalar input signal tracking device to non-linear, vector tracking device is justified. Now this type of modified input will resolve the problem of bumps in speed wave. Moreover, closed loop transfer function will be acting as low pass filter to make it replica of PLL.

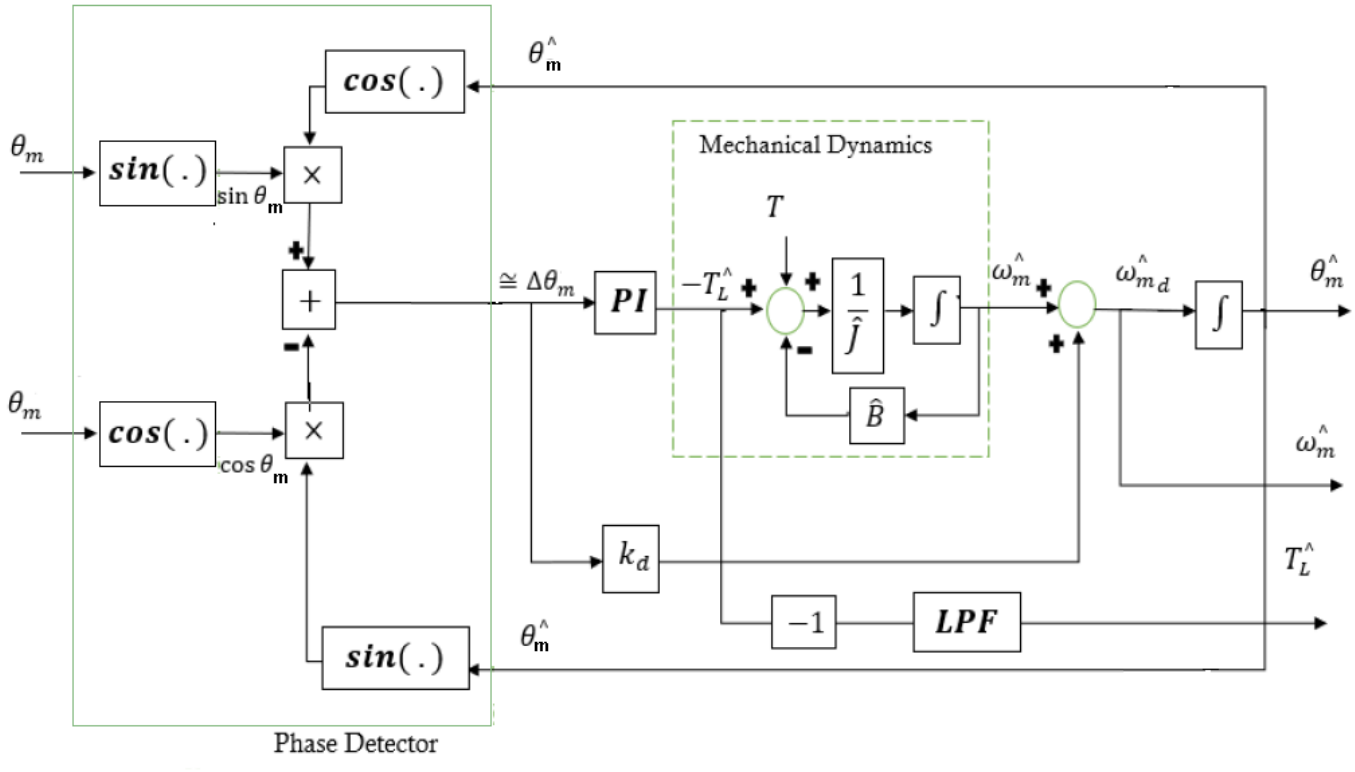

Figure 4.3.1: Block Diagram of Vector Tracking Observer

4.3.1 Design and Tuning of Vector Tracking Observer in s-domain

Basic simplified structure of VTO [17] is given in figure 4.3.1.1 to assist understanding and tuning. Non-Linear phase detector is ignored here as it does not contribute to tuning of observer.

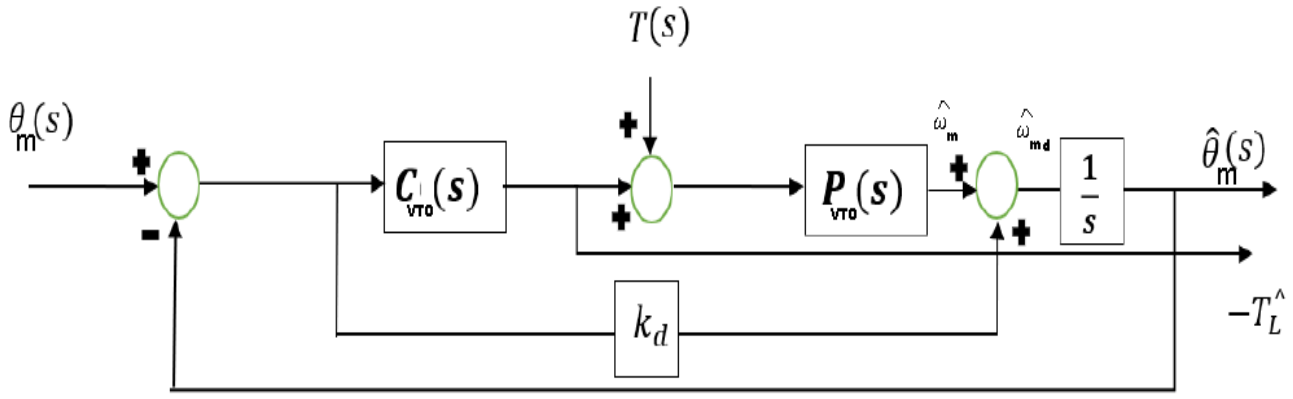

Figure 4.3.1.1: Structure of VTO in Continuous-time Domain

Same structure is expanded and shown in figure 4.3.1.2. It is to elaborate controller type, its gains and mechanical model of the machine.

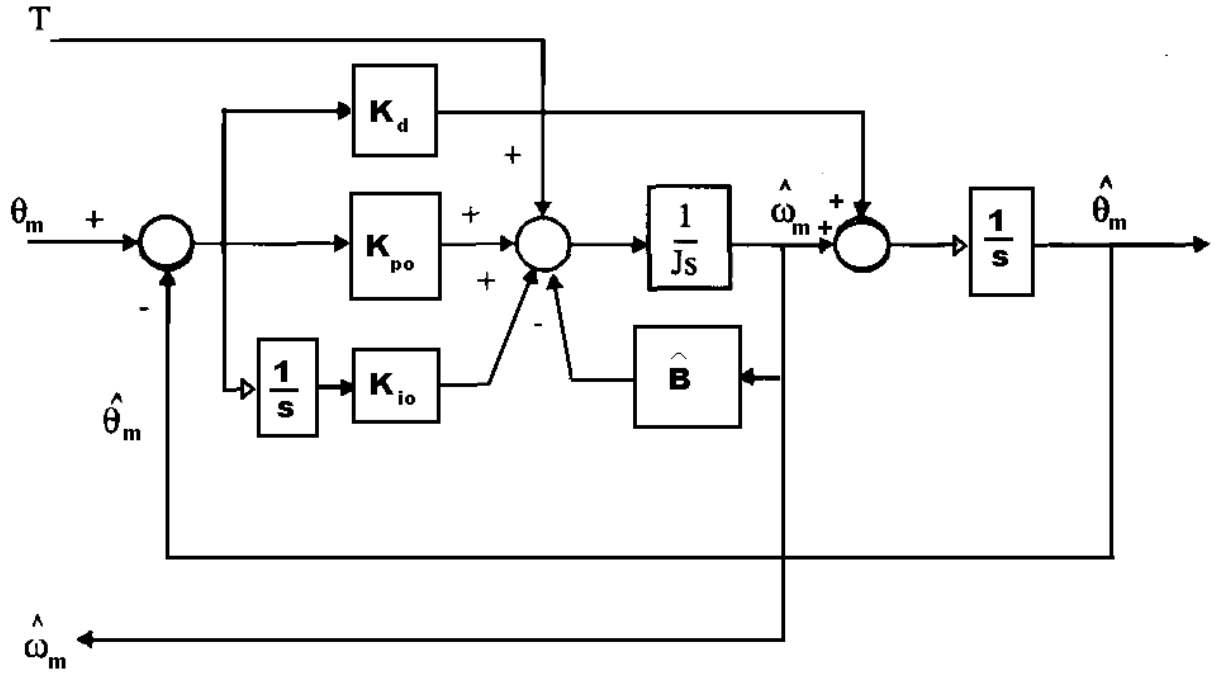

Figure 4.3.1.2: Expanded Structure of Position Observer in Continuous-time Domain

Controller is PI controller here and its transfer function is given as;

$$C_{VTO}(s) = K_{po} + \frac{K_{io}}{s} = \frac{K_{po}s + K_{io}}{s} = K_{io}\frac{\frac{K_{po}s}{K_{io}} + 1}{s} \qquad (4.3.1.1)$$

Mechanical plant model is given as;

$$P_{VTO}(s) = \frac{1}{\hat{J}s + \hat{B}} = \frac{\frac{1}{\hat{B}}}{\frac{\hat{J}s}{\hat{B}} + 1} \qquad (4.3.1.2)$$

Transfer function of mechanical model combined with PI controller is given as;

$$TF_{VTO}(s) = C_{VTO}(s) * P_{VTO}(s) = \frac{K_{io}}{\hat{B}}\frac{\frac{K_{po}s}{K_{io}} + 1}{s\left(\frac{\hat{J}s}{\hat{B}} + 1\right)} \qquad (4.3.1.3)$$

Here, one thing is to be highlighted that transfer functions related to current loop include 'i' and the ones related to speed observer are marked with 'vto'. To make zero-pole cancellation, gains can be chosen such as;

$$\frac{K_{po}}{K_{io}} = \frac{\hat{J}}{\hat{B}} \tag{4.3.1.4}$$

So mechanical model and PI controller transfer function reduces to;

$$TF_{VTO}(s) = \frac{K_{io}}{s\hat{B}}$$

Seen from figure 4.3.1.2, overall open loop transfer function becomes;

$$OLTF_{VTO}(s) = \frac{TF_{VTO}(s) + K_d}{s} = \frac{\left(\frac{K_{io}}{s\hat{B}} + K_d\right)}{s}$$

$$OLTF_{VTO}(s) = \frac{K_{io} + s\hat{B}K_d}{\hat{B}s^2} \tag{4.3.1.5}$$

Closed loop transfer function (CLTF) can be expressed as follows;

$$CLTF_{VTO}(s) = \frac{OLTF_{VTO}(s)}{1 + OLTF_{VTO}(s)} = \frac{\frac{K_{io}}{\hat{B}} + sK_d}{s^2 + sK_d + \frac{K_{io}}{\hat{B}}}$$

To choose gain values, closed loop transfer function will be compared with standard second order transfer function.

$$CLTF_{VTO}(s) = \frac{{\omega_n}^2 + s2\zeta\omega_n}{s^2 + s2\zeta\omega_n + {\omega_n}^2} = \frac{\frac{K_{io}}{\hat{B}} + sK_d}{s^2 + sK_d + \frac{K_{io}}{\hat{B}}} \tag{4.3.1.6}$$

Here ω_n is natural frequency of the system, which is related with bandwidth of the loop by the following relation.

$$\omega_n = 2\pi f_{BW\_VTO} \tag{4.3.1.7}$$

Bandwidth of the speed observer should be high enough to provide good disturbance rejection. But in this case, observer will tend to track any step change at the input reference which is not desired. Considering this aspect, bandwidth should be small enough to overcome any such undesired step change, allowing more disturbances to be injected into the system. By considering aforementioned situations, it can be concluded that a tradeoff is to be made by wisely choosing bandwidth [18].

To complete the controller design in s-domain equations 4.3.1.4, 4.3.1.6 and 4.3.1.7 can be used to calculate all three gains.

$$K_d = 4\pi\zeta f_{BW\_VTO} \tag{4.3.1.8}$$

$$K_{io} = 4\hat{B}\pi^2 {f_{BW\_VTO}}^2 \tag{4.3.1.9}$$

$$K_{po} = \frac{\hat{J}}{\hat{B}} K_{io} \tag{4.3.1.10}$$

4.3.2 Design and Tuning of Vector Tracking Observer in z-domain

Simplified closed loop vector tracking observer in discrete domain is shown below in figure 4.3.2.1. Expanded structure is not shown as PI controller and plant functions are same as shown in figure 4.3.1.2. Here, controller and plant will be driven in discrete domain as explained in section 3.1.2.

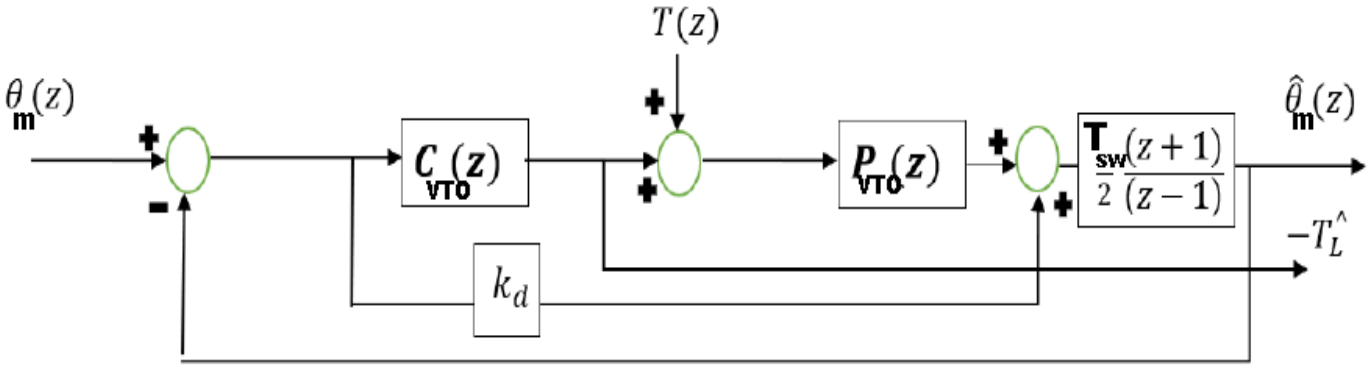

Figure 4.3.2.1: Structure of VTO in Discrete-time Domain

PI controller in z-domain can be written as;

$$C_{VTO}(z) = K_{po} + K_{io}T_{sw}\frac{z}{z-1}$$

$$C_{VTO}(z) = \frac{K_{po}z - K_{po} + K_{io}T_{sw}z}{z-1} = \frac{(K_{po} + K_{io}T_{sw})z - K_{po}}{z-1}$$

$$C_{VTO}(z) = (K_{po} + K_{io}T_{sw})\left(\frac{z - \frac{K_{po}}{K_{po} + K_{io}T_{sw}}}{z-1}\right) \tag{4.3.2.1}$$

Plant function for the observer can be derived using mechanical model equation and ZOH transfer function.

$$P_{VTO}(z) = (1 - z^{-1})\, Z\left\{\frac{P_{VTO}(s)}{s}\right\}$$

$$P_{VTO}(z) = (1 - z^{-1}) Z\left\{\frac{1}{s(\hat{J}s + \hat{B})}\right\} = \frac{1}{\hat{B}}\left(\frac{1 - e^{-1-e^{-\hat{B}/\hat{J}T_{sw}}/\hat{J}T_{sw}}}{z - e^{-\hat{B}/\hat{J}T_{sw}}}\right) \quad (4.3.2.2)$$

So transfer function containing PI controller and plant model becomes;

$$TF_{VTO}(z) = \frac{(K_{po} + K_{io}T_{sw})}{\hat{B}}\left(\frac{z - \frac{K_{po}}{K_{po} + K_{io}T_{sw}}}{z - 1}\right)\left(\frac{1 - e^{-\hat{B}/\hat{J}T_{sw}}}{z - e^{-\hat{B}/\hat{J}T_{sw}}}\right)$$

To simplify the expression, all constant terms can be lumped into one parameter. Let's say

$$\frac{(K_{po} + K_{io}T_{sw})(1 - e^{-\hat{B}/\hat{J}T_{sw}})}{\hat{B}} = K$$

So

$$TF_{VTO}(z) = K\left(\frac{z - \frac{K_{po}}{K_{po} + K_{io}T_{sw}}}{z - 1}\right)\left(\frac{1}{z - e^{-\hat{B}/\hat{J}T_{sw}}}\right) \quad (4.3.2.3)$$

To reduce the order of system and simplify the analysis, zero and pole can be cancelled by choosing appropriate gain values as shown in equation 4.3.2.4.

$$\frac{K_{po}}{K_{po} + K_{io}T_{sw}} = e^{-\hat{B}/\hat{J}T_{sw}} \quad (4.3.2.4)$$

Assuming that, we are successful to make exact zero-pole cancellation, equation 4.3.2.3 can be written as;

$$TF_{VTO}(z) = \frac{K}{z - 1} \quad (4.3.2.5)$$

But this transfer function does not include effect of derivative term, given directly to estimated unenhanced speed, and integral function to compute position. Over-all open loop transfer function can be computed as follows;

$$OLTF_{VTO}(z) = \left(\frac{K}{z - 1} + K_d\right)\left(\frac{T_{sw}}{2} * \frac{z + 1}{z - 1}\right)$$

$$OLTF_{VTO}(z) = \frac{(K + zK_d - K_d)(z + 1)T_{sw}}{2(z - 1)^2} \quad (4.3.2.5)$$

Closed loop transfer function is given as follows;

$$CLTF_{VTO}(z) = \frac{OLTF_{VTO}(z)}{1 + OLTF_{VTO}(z)}$$

$$CLTF_{VTO}(z) = T_{sw} \frac{K_d z^2 + Kz + (K - K_d)}{z^2(K_d T_{sw} + 2) + z(KT_{sw} - 4) + (2 + KT_{sw} - K_d T_{sw})} \quad (4.3.2.6)$$

To analyze poles of closed loop system, denominator polynomial must be examined. This second order polynomial will result two poles. Slower pole will dominate dynamic traits of the system.

5. Hardware and Software Setup

This chapter describes details about hardware used to accomplish the task and its interfacing. It discusses how different peripherals are configured to make them useful for drive control purpose and how signals are received and manipulated. Available hardware comprises of some definite structure and can't be changed, so first hardware setup will be discussed and then software algorithm will be developed so as to make the two compatible with each other.

5.1 Hardware Setup

Electric motors, DAC, oscilloscope, current sensor and power stage are major hardware components. Here, only relevant aspects, useful for development of control algorithm are detailed.

5.1.1 Electric Motors

For the complete experiment, two IPMSMs are used which are connected through a shaft. One is the motor to be controlled and other is working as load. Motor is equipped with incremental encoder. Motor electrical and mechanical parameters are given below.

Parameter	Value
Rated Current	3.6A (rms)
Voltage Constant	0.0598 Vs/rad
Resistance	2.44 ohm
Q-axis Inductance	7.52 mH
D-axis Inductance	5.6 mH
Pole Pairs	4
Torque Constant	0.45 Nm/A
Rotor Inertia	0.45e-4 kg/m²
Encoder maximum pulse count	10,000

Table 5.1.1.1: Characteristics of Electrical Motor and Encoder

Mathematical model of IPMSM is developed in chapter 2. Tuning of controller for available motor is discussed in chapter 3. Same theoretical concepts will be realized for experimental work.

5.1.2 HV Motor Control and PFC Kit

High Voltage motor control and Power Factor Correction (HVCntrl+PFC) kit [13], developed by Texas Instruments, is deployed which is a very versatile package. Macros of this kit are shown in figure 5.1.2.1 and only relevant elements are discussed in detail later on.

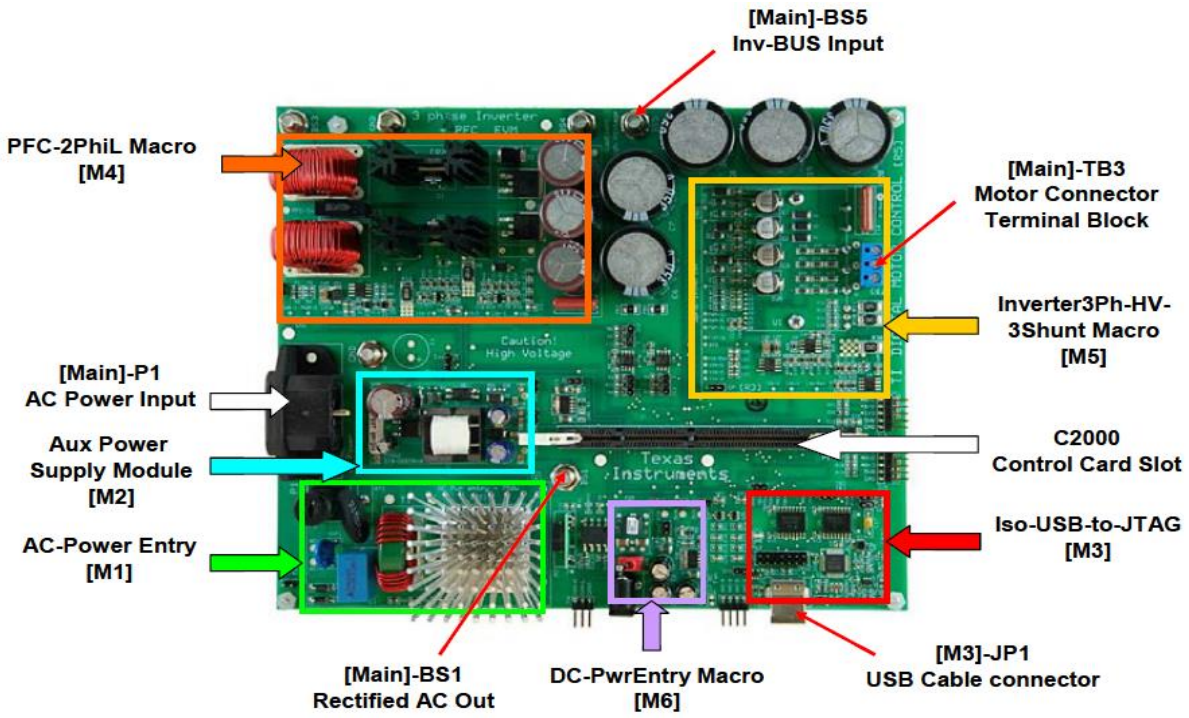

Figure 5.1.2.1: Layout of High Voltage Motor Control and PFC Kit

This kit consists of F28335 control card, high voltage DMC (digital motor control) board and an AC power cord. DMC board of the kit takes AC power input from main supply and rectifies it. This rectified voltage can be used for the input of Power Factor Correction (PFC) stage or used to power DC-link directly for inverter operation. PFC stage will increase the efficiency of the system, but this stage is ignored for experimental work of this thesis. DC-link serves as bridge between AC mains and three phase inverter. This kit includes necessary protection also to save the system in case of heavy inrush currents, short circuits or other faults. If power flow from main supply is higher than limit then mounted fuse (10A, 250V) serves its purpose. According to power requirements of the motor, fuse can be changed.

This kit has isolated CAN (controller area network) interface for communication over CAN bus. The CAN interface is isolated from the high voltages on the board using Texas Instruments ISO1050 isolated CAN transceiver with 4000V-Vpeak Isolation and Texas Instruments DCH01Series miniature 1W, 3kV isolated DC/DC converter module.

This kit allows interfacing of up to four DAC (digital to analog converter) chips to display system variables on oscilloscope. SCI (serial communication interface) interfacing is another option available. Using this kit, Quadrature Encoder Pulses (QEP) and Hall sensor output can be easily dealt with, to determine the speed and position of the rotor. This kit has allocated resources for both.

A heat sink is mounted underneath the board to the motor inverter and a DC fan is attached to this heat sink to increase airflow. This kit comprises of voltage and current sensors also. For this experimental work, we are using only three of the many sensors. Two phase currents and DC-Link voltage readings are read through Analog to Digital Converter (ADC). Signal conditioning circuit is also included on HV motor control and PFC kit to adjust amplitude of sensor signals as per ADC input requirements. How different signals are conditioned, is detailed in section 5.1.3. And how ADC is configured to read those signals, is detailed in section 5.2.2.

5.1.3 Signal Conditioning

5.1.3.1 Sensing and Conditioning of Phase Currents

As mentioned above, HV motor control and PFC kit includes all three phase current sensors. These sensors are mounted on the lower side of inverter legs. Figure 5.1.3.1.1 shows the placement of current sensors.

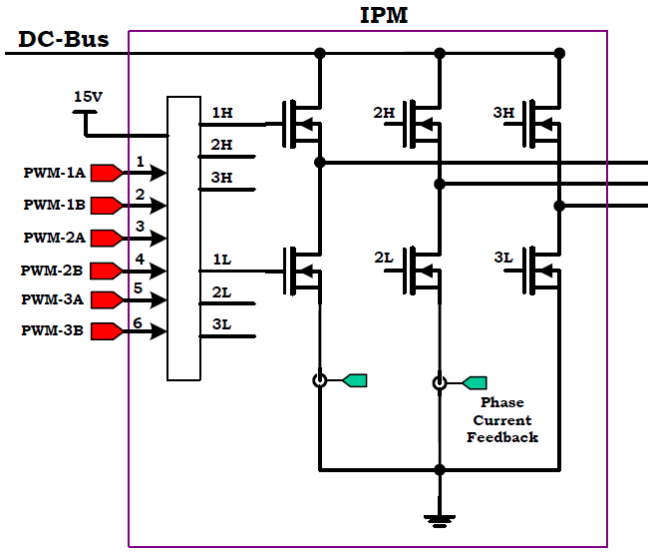

Figure 5.1.3.1.1: Placement of Phase Current Sensors on HVDMC and PFC Kit

In the diagram, only two phase current sensors are shown, while hardware has the capability to sense third one also. Nonetheless, it is important to mention here that we will also read two current feedback signals and compute third one. Because ADC reads signals in its natural sequence one by one and for control implementation, it is desired to read/sample all phase signals in once (detailed in section 5.2.1.2.2). So to make time lag as minimum as possible, mentioned strategy is used.

ADC module can read analog signal ranging from 0-3.3V. So to make all the possible actual values read for processing, they must be adjusted accordingly. This kit contains appropriate circuitry for the purpose which is shown in figure 5.1.3.1.2. This circuit is same for all current feedback signals so here it is shown only for one phase.

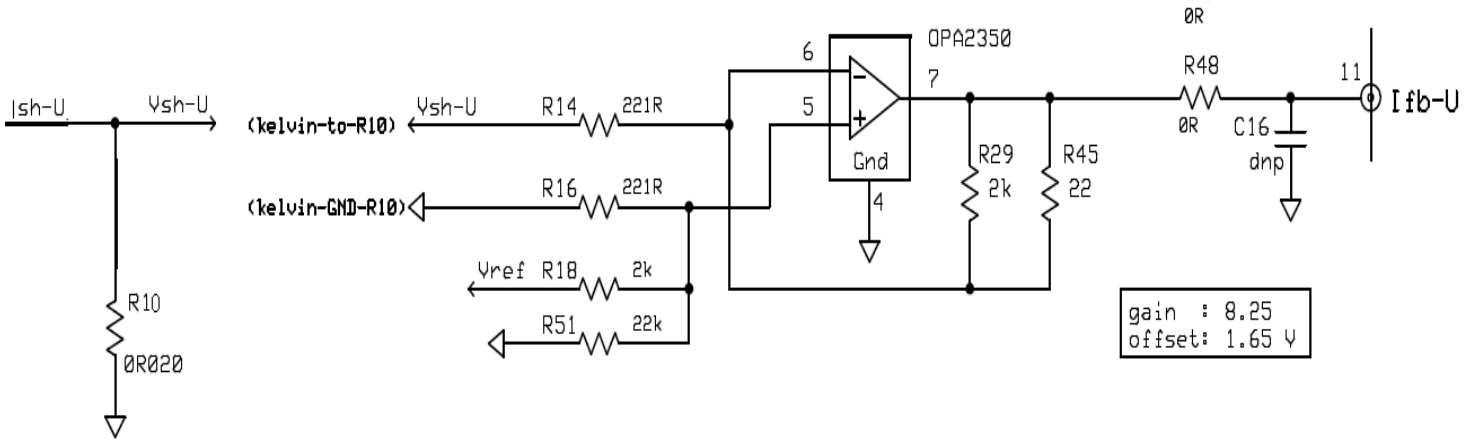

Figure 5.1.3.1.2: Signal Conditioning Circuit for Phase-Currents

As depicted in the diagram, current is transformed into voltage quantity. This will help improve sensitivity issues and further processing also becomes easier. Afterwards, it is amplified and given offset. If for phase current I_{sh}, ADC reads value I_{fb}, then realtion can be expressed as follows;

$$I_{fb} = I_{sh} * 0.02 * 8.25 + 1.65 \qquad (5.1.3.1.1)$$

Actual maximum current range for this setup is 10A so sensor-read or actual current and input to ADC or conditioned signal will be given as shown in figure 5.1.3.1.2.

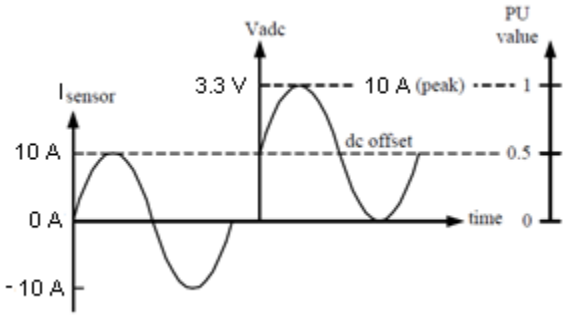

Figure 5.1.3.1.2: Phase Current Read using Sensor, Respective Input signal to ADC and its Per-unit Representation

5.1.3.2 Sensing and Conditioning of Voltages

As it is explained for current sensor feedback that signal conditioning is required. Likewise, voltage signals are to be adjusted to make them read using ADC module. For this work, only DC-link voltage is read. Kit contains three more voltage sensors to read phase voltages also.

Signal conditioning for voltages is simpler than current signals because it has only positive values. It refers that only scaling is required and not shifting. Circuitry for voltage conditioning is shown below in Figure 5.1.3.2.1.

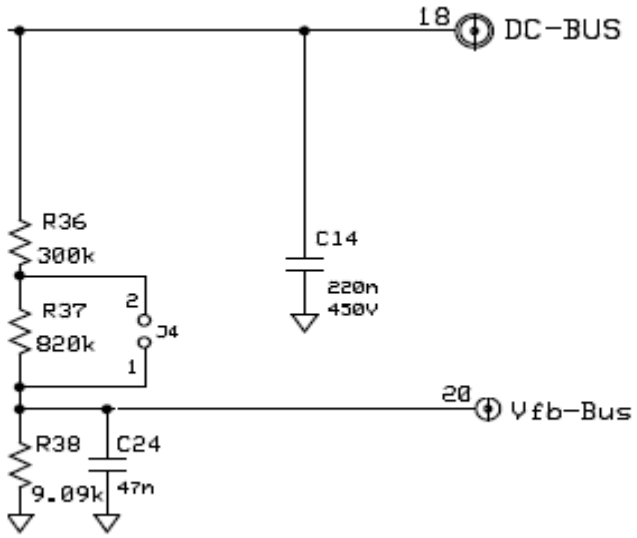

Figure 5.1.3.2.1: Signal Conditioning Circuit for DC-link and Phase Voltages

Jumper J4 shown in diagram, gives feasibility to change scaling factor. For our case, jumper is left open so actual DC-link voltage $V_{DC}$and feedback signal for ADC $V_{fb-Bus}$is related as given in equation 5.1.3.2.1.

$$V_{fb-Bus} = \frac{9.09k}{9.09k + 820k + 300k} V_{DC} \qquad (5.1.3.2.1)$$

Using this conditioning circuit, maximum voltage value of 410V can be read for processing purpose.

5.2 Software Setup

Once the necessary understanding of hardware tools is made, software setup can be made. Though, for configuring many peripherals. More information regarding hardware will be needed which can be mentioned at that same point to make the things clear.

Control algorithm is developed using PSIM add-on option. It generates C code from PSIM schematics. It requires user to mention hardware target. In the schematic, libraries from no other hardware target can be used except the selected one. This hardware can be set in SimCoder tab in Simulation Control block as shown in figure 5.2.1.

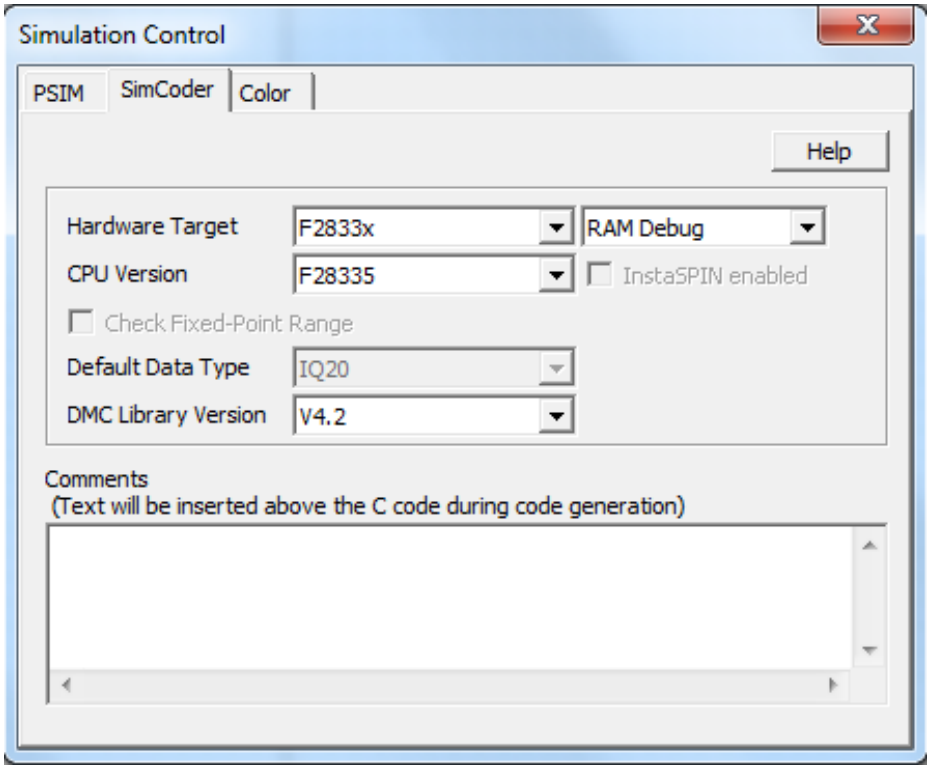

Figure 5.2.1: Hardware Selection to use SimCoder Tool

For the experiment, floating type hardware F28335 is used so appropriate choices are made to setup the project. RAM Debug mode offers easy debugging of schematic so it is chosen initially. Code compiled in release mode is faster than code in debug mode so later on one can switch to RAM Release and consequently to Flash Release or Flash RAM Release mode.

Before we proceed to form schematic, it is important to mention that C code can be generated only when system is developed in discrete domain. Any component which does not offer the option to be sampled on set sampling period, can't be compiled and will generate errors. For developing the complete schematic, elements from F2833x hardware targets are used mainly. Few elements from SimCoder library, which are hardware independent, are also used.

SimCoder also creates the complete project files for the TI Code Composer Studio development environment where the code will be compiled, linked, and uploaded to the DSP.

Complete software setup will consist of these three elements essentially;

1. Hardware and peripheral configurations
2. Determining real-time DSP signals
3. Development of control schematics

5.2.1 Hardware and Peripheral Configurations

5.2.1.1 Hardware Configuration

F28335 DSP has 88 GPIO ports (GPIO0 to GPIO 87), and each port may be configured for different functions but in one program one GPIO can serve only one functionality. Which functions, a specific port can serve, is listed in hardware configuration block. Hardware configuration block consists of list of all GPIO ports and all possible functions for them. If complete schematic consists of any peripheral blocks, using any function of GPIOs, respective option in hardware configuration block must also be set for the same GPIOs. For example, PWM123 is used to supply gating signals. GPIO ports 0-5 are associated with PWM123 so function of GPIOs will be decided through hardware configuration block as shown in figure 5.2.1.1.1.

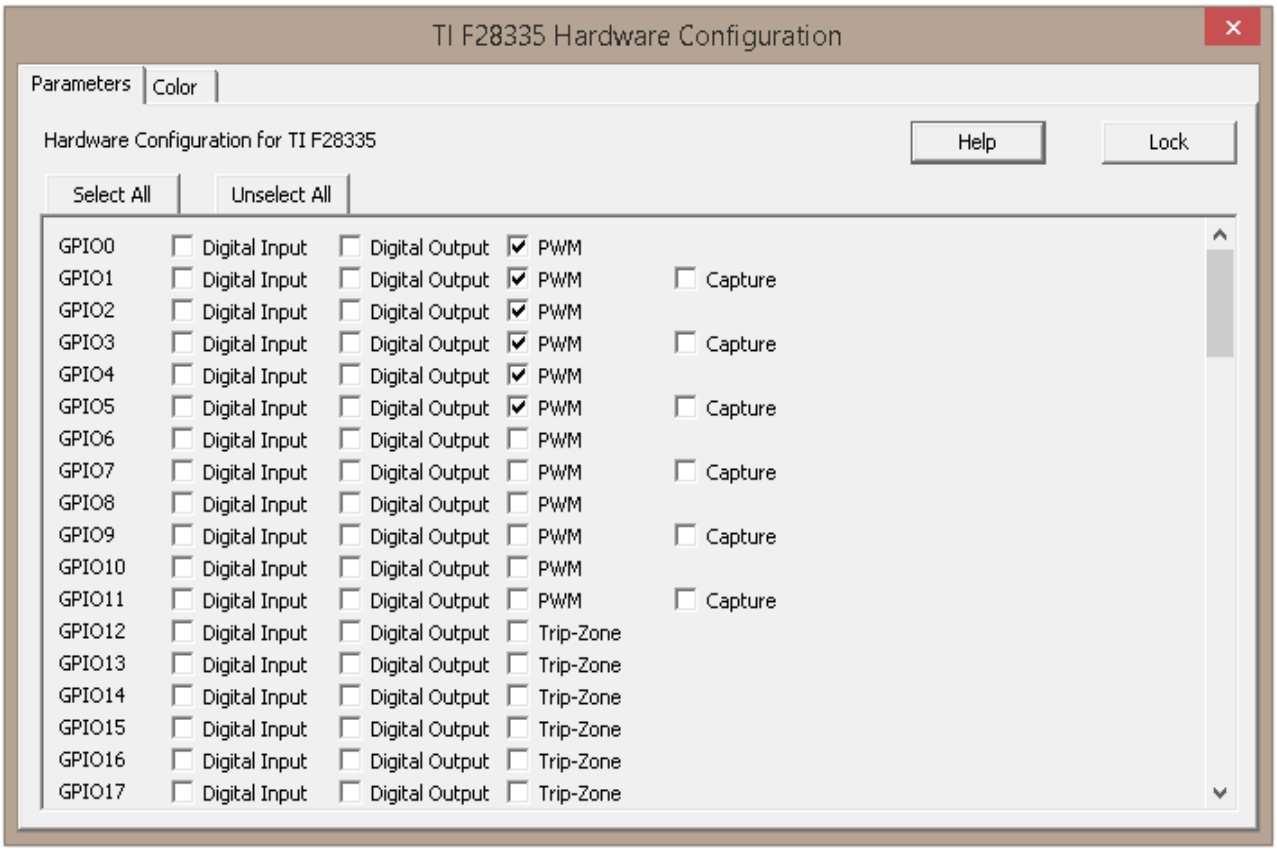

Figure 5.2.1.1.1: Hardware Configuration in SimCoder

5.2.1.2 Peripheral Configurations

SimCoder gives feasibility to use different processor peripherals in a convenient way. Only the peripherals, which are used in the control schematic, are discussed in this section.

5.2.1.2.1 Configuration of Pulse Width Modulator

The F2833x DSP provides 6 sets of PWM outputs: PWM 1 (GPIO0 and GPIO1), PWM 2 (GPIO2 and GPIO3), PWM 3 (GPIO4 and GPIO5), PWM 4 (GPIO6 and GPIO7), PWM 5 (GPIO8 and GPIO9), and PWM 6 (GPIO10 and GPIO11). Each set has two outputs that are complementary to each other. For example PWM 1 has a positive output PWM 1A and a negative output PWM 1B, except when the PWM operates in a special operation mode. All options for generation of PWM are discussed in [14]. For this thesis work, three phase PWM generator is used with PWM123. Figure 5.2.1.2.1.1 shows the configuration block for three phase PWM.

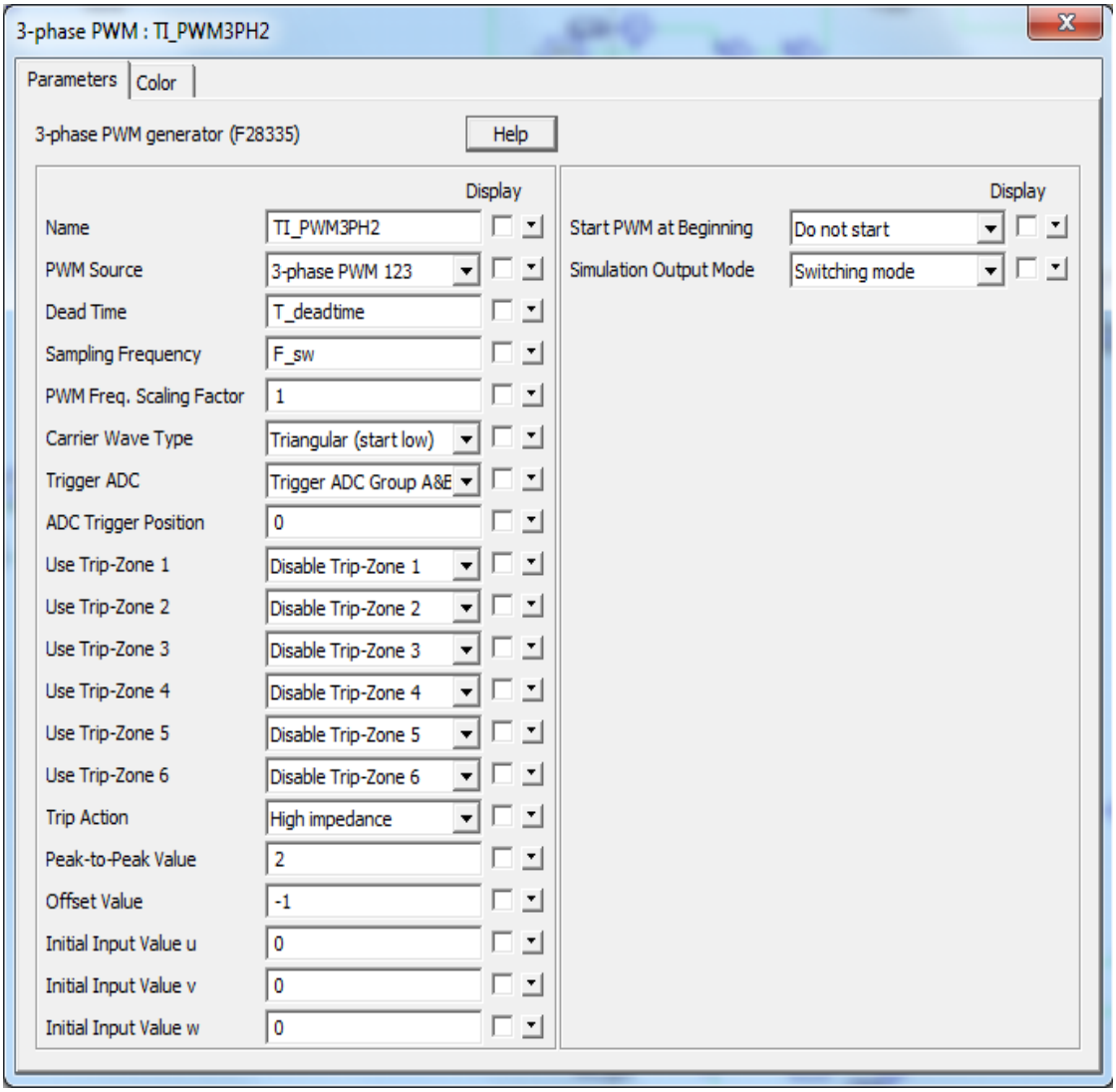

Figure 5.2.1.2.1.1: Configuration of Pulse Width Modulator

Starting from the very first entry in the block, it is mentioned, which PWM associated GPIOs will be operated through this block. If there is flexibility in utilization of hardware, then either PWM123 or PWM456 can be used. While using HV digital motor control and PFC kit, we are bound to use PWM123 as it is feeding 3-phase inverter embedded on the kit.

For safe operation, it is necessary to introduce appropriate dead-time as explained in section 3.3.2. Here, this time is given in seconds.

Sampling frequency, given in Hertz, determines how often duty cycle of PWM signal will be updated.

The scaling factor between the PWM frequency and the sampling frequency can be 1, 2, or 3. That is, the PWM frequency (the frequency of the PWM output signals used to control switches) can be multiples of the sampling frequency. For example, if the sampling frequency is 10 kHz and the scaling factor is 2, it means that the PWM frequency is 20 kHz. Switches will switch at 20 kHz, but the gating signals are updated once per two switching cycles at 10 kHz.

Carrier wave can be triangular or sawtooth wave. Both waves can be set to start from high or low level. This option combined with the sampling instant determines performance of the system as explained later in the same section.

ADC can be set to operate irrespective of PWM or any one group of ADC or both groups can be triggered by respective PWM. At what instant with respect to PWM wave, ADC will be triggered is determined by ADC trigger position. This value can vary from 0 to 1. For example, if ADC trigger position set to 0, ADC will read signals at the very start of PWM cycle. It should be ensured that ADC does not read signals at switching instants, because harmonics will be introduced and we will not be reading true average value of current specifically. If ADC reads signals at the instants when there are no harmonics, then filter for these signals can be skipped. This can be done by sampling currents at peaks of carrier wave. In settings above, PWM carrier wave, is made to start from low level. And sampling is done at 0 instant of carrier wave so average value is read through ADC.

F28335 DSP offers extra protection of system by introducing trip-zones to handle external faults, specific GPIOs are allotted for all trip-zones. A PWM generator can use any number of trip-zone signals and a trip-zone signal can be associated with any number of PWM generators. Anyhow, none of the trip-zones is used for this thesis work. If some trip action is taken, then switches of inverters are made to respond as per settings. In this case, if system is made to trip, then all switches will be opened instantaneously.

Carrier wave amplitude can be set according to maximum amplitude of reference voltage signals or per-unit values. Here per-unit implementation was easy so carrier wave ranges from -1 to 1.

Initially, all switches are desired to be open so all three inputs are set to zero.

It is necessary to have full control over the operation and PWM being the core element, need special attention. Considering this aspect, PWM block is kept un-activated unless a separate command is given through CCS window. So start and stop blocks are used to run and stop respective PWM block as shown in figure 5.2.1.2.1.2.

Which PWM source will be started and stopped from these blocks, is specified in PWM source option tab. Same input variable will activate one of these as NOT gate is used to give inverted logic state to both with respect to each other. One start-stop function can control only one PWM function generator.

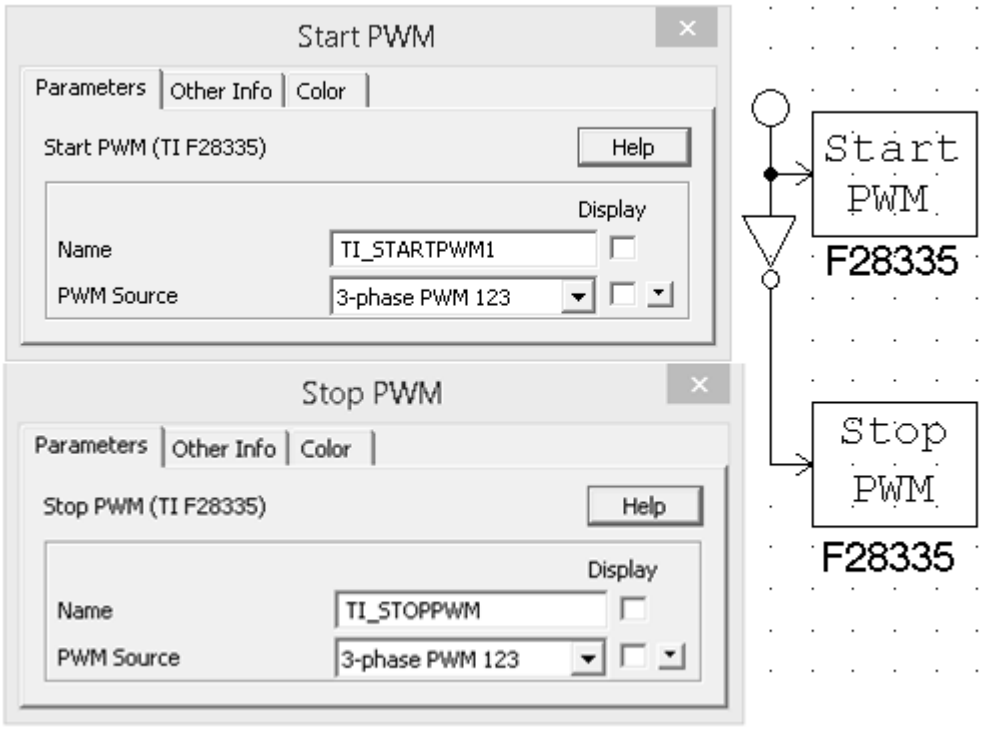

Figure 5.2.1.2.1.2: Controlling Generation of PWM using Start-Stop Command

5.2.1.2.2 Configuration of Analog to Digital Converter

The F28335 DSP provides a 12-bit 16-channel ADC which is divided into two groups A and B. the input range of A/D converter is from 0V to 3.3V. A/D converter is used in start/stop mode synchronized with PWM block, as mentioned in section 5.2.1.2.1. If there are more than one PWM blocks in schematic, only one is allowed to trigger ADC. All other PWM blocks must be set so they don't trigger ADC.

In section 5.1.3, it is detailed that all signals are conditioned to range from 0V to 3.3V so DC mode will be used. Gain is made unity to make the things simple. However, retrieving, actual DSP signal values from ADC is detailed in section 5.2.2.

In [13], it is detailed how ADC resources are allocated for different signals read from physical circuit. Here, we present some selective data in table 5.2.1.2.2.1.

Signal Name	ADC Channel No Mapping	Function
I_{fb-U}	ADC-B3, A1	Low side U-phase current sense

I_{fb-V}	ADC-B5, B1	Low side V-phase current sense
I_{fb-W}	ADC-A3, A5	Low side W-phase current sense
V_{fb-Bus}	ADC-A7	DC-link voltage sense

Table 5.2.1.2.2.1: Resource Allocation for ADC

ADC can't sample signals at its all channels in once. Instead, it starts from A0 and goes till A7 and then starts from B0 and goes till B7 one by one. For efficient vector control implementation, it is desired that all phase currents must be sampled at once. Moreover, two phase currents are enough to implement control. Because motor winding is wye configured without neutral so $I_U + I_V + I_W = 0$. If two currents are known, third one can be found.

So here an effort will be made to choose those ADC channels which receive their samples with minimum time lag. As it can be seen that each phase current sensor signal is hardwired with two ADC channels making the task easy. Considering all these aspects, we have selected ADC channel B3 and B5 to read phase U and phase V currents respectively.

For DC-link voltage, there is no such issue to be considered and it is read from ADC channel A7. Channel selection is made clear in figure 5.2.1.2.2.1.

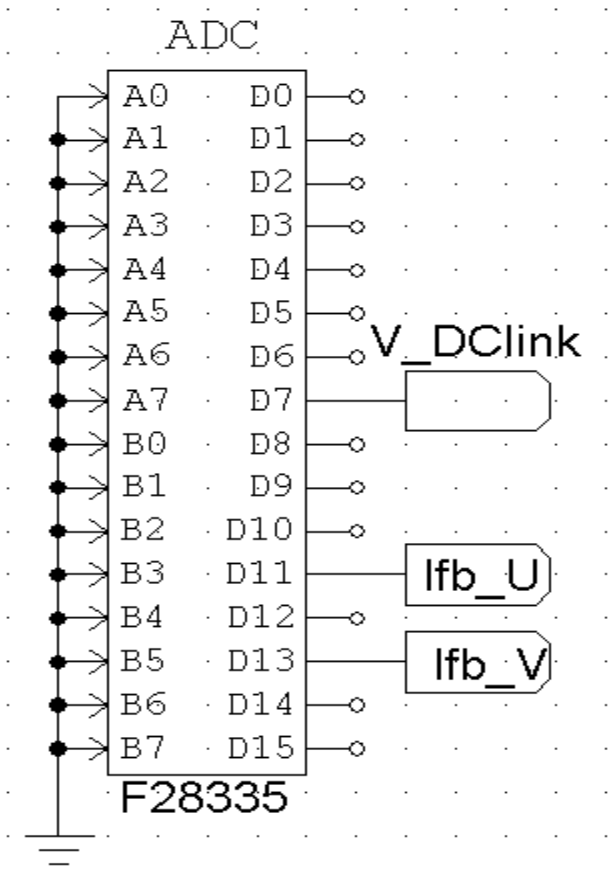

Figure 5.2.1.2.2.1: Receiving Conditioned DSP Signals at Allocated ADC outputs

It is to be made clear that all input pins of ADC channels must be grounded in schematic to avoid errors.

5.2.1.2.3 Configuration of Encoder

The F2833x DSP has two options for encoder interfacing. Encoder 1 can be at either Port GPIO 20-21, or Port GPIO50-51. Encoder 2 is at Port GPIO24-25. It is important to mention that Encoder 1 at Port GPIO20-21 and at Port GPIO50-51 uses the same inner function blocks, and cannot be used at the same time.

In section 1.1.2, it is explained that to make the direction read, slots of two tracks are in quadrature. Apart from that there is one zero mark. Mapping same concept in software, the eQEP (enhanced quadrature encoder pulse module) inputs include two pins for quadrature-clock mode or direction-count mode, an index (or 0 marker), and a strobe input. However, either index mark or strobe input is used to latch the encoder's initial position. Figure 5.2.1.2.3.1 shows encoder block configuration and relevant schematic.

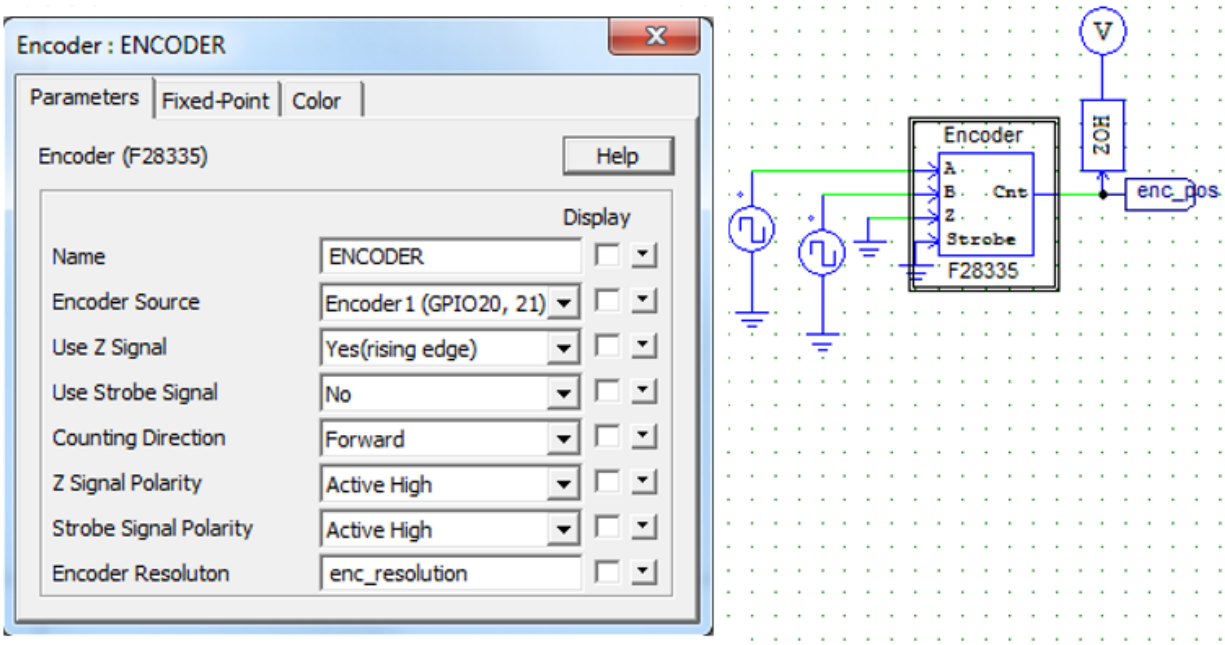

Figure 5.2.1.2.3.1: Configuration and schematic for Encoder Interfacing

In schematic, all inputs ports of encoder block must be given some signal. Or they must not be in the floating state. Here, A and B pins are given square waves similar to signals generated by actual encoder. And zero mark and strobe signals are grounded. Encoder block gives encoder position in integer numbers ranging from 0 to maximum pulse count of encoder. This count is referred to as encoder resolution in configuration block. This resolution is four times the number of lines on A or B row as explained in section 1.1.2.

This encoder is using encoder 1 resources. Z signal is used to latch encoder position at its initial state at its rising edge. And motor running in anti-clockwise direction will cause encoder

reading to go in forward direction. Z signal polarity is chosen to be high because in mounted encoder, inner track is solid with just one slit. This slit makes zero signal high once in a complete rotation.

Encoder resolution being the most important one, determines if angle is read correctly or not. If it is set to 0 then encoder counter will keep on counting and will not reset. But if the resolution is set to 200, for example, counter will start from 0 and count up to 200 and reset to zero. It should be verified that in one mechanical rotation, encoder counter must reset only once. And this reset point must be met with zero signal.

5.2.1.2.4 Configuration of Serial Communication Interface (SCI)

The F28335 DSP provides the function for serial communication interface (SCI). Through SCI, data inside the DSP can be transferred to a computer using an external RS-232 cable. PSIM also provides all the necessary functions to transmit and receive data on both the DSP and computer sides, and to display the data on the computer using its easily configurable DSP oscilloscope. This provides a very convenient way to monitor, debug, and adjust the DSP code in real time. SCI configuration block is used to make settings for SCI and SCI input and /or SCI output block is used to receive signals on computer or give commands in run-time. Figure 5.2.1.2.4.1 shows SCI configuration block with settings made for this work.

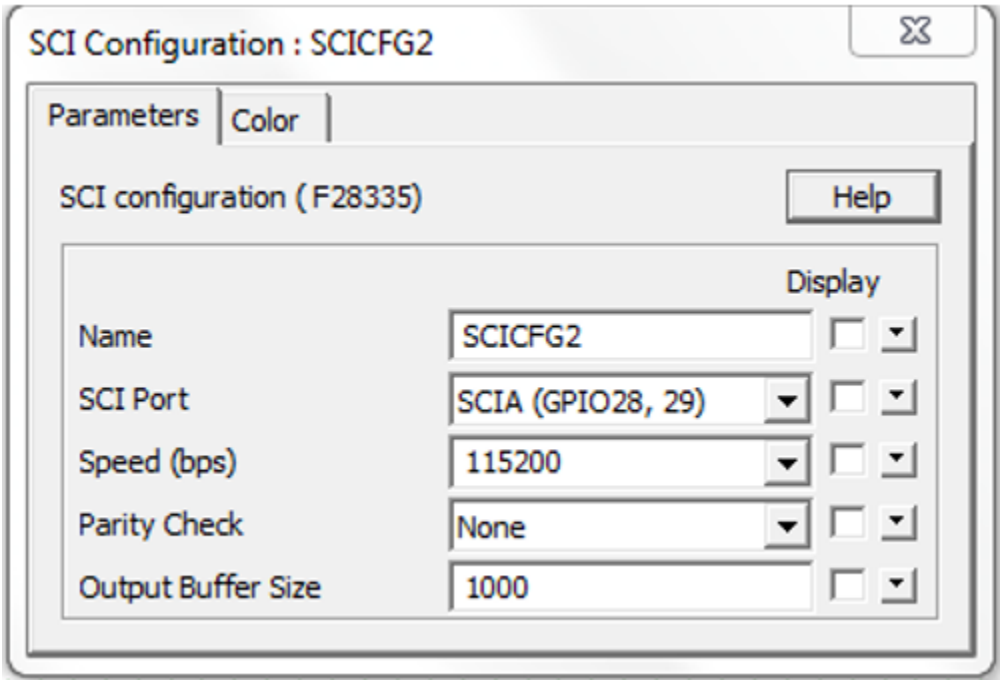

Figure 5.2.1.2.4.1: Configuration of SCI in SimCoder

There are 7 sets of GPIO ports that can be used for SCI detailed in TI provided manual specified for SCI. Any set of ports can be used, but it must be kept in mind that these GPIOs must not be used for any other purpose. There are various options for SCI communication speeds in bps (bits per second). Here 115200 bps is chosen. If any error check for transferred data is needed,

it can be made in parity check select box. Buffer for SCI is allocated in RAM area of DSP. Each buffer has capability to store one data point which consists of three 16-bit words. Buffer size should be large enough, in order to collect more data points especially if large number of variables is being observed in DSP oscilloscope. But internal DSP memory is limited so very large buffer size might cause interference with normal DSP operation. Thus a trade-off is to be made here and buffer size should be chosen carefully.

It must be noted that either command can be given through SCI input variable using DSP oscilloscope in PSIM or through watch window in CCS. Both can't be used together. Deactivating SCI blocks in PSIM schematic will automatically enable variables in watch window, if relevant expressions are already added.

5.2.1.2.5 Configuration of Serial Peripheral Interface (SPI)

By using the SPI blocks in the TI F833x Target library, one can implement the function to communicate with external SPI devices (such as external A/D and D/A converters) easily and conveniently. It is another alternative to SCI so DSP signals could be displayed on actual oscilloscope. For the thesis work, SPI is configures for DAC. Configuration depends upon DAC chip used.

For this experimental setup, AD7568 is used which contains eight 12-bit DACs in one monolithic device. The DACs are standard current output with separate $V_{ref}, I_{OUT1}, I_{OUT2}$ and R_{FB} terminals. It is a serial input device. Data is loaded using $\overline{\text{FSIN}}$ (Frame synchronization signal for input data), CLKIN (data is clocked into input shift register on falling edges of CLKIN) and SDIN (serial data input). One address pin, A0, sets up a device address, and this feature may be used to simplify device loading in a multi-DAC environment.

All DACs can be simultaneously updated using the asynchronous $\overline{LDAC}$ (load DACs) input and they can be cleared by asserting the asynchronous $\overline{CLR}$ (clear DACs) input.

The device accepts a 16-bit word. The first bit (DB15) is the DAC MSB (most significant bit), with the remaining bits following. Next comes the device address bit, A0. If this does not correspond to the logic level on pin A0, the data is ignored. Finally come the three DAC select bits. These determine which DAC in the device is selected for loading. DSP signals, to be displayed are connected with SPI output device and DAC number is put to display the data on respective channel ranging from 0 to 7.

To configure SPI using PSIM, there are two blocks named SPI configuration block and SPI device. They are connected as shown in figure 5.2.1.2.5.1.

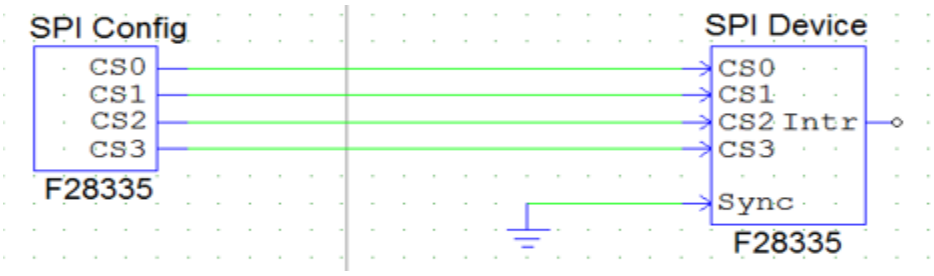

Figure 5.2.1.2.5.1: Connecting SPI device with Configuration Block to Retrieve Respective Configuration Setup

How these blocks are set, is shown in figure 5.2.1.2.5.2.

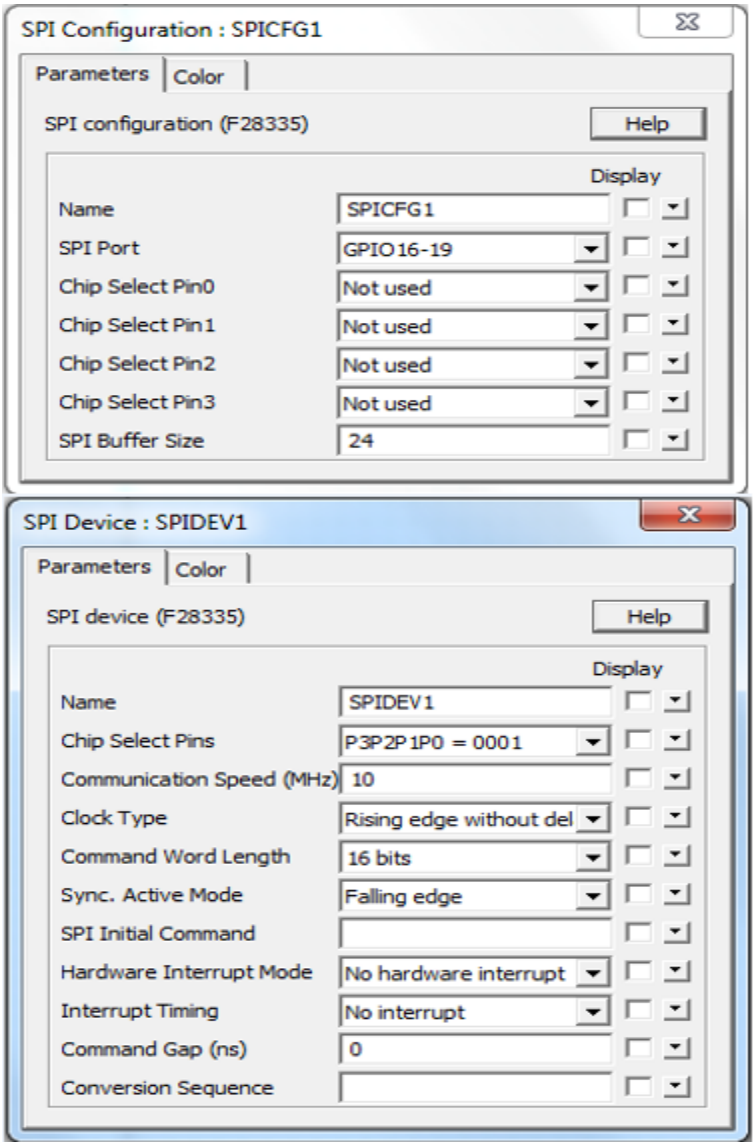

Figure 5.2.1.2.5.2: Configuration of SPI Device

In this experiment, only one chip is used so chip select pins are not used. This option needs to be set for multi-chip environment. Chip select pins of SPI configuration block will be connected with SPI device block to make sure that settings made, are for respective device. Which ports will be used for communication of data for connected device, is set in configuration block. Buffer size is chosen such as data is not lost for any channel of device and DSP function doesn't get affected as explained in section 5.2.1.2.4 for SCI.

AD7568 clock frequency is 10MHz and word length is 16 bits as explained above. It synchronizes its data on falling edge and receives on rising edge of clock without any delay. Chip select pins are not serving any purpose here. Our connected device has eight channels. So eight DSP signals can be displayed simultaneously using eight SPI output devices.

DSP signal will be connected with SPI output device and mentioned in its settings, which channel will display this signal as shown in figure 5.2.1.2.5.3.

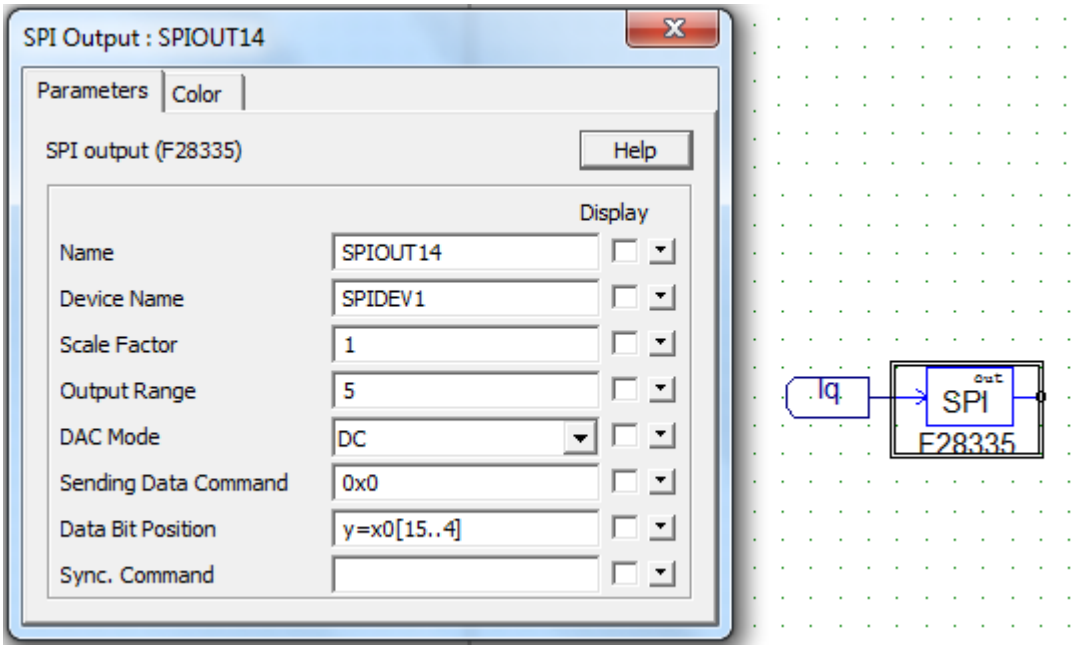

Figure 5.2.1.2.5.3: Setting SPI output to display Real-time DSP Signal

This SPI output device is using settings of SPI device SPIDEV1 of figure 5.2.1.2.5.2 so it is mentioned in device name block. Signal is communicated without using any scaling. DAC devices usually have maximum output range of 5V. This must be mentioned that if signal, to be displayed, has negative values or amplitude higher that 5V then its amplitude must be shifted and scaled to bring it to display range of DAC. Channel '0' of DAC chip will display the signal so channel number is specified in sending data command option. As mentioned above, for this DAC device, word is formed with 12 most significant bits being the data bits. Which part of the word, this DSP signal will constitute for, is specified in data bit positions. Synchronization command is same as that of respective device so it is left empty.

5.2.2 Determining Real-time DSP Signals

Once all peripherals are set and necessary understanding regarding signals received from hardware is made, we can proceed to process signals coming from encoder and ADC module. It is to be kept in mind that all the mentioned signals are either conditioned in hardware or are providing indirect information like that of encoder. Following section is about retrieving actual DSP signals.

5.2.2.1 Determining DC-link Voltage

In section 5.1.3.2, it is detailed how DC-link voltage is modified to be fed to ADC module. In order to develop control algorithm, real DC-link value is calculated using equation 5.2.2.1.1 which is a modified form of equation 5.1.3.2.1.

$$V_{DC} = \frac{9.09k + 820k + 300k}{9.09k} V_{fb-Bus} \qquad (5.2.2.1.1)$$

Here, V_{DC} is actual DC-link voltage and V_{fb-Bus} is scaled DC-link voltage received through ADC.

5.2.2.2 Determining Phase Currents

Exactly the way, actual DC-link voltage is computed, Phase currents will be determined using equation 5.2.2.2.1.

$$I_{sh} = \frac{I_{fb} - 1.65}{0.02 * 8.25} \qquad (5.2.2.2.1)$$

I_{sh} is actual phase current and I_{fb} is conditioned phase current as described in section 5.1.3.1. Once actual U and V phase currents are calculated, W phase current is calculated as per figure 5.2.2.2.1.

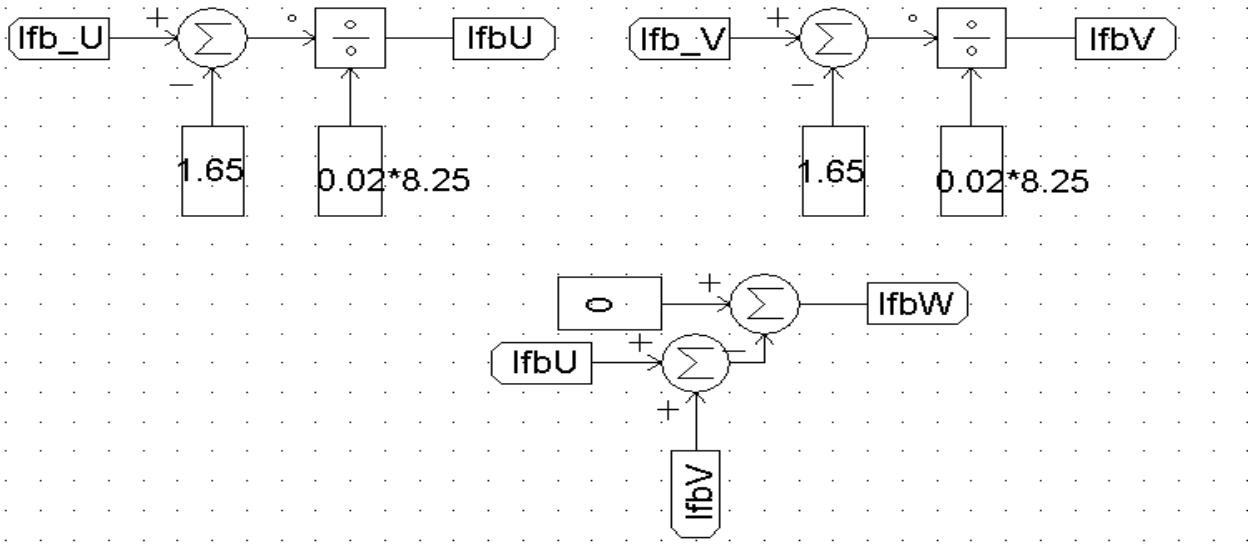

Figure 5.2.2.2.1: Schematic to Get Actual Phase Currents

5.2.2.3 Determining Mechanical and Electrical Angle of Rotor

From encoder counter reading mechanical angle can be obtained directly using encoder resolution. As it is explained that for one complete mechanical rotation, counter reading goes until maximum pulse count of encoder which is referred to as encoder resolution in SimCoder encoder block. To keep the whole setup synchronized, this terminology will be followed. Encoder output manipulated with appropriate gain results mechanical angle as shown in figure 5.2.2.3.1.

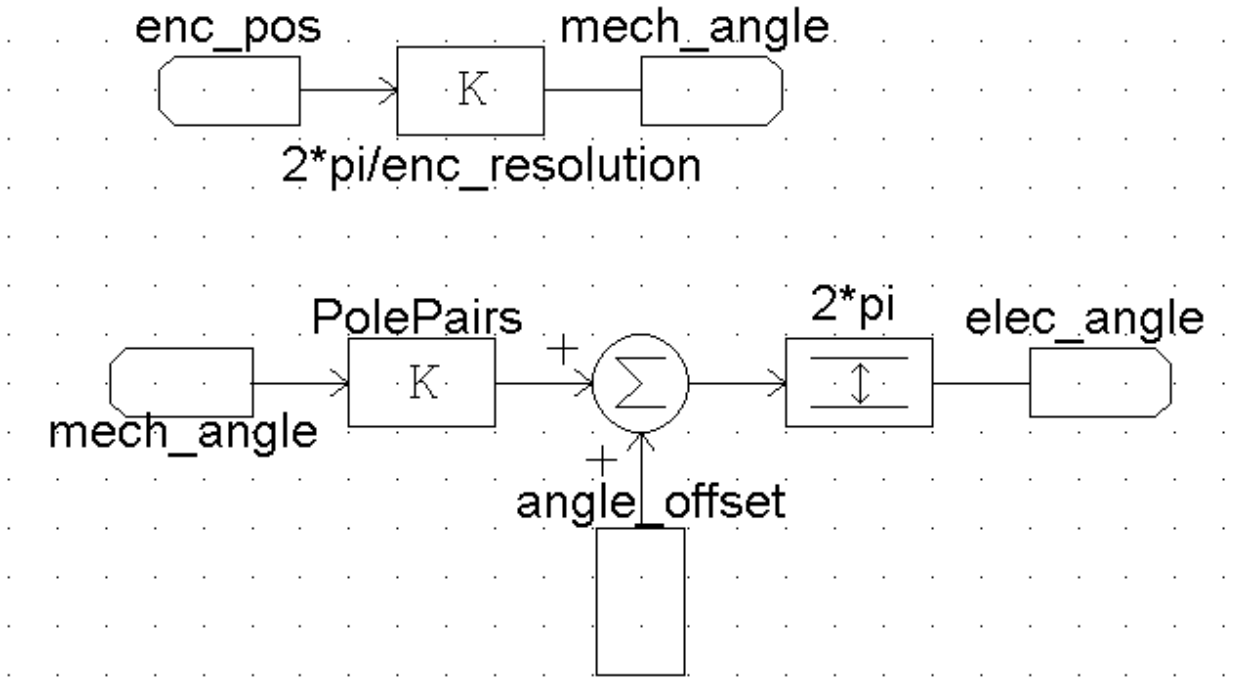

Figure 5.2.2.3.1: Schematic to Calculate Rotor Mechanical and Electrical Angle from Encoder Reading

Electrical and mechanical angles are related to each other by number of pole pairs as explained previously in chapter 2. Apart from that, difference in position between zero mark of encoder and rotor quadrature axis is discussed in section 1.1.2.1. Offset angle is calculated in section 6.1.5 through experimental setup. Considering all these aspects, electrical angle is also calculated in the schematic shown in figure 5.2.2.3.1.

For calculation of electrical angle range limiter is also used which resets to its lower limit 0 after reaching it upper limit 2π. Even if this limiter is removed, system will work well.

5.2.2.4 DSP Currents in Synchronous Reference Frame

To develop field oriented control, q and d-axis currents need to be calculated using phase currents and electrical angle as explained in section 2.2. PSIM has in-built block for axis transformation, but for the sake of better understanding and to comply with theoretical concepts, axis transformation is done as shown in figure 5.2.2.4.1.

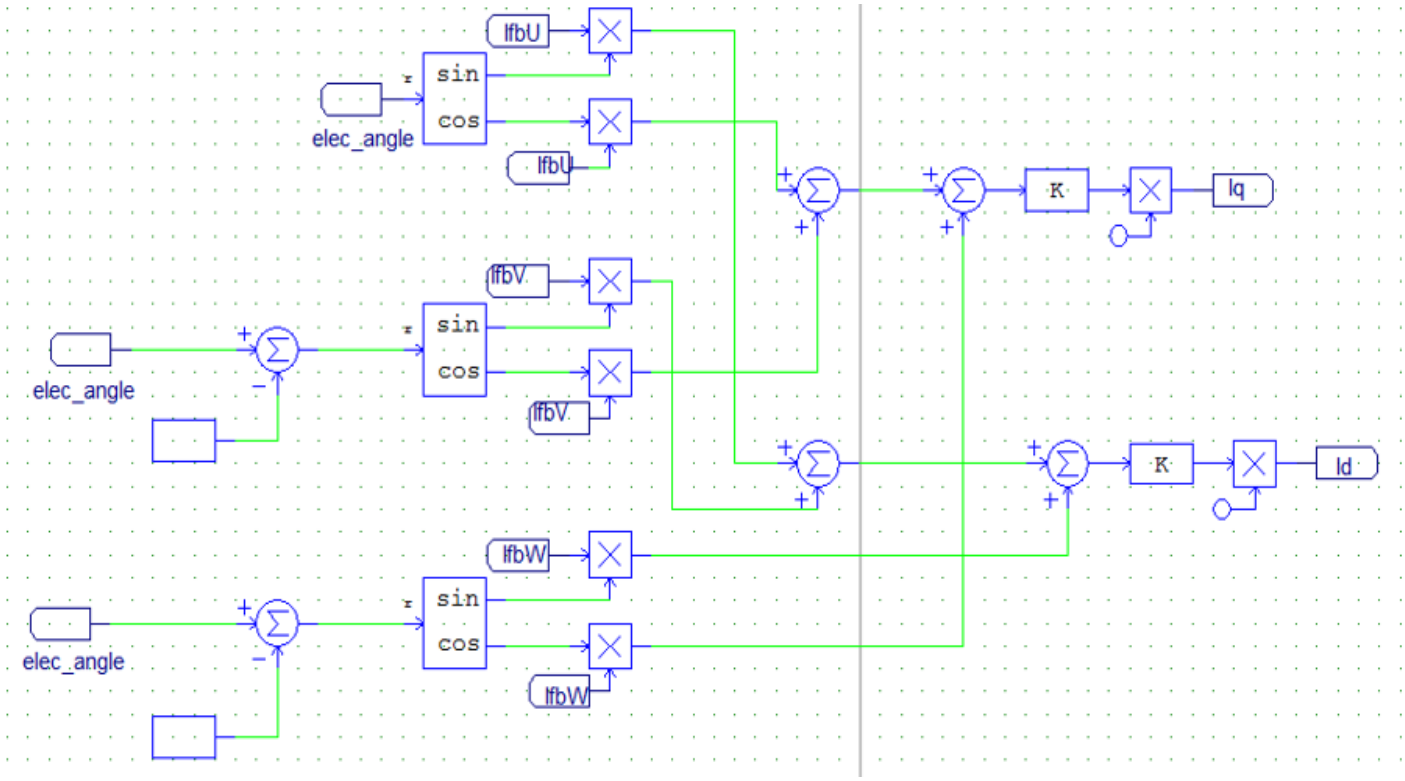

Figure 5.2.2.4.1: Schematic to calculate Synchronous Reference Frame Currents from Phase Currents

Electrical angle is shifted by 2π/3 and 4π/3 for V phase and W phase currents respectively. According to discussion made in section 2.2, a constant multiplication is also made to ensure amplitude conservation in transformation.

5.2.3 Development of Control Schematic

In this section cross-coupling decoupling and complex vector controllers will be implemented in PSIM schematic. Elements required to develop current vector controller are made available by computing real-time phase currents, electrical angle and currents in synchronous reference frame. Electrical parameters of motor are determined in section 6.1 and how these parameters will be used to determine control gains, is discussed in section 3.1.1 and 3.1.2 for continuous and discrete time systems respectively.

For both type of controllers, it is necessary to know electrical speed of rotor to make cross-coupling decoupling compensation or to introduce complex term in the controller. Further, dead-time compensation is needed for both type of controllers for compensation of inverter's non-linear behavior as described in section 3.3.2.

5.2.3.1 Implementing Vector Tracking Observer (VTO)

Implementation and tuning of vector tracking observer is discussed in chapter 4. Schematic of vector tracking observer is implemented in PSIM to get speed estimate based on same concepts. This schematic is shown in figure 5.2.3.1.1. In this schematic, mechanical angle is

used as input to tracker so result is also mechanical speed. Alternatively, electrical angle can be used to get directly electrical speed also. Both, enhanced and un-enhanced speed estimates are highlighted in figure 5.2.3.1.1. Figure also shows how load torque estimate is obtained from VTO and how electromechanical torque is given as feed forward to improve the response as described in section 4.1.

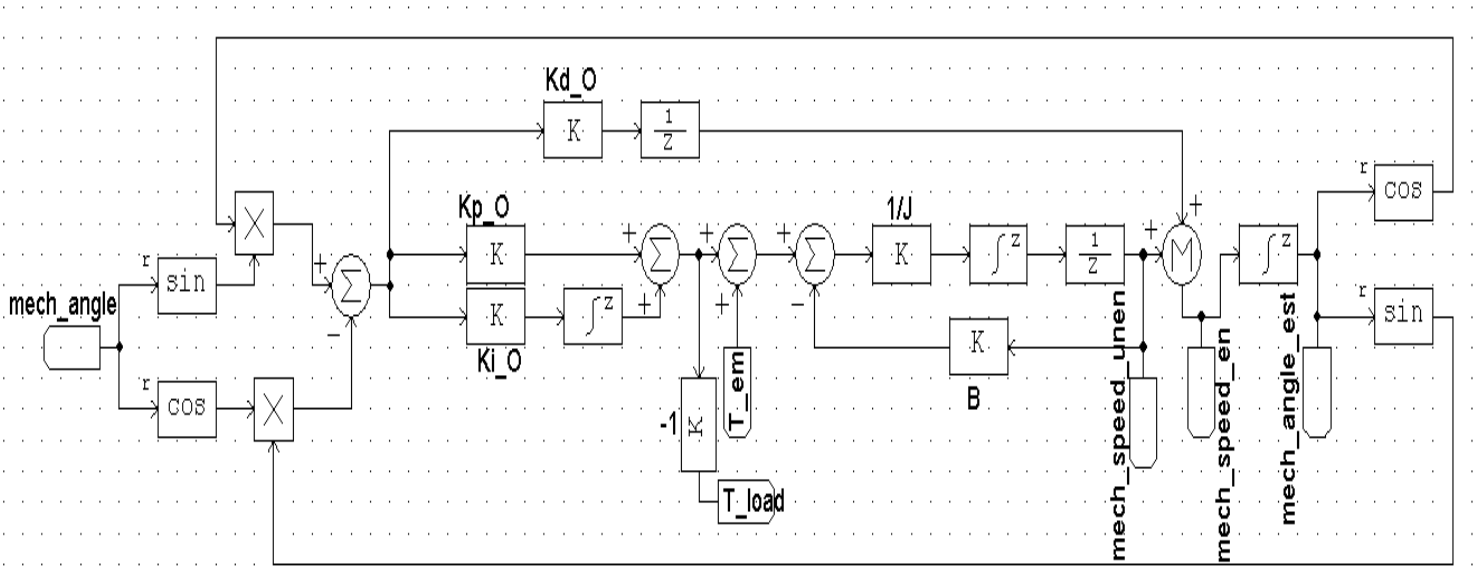

Figure 5.2.3.1.1: Schematic of Vector Tracking Observer

Gains in controller are marked with letter 'O' to show these ones are associated with observer. J and B, in plant model, stand for inertia and friction respectively. To determine electrical speed from mechanical speed, any of the two, enhanced or un-enhanced mechanical speed can be used. Here, un-enhanced speed is used because it is less effected by sudden change in position error and results more smooth output. Mechanical speed is multiplied with number of pole pairs of machine to get electrical speed as shown in figure 5.2.3.1.2.

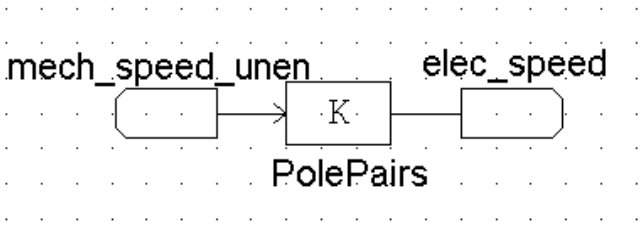

Figure 5.2.3.1.2: Schematic to Obtain Electrical Speed

5.2.3.2 Implementing Cross-Coupling Decoupling Current Controller

Concept of cross-coupling and decoupling is explained in section 3.2.1. To develop this type of controller calculation of compensation voltages is necessary. Computation of d and q axis compensation voltages is made in schematic depending on real-time DSP signals as shown in

figure 5.2.3.2.1. Concept of back-EMF is also described for controller implementation. Its computation is also shown in figure 5.2.3.2.1.

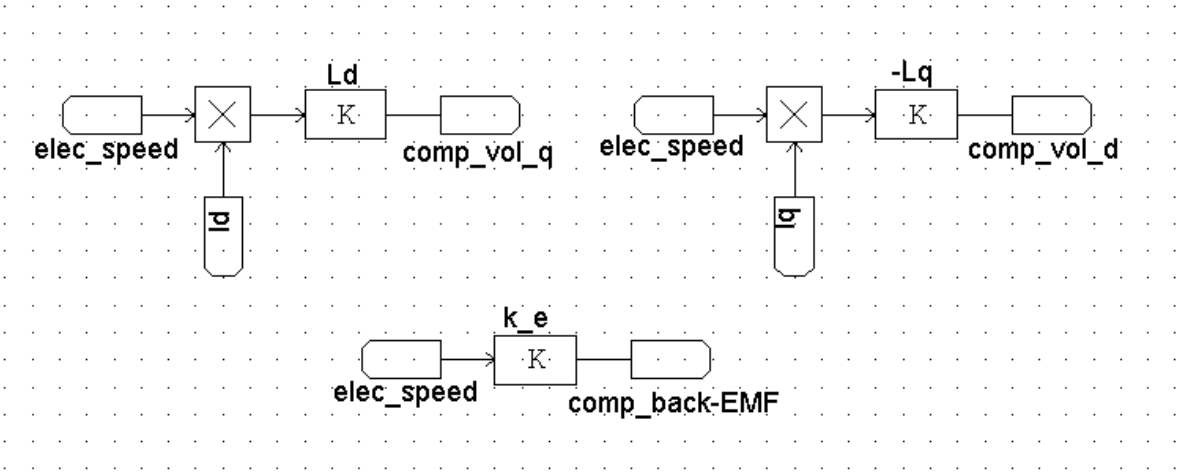

Figure 5.2.3.2.1: Calculation of Compensation Voltages for Cross-coupling Decoupling Type Synchronous Frame PI Current Regulator

Back-EMF constant used in computing back-EMF compensation is same electrical constant calculated in section 6.1.4.

Ignoring dead-time compensation for now, all elements required for controller development are discussed in schematics also. Calculation of gains for both d and q axis will be made using respective electrical parameter values determined in section 6.1. Controller implementation in discrete-time domain is also discussed in section 3.1.2. Anti-windup algorithm is also discussed, which will be incorporated in the following implementation.

In figure 5.2.3.2.2 PI current controller with cross-coupling decoupling is shown. Q and d axis voltages, coming from PI controllers might be high enough to cause over-modulation explained in section 1.1.3.3. So saturation is applied which limits square-root of squared voltages on the basis of DC-link voltage. Collective voltages before and after application of saturation are referred to as unsaturated and saturated voltage respectively. Their difference is used for anti-windup feedback calculation along with signs of original q and d axis controller voltages. Moreover, ratio of saturated and unsaturated voltages is made to scale q and d axis controller voltages, which is final demand voltage fed to the inverter. While configuring PWM block, amplitude of carrier wave is kept unity. So voltage demands should also be made in per unit values. For this reason, after scaling voltages for specific saturation level, they are transformed into per-unit quantities by manipulating with DC-link voltage. This finalizes discussion regarding cross-coupling decoupling type current vector controller. Dead-time compensation will be discussed in the very end which is general and not specified to any type of control technique.

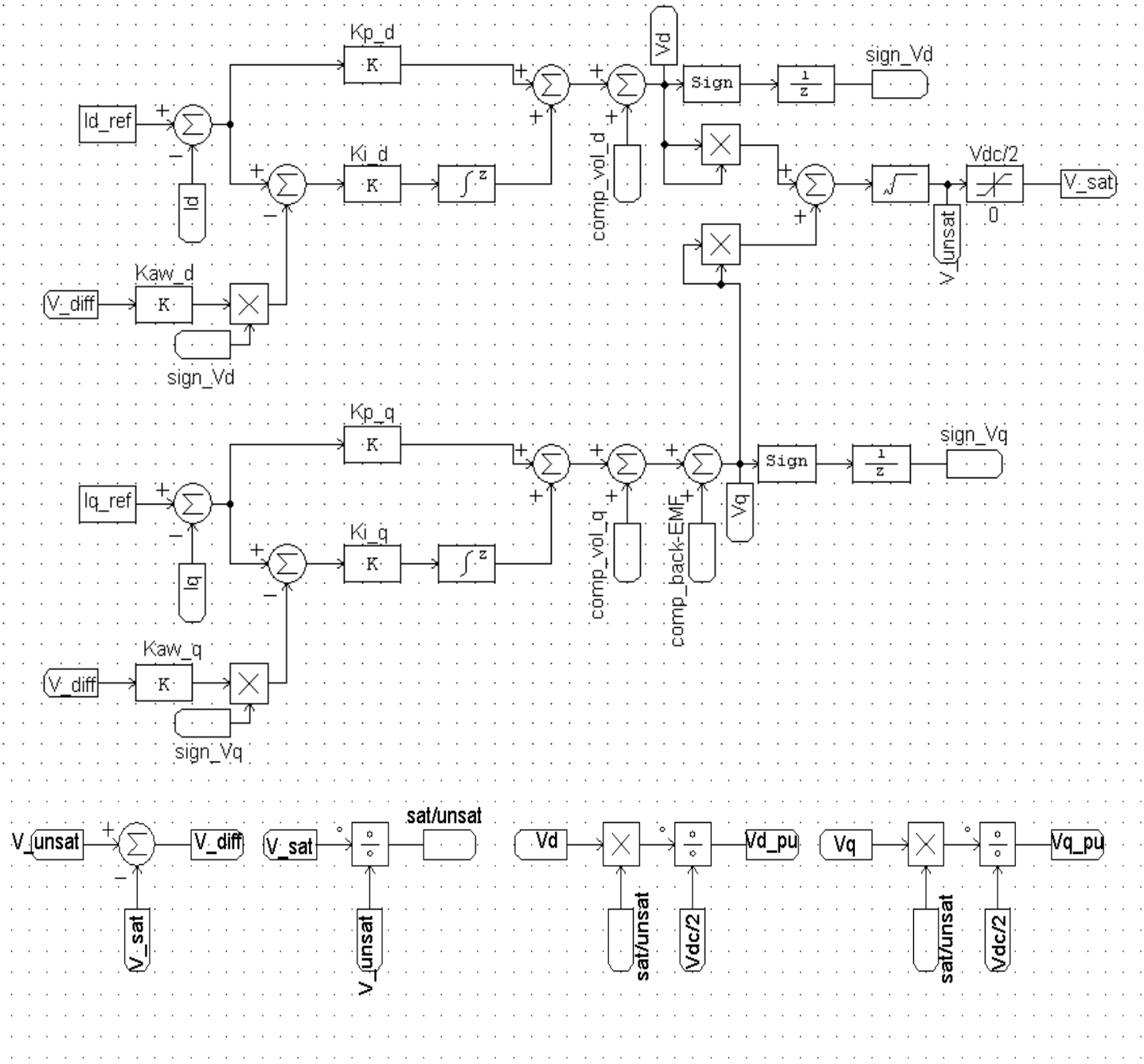

Figure 5.2.3.2.2: Schematic of Synchronous Frame PI Current Regulator with Cross-coupling Decoupling

5.2.3.3 Implementing Complex Vector Current Controller

In section 3.2.2, detailed discussion is made regarding movement of plant pole with speed of motor which leads to the need to develop complex vector controller, whose zero is also dependent upon speed of motor. In this way, zero-pole cancellation happens in almost full operation range, making the system to behave in more ideal way. Complex vector current controller is developed as part of the thesis. Detailed schematic is shown in figure 5.2.3.3.1. Same gains as calculated in section 3.1.2 are used here. Q and d axis compensation voltages

made to nullify cross-coupling effect are removed here and PI controller is modified. Back-EMF compensation is irrelevant of controller type. Currently, dead-time compensation will be ignored here as well. Moreover, saturation and anti-windup technique is also exactly the same as that of cross-coupling decoupling regulator. Anti-windup gain is different here as described in section 3.3.1.2.

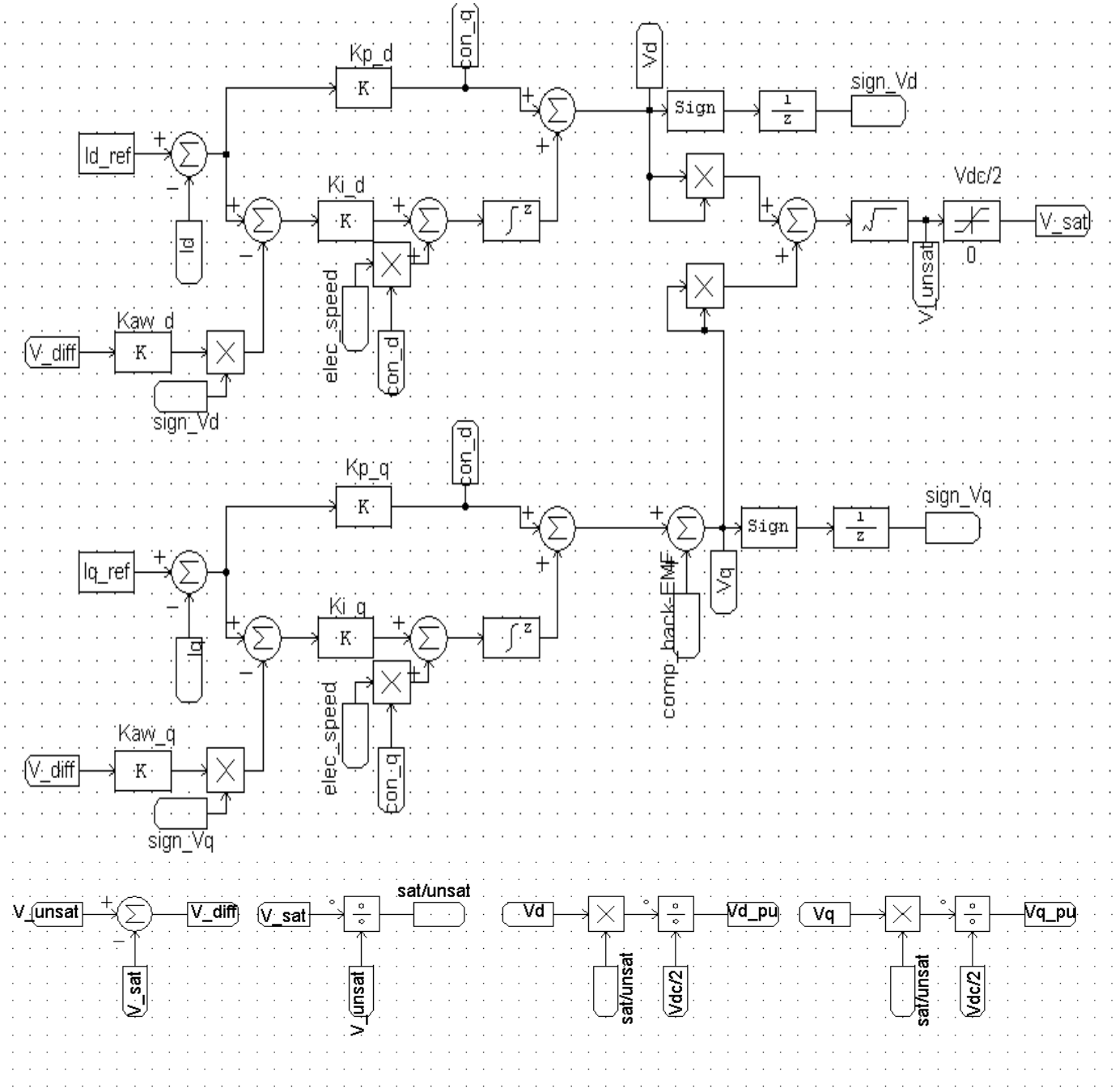

Figure 5.2.3.3.1: Schematic of Complex Vector Synchronous Frame PI Current Regulator

5.2.3.4 Dead-time Compensation and Start-up of Drive

In section 5.2.3.2 and 5.2.3.3, per-unit voltages in synchronous reference frame are formed for Pulse Width Modulator so that gating signals for inverter could be made available. But before that non-ideal behavior of inverter, discussed in section 3.3.2, is to be considered. Equation 3.3.2.2 and 3.3.2.3 are used to calculate alpha and beta dead-time compensation voltages. Relevant schematic is given in figure 5.2.3.4.1.

One thing is important to mention here, as d-axis current is kept at zero level for all experiments so θ^*term, mentioned in equations, is ignored to make dead-time compensation.

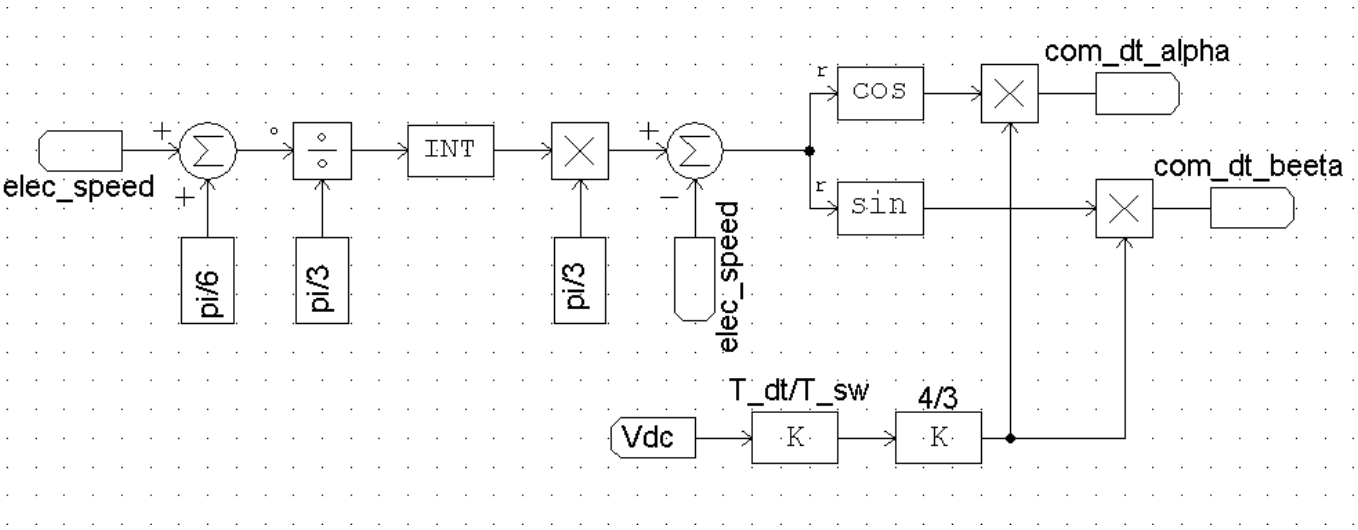

Figure 5.2.3.4.1: Schematic to Compute Dead-time Compensation Voltages in Stationary Reference Frame

These compensation voltages are not in per-unit values so before applying to drive circuitry, they must be converted. Block labelled with “INT” truncates its input to digit to give sector in six sector space.

In section 1.1.3, PWM strategies are discussed and advantages of using Space Vector Pulse Width Modulation (SVPWM) over Sinusoidal Pulse Width Modulation (SPWM) are detailed. For this thesis work also, in-built SVPWM block from SimCoder library is used. Block inputs need to be given in transformed stationary reference frame. So transformation is also emerged here. Figure 5.2.3.4.2 shows reference frame transformation, Dead-time compensation in per-units and start-up of drive.

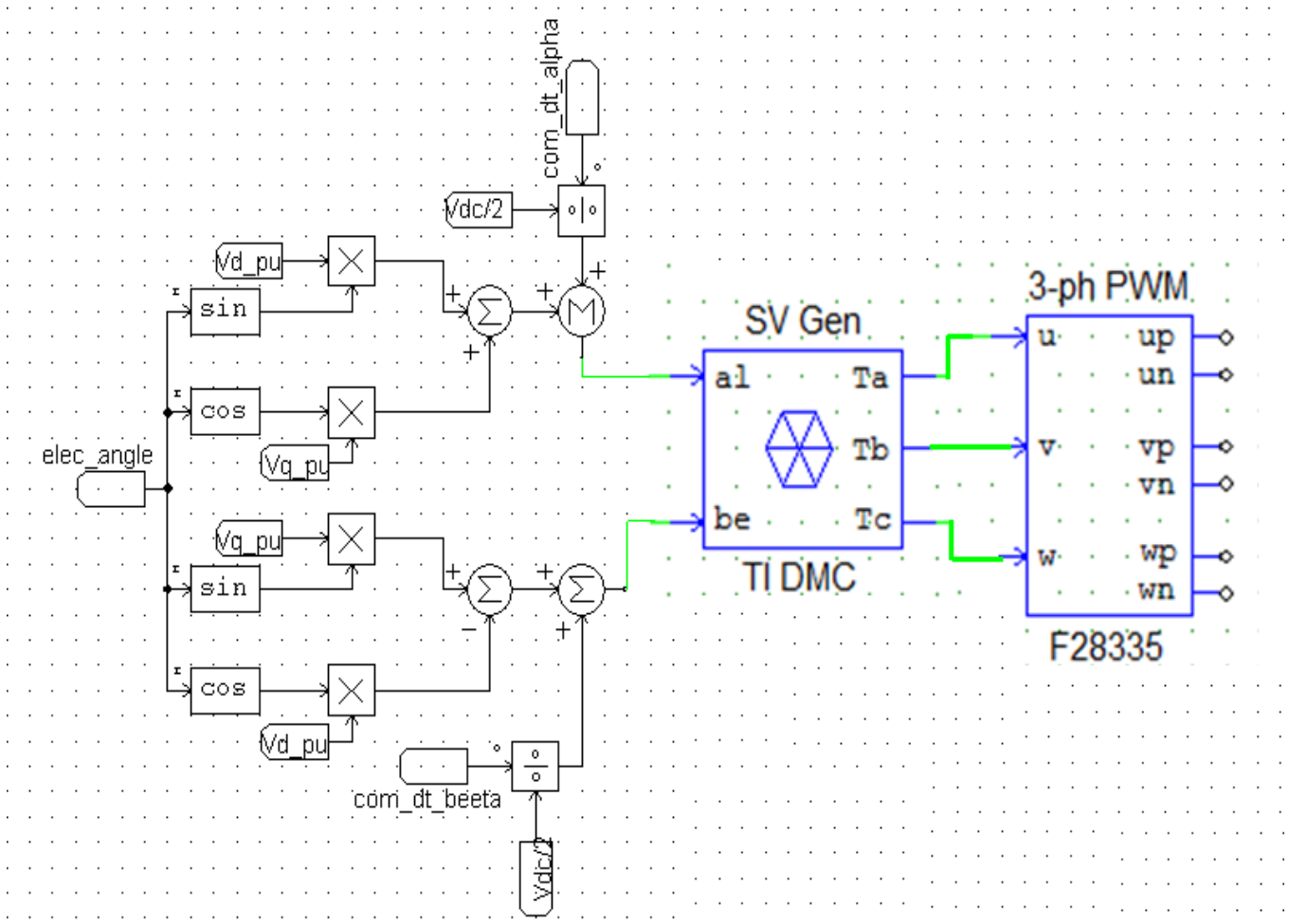

Figure 5.2.3.4.2: Schematic to Transform Command Voltages and Start-up of drive

This completes development of schematic. The code generated from this schematic can be downloaded into controller and run directly.

6. Pre-Commissioning of the Electric Motor and Experimental Results

This chapter presents all the results which validate speed estimation methods discussed in chapter 4 and developed in chapter 5. Moreover, two types of synchronous frame PI current regulators are discussed in chapter 3 and developed in chapter 5. Current tracking capability of both type of controllers and their transient response is validated through experiment and results are shown in section 6.3.

Before Plunging to calculation of controller gains, it is necessary to know characteristic electrical parameters of the motor under consideration. Process to determine these parameters is termed as pre-commissioning. Section 6.1 details the experiments for pre-commissioning.

6.1 Determining Electrical Characteristics of IPMSM

To realize Field-Oriented Control (FOC), electrical parameters of motor must be known. These parameters are needed to determine the PI controller gains to get the desired closed loop performance. This section describes simple experiments [21] that are performed to determine number of pole pairs, stator resistance, d and q axes inductances, electric/ BEMF constant and offset angle between z-pulse of encoder and quadrature axis of motor.

6.1.1 Pole pairs

Pole pairs define ratio between mechanical and electrical quantities of motor like position and speed. Sets of north and south segments on rotor represent motor pole pairs.

To determine pole pairs, motor can be run in open loop by setting some frequency and amplitude modulation ratio. Mechanical angle obtained by encoder should be plotted against some electrical quantity like current, sensed by current sensor. If current sensor is not available, the motor under consideration should be run by some other motor at fixed mechanical speed and back-EMF might be plotted with mechanical angle. In the figure 6.1.1.1, phase current and mechanical angle is shown.

It is clear from the diagram that in one mechanical rotation, current which is electrical quantity is having four complete rotations. So motor has four pole pairs or eight poles.

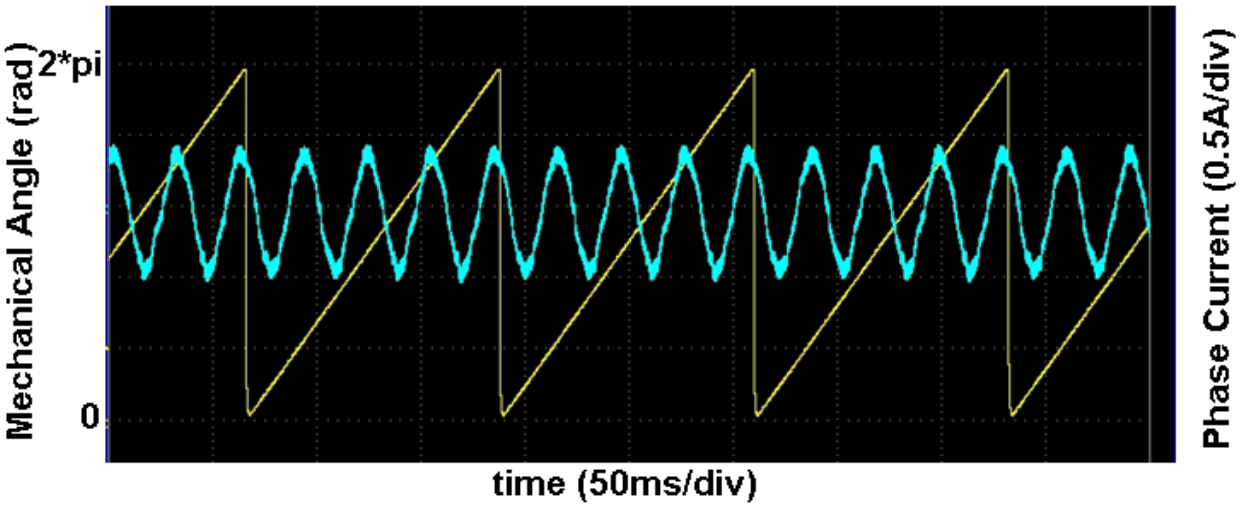

Figure 6.1.1.1: Rotor Mechanical Angle and Phase Current to Determine Number of Pole Pairs

6.1.2 Resistance Calculation

Resistance of the stator winding $R_s$is defined as resistance between phase terminal and center of the winding. Value of resistance is temperature dependent. In the motor's datasheet, motor resistance is given at 25°C. The resistance, measured in this experiment will also be considered same and it can be modified as follows for different temperatures.

$$R_s = R_0(1 + \alpha\Delta t)$$

R_0 is resistance at 25°C. α is constant determined by material and Δt is temperature difference such as T-25°C.

To determine stator winding resistance, pre-determined value of DC current is injected between two windings of the stator and voltage is measured across them.

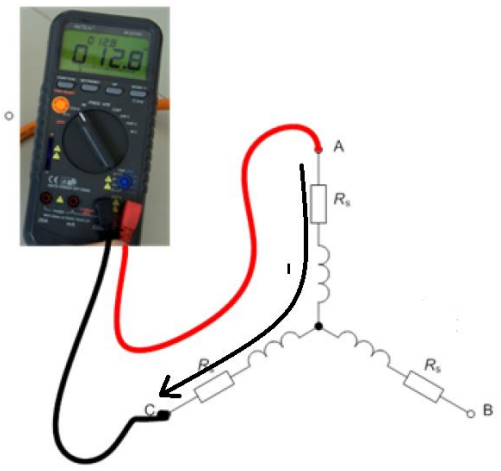

Figure 6.1.2.1: Setup to Determine Stator Winding Resistance

Value of current is known already so resistance is calculated.

$$R_l = \frac{V}{I}$$

The motor under consideration has wye winding arrangement. So calculated value is that of two phases. Phase resistance is as follows.

$$R_s = \frac{R_l}{2} = \frac{4.88\Omega}{2} = 2.44\Omega$$

6.1.3 Synchronous Inductances

In the case of non-salient rotor, q and d axis inductances will be same. It is shown in section 2.3.1 that IPMSM rotor has salient structure so both inductances will be different from each other. For the case of IPMSM, q-axis inductance is higher than that of d-axis inductance. Inductance value changes as current is increased and magnetic circuit enters saturation region. This concept is summarized in figure 6.1.3.1.

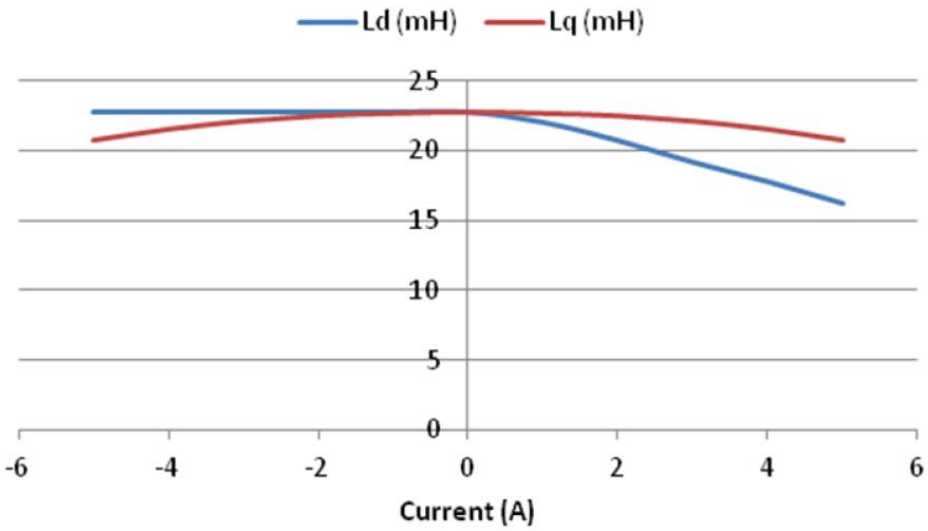

Figure 6.1.3.1: Inductance Variation as a Function of Current for IPMSM

Here, linear region will be assumed and inductances will be calculated. Balanced three phase current supply must be ensured. Depending on the electrical angle of the rotor θ_e, q or d axis inductance will be measured, after rotor will be aligned with specific axis, using equivalent electrical circuit of stator winding shown in figure 6.1.3.2.

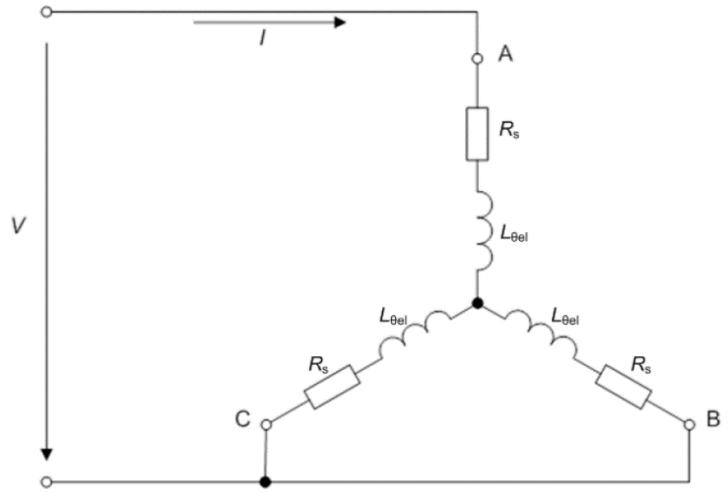

Figure 6.1.3.2: Inductance Measurement Circuit

To align the rotor along d-axis, phase A is connected to positive potential and B and C are grounded. Likewise, to align rotor along q-axis, phase B terminal is given positive potential, phase C terminal is grounded and phase A terminal is floating. This alignment strategy is shown below.

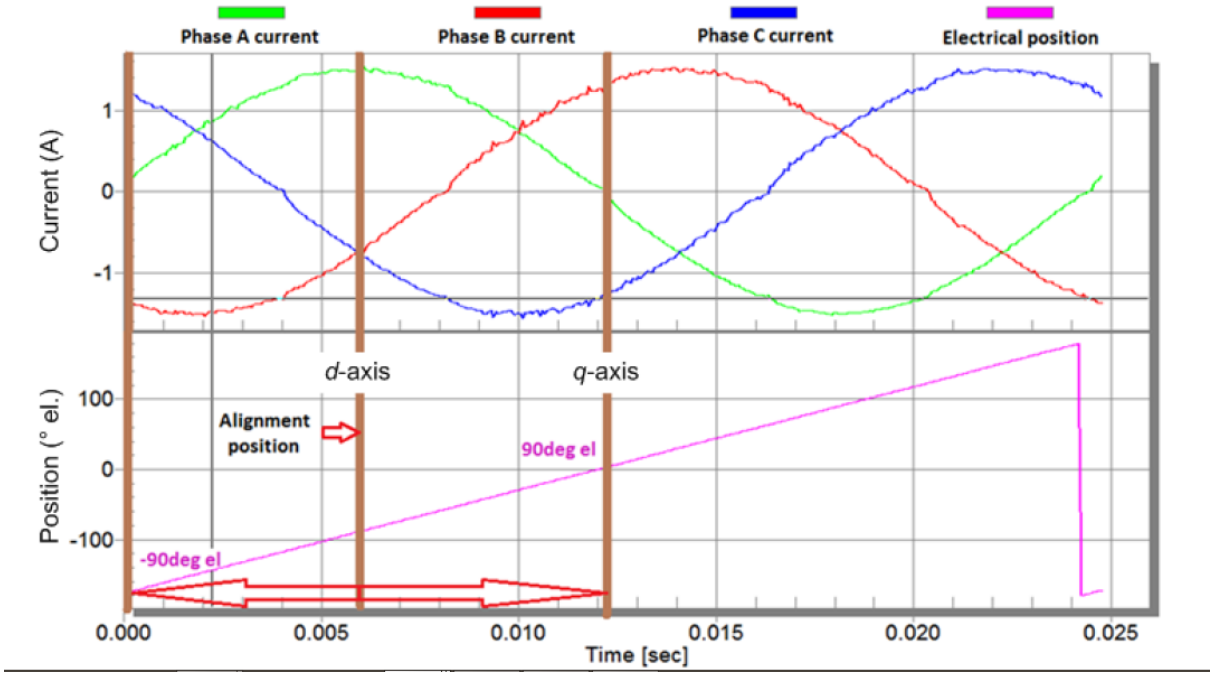

Figure 6.1.3.3: Explanation of q and d-axis alignment

Once the rotor is locked in its position for q or d axis. Step voltage is applied across the circuit shown in figure 6.1.3.2, when phase A terminal is at high potential and Phase terminals B and C are grounded. The current response is that of first order RL circuit.

$$i = \frac{V}{R}\left(1 - e^{-\frac{t}{\tau}}\right)$$

Here τ is time constant of the circuit given as

$$\tau = \frac{L}{R}$$

Let's 'L' is the total inductance of serial-parallel connection of the stator winding. When rotor aligned with d-axis, $V_d = \frac{2}{3}V$ and $V_q = 0$ and I_d is same as$I$. It can be concluded that$L_d = \frac{2}{3}L$;

Similarly, when rotor is aligned with q-axis, $V_q = \frac{2}{3}V$ and $V_d = 0$ and I_q is same as$I$ leading to $L_q = \frac{2}{3}L$. Resistance seen from the terminals of circuit is also $\frac{3}{2}R_s$.

For both q and d-axis inductance measurement current response for unit step voltage is given in figure 6.1.3.4 and 6.1.3.5 respectively.

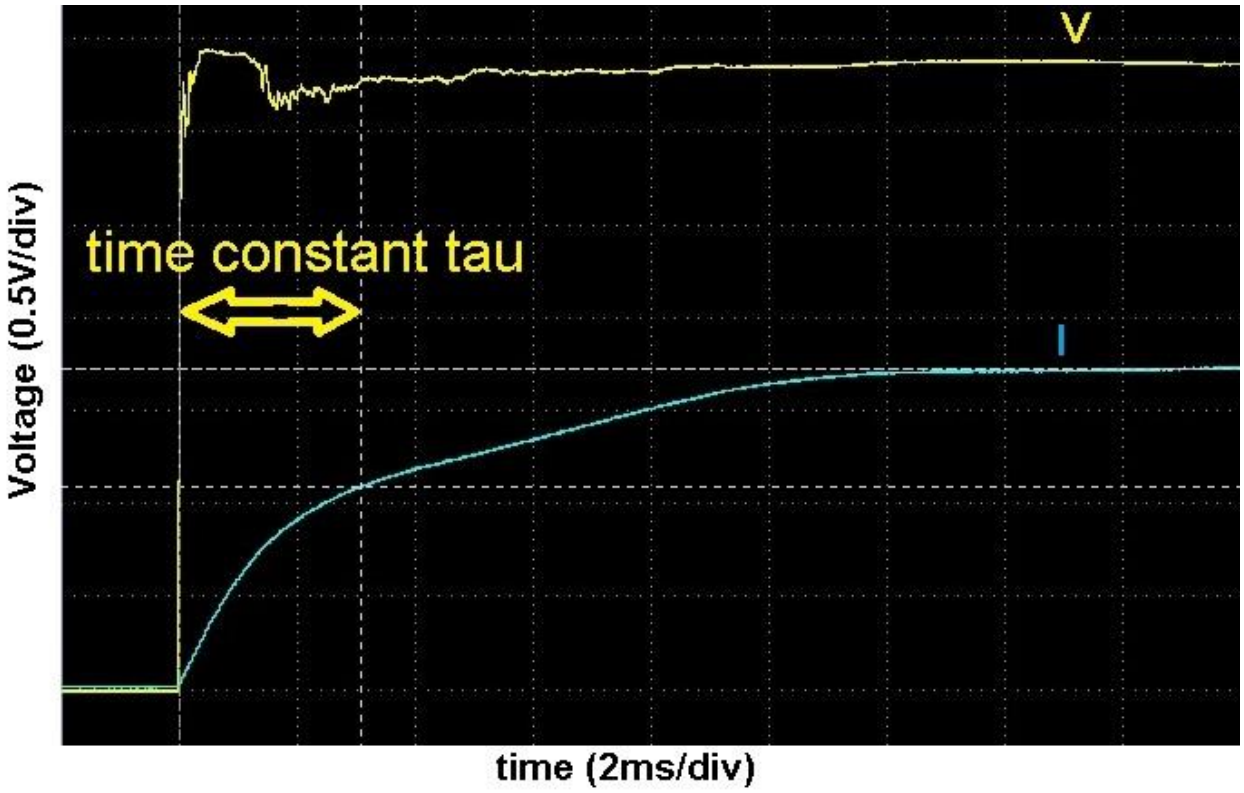

Figure 6.1.3.4: Current Step Response Waveform for Q-axis Inductance Measurement

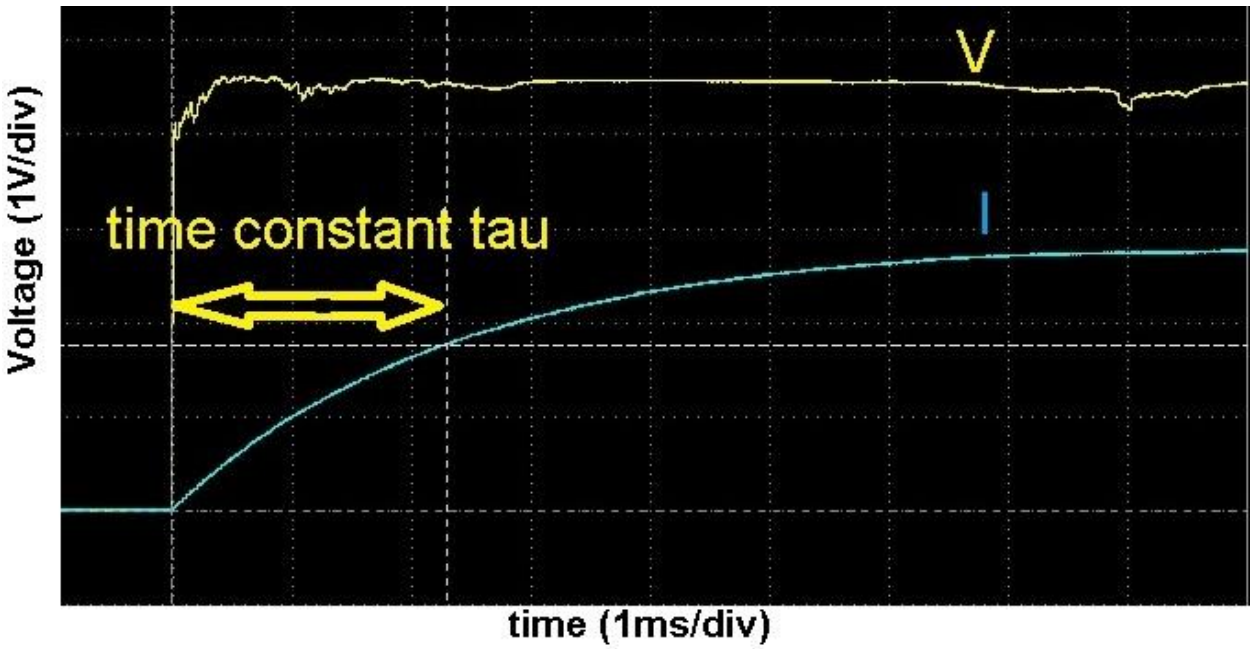

Figure 6.1.3.5: Current Step Response Waveform for D-axis Inductance Measurement

From the above figures, time constants for both q and d-axis aligned rotor is determined. Phase resistance is determined in section 6.1.2. So d and q axis inductance is calculated as follows.

$$L_q = \tau_q R_s = 3.08m * 2.44 = 7.52mH$$

$$L_d = \tau_d R_s = 2.3m * 2.44 = 5.6mH$$

6.1.4 Back-EMF constant

Flux linkage constant also named as back-EMF constant and electrical constant of the machine is determine by measuring peak phase voltages of motor in no-load condition at constant speed. Motor is rotated by some other electric machine through its shaft. This constant gives ratio between back-EMF voltage and angular electrical speed. Setup shown in figure 6.1.4.1 is used to run this experiment.

If neutral point of motor is not accessible then an artificial neutral point can be created using wye connected resistors or line-line voltage can be measured and manipulated appropriately to get line-neutral voltages.

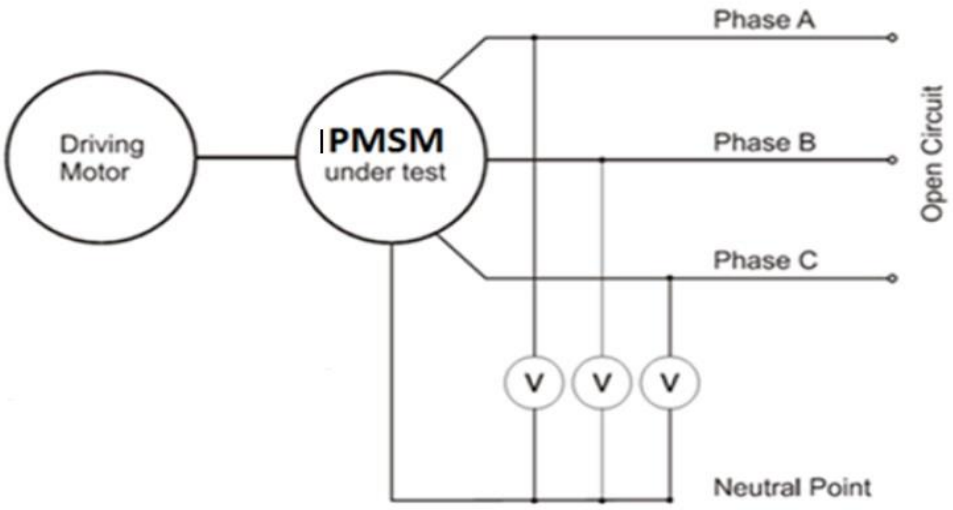

Figure 6.1.4.1: Setup to measure Back-EMF Constant

With the setup of figure 6.1.4.1, all three phase back-EMF voltages are measures and plotted. Result is shown in figure 6.1.4.2.

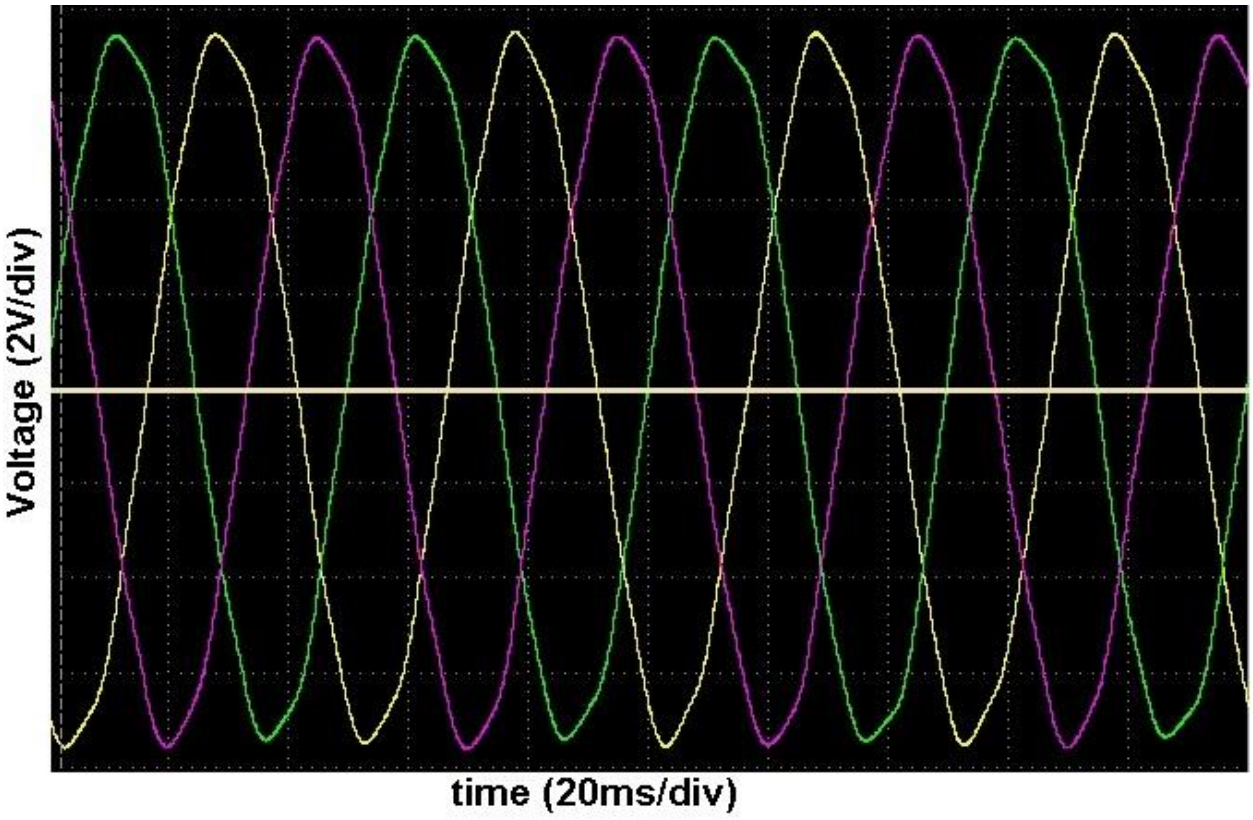

Figure 6.1.4.2: Phase Back-EMF Voltages to Measure Electrical Constant of the Machine

Finally, constant is calculated using the following expression.

$$\lambda_{pm} = k_e = \frac{V_{pk}}{\omega_e} = \frac{\frac{V_{pk-pk}}{2}}{2\pi * f_e} = \frac{7.49 * 50.32m}{2\pi} = 0.0598Vs/rad$$

6.1.5 Offset angle of the motor

In section 1.1.2.1, it is explained that position difference between z-pulse of the encoder and q-axis of the motor is observed commonly. For the given motor, this offset angle is determined by plotting back-EMF phase voltages with z-pulse of the encoder as shown in figure 6.1.5.1.

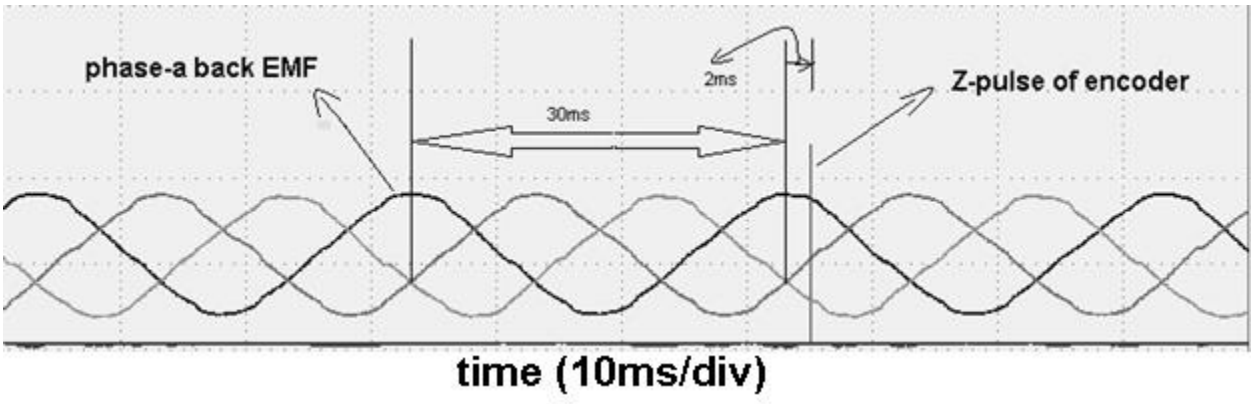

Figure 6.1.5.1: Phase Back-EMF Voltages and Z-Pulse of Encoder to Calculate Offset Angle

Phase difference between peak of phase-a back-EMF and encoder z-pulse corresponds to offset angle and calculated below.

$$\theta_{offset} = \frac{2\pi}{30m} * 2m = 0.42rad$$

6.2 Experimental Set-up

Complete hardware setup is discussed in chapter 5. Figure 6.2.1 presents an overview of this setup. This diagram highlights the main features of each element of hardware specially HVCntrl and PFC kit.

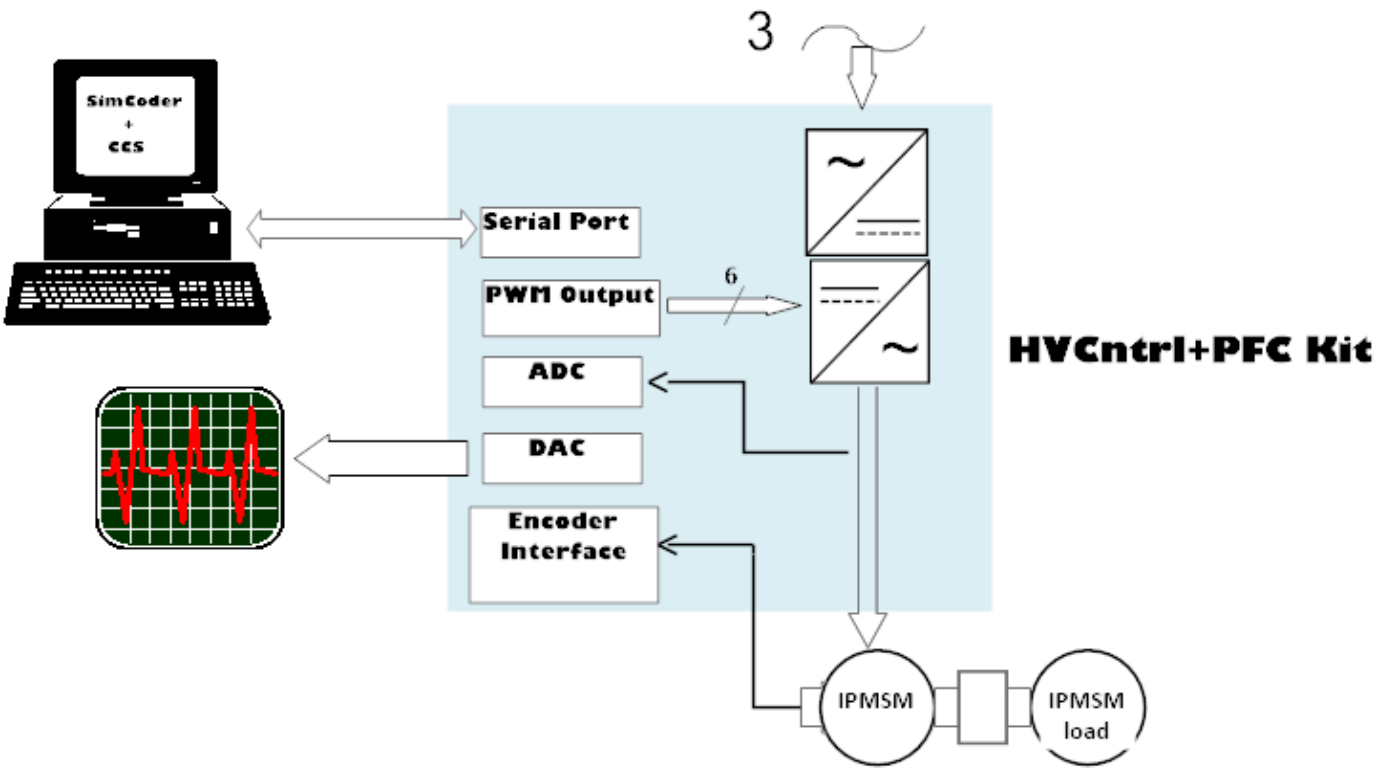

Figure 6.2.1: Harware Setup for Experimental Work

All elements of hardware are discussed in detail in chapter 5. For respective setup, detailed control software is also developed in section 5.2.

6.3 Experimental Results

This chapter discusses all the results obtained from mentioned control algorithms. First, results of luenberger observer and vector tracking observer will be shown. After that need for dead-time compensation will be demonstrated and results obtained from various compensation techniques will be shown. Finally, step current responses for developed controllers will be demonstrated.

6.3.1 Speed Estimation

6.3.1.1 Position and Speed Estimation from Luenberger Observer

Luenberger observer discussed in section 4.1, if tuned well, gives good estimate of rotor position. Figure 6.3.1.1 shows actual position obtained from incremental encoder and estimated position resulting from observer.

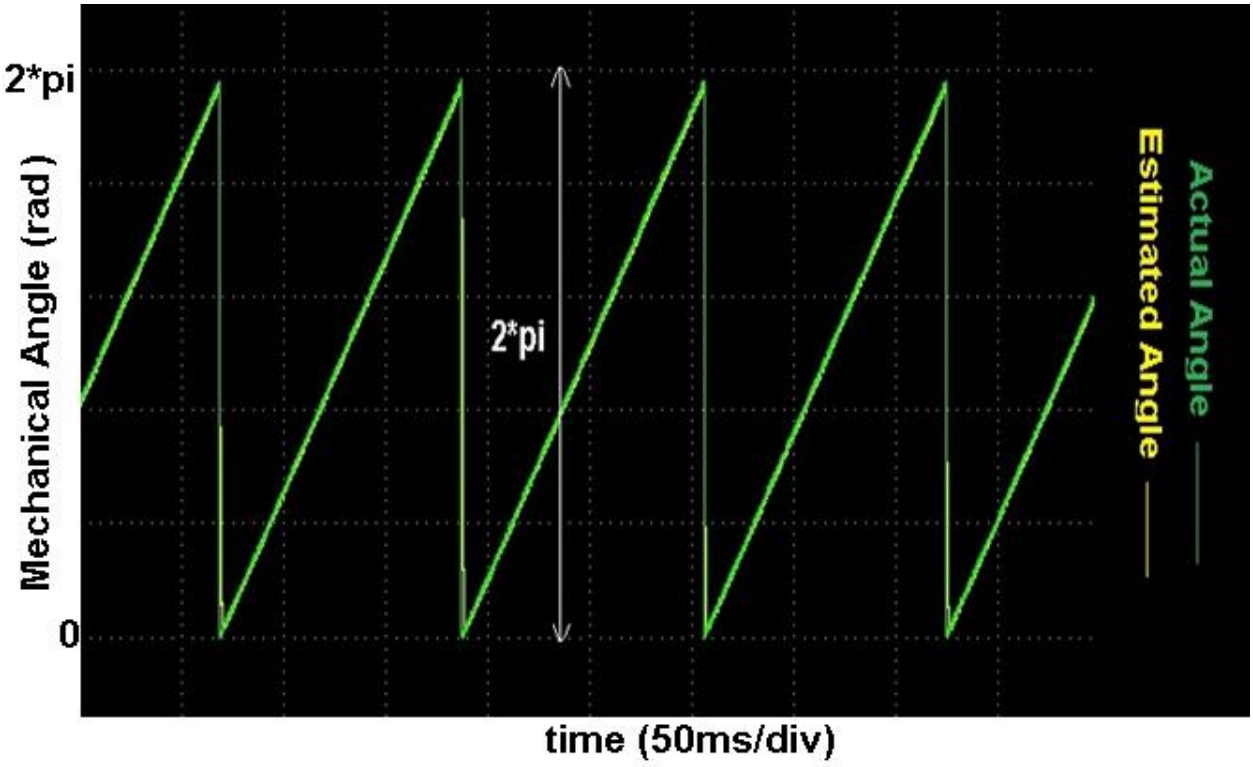

Figure 6.3.1.1: Position Tracking Capability of Luenberger Observer

Result shows that observer is tracking position input well. There is little noise at the moment when encoder counter resets at the end of each mechanical rotation which can be minimized by suitable selection of damping ration and observer bandwidth in continuous domain and pole placement variation in discrete domain. This observer is easy to implement but it has a problem in its speed estimate because encoder counter resets every mechanical cycle. This issue is discussed in section 4.1 in detail. Speed estimate from this observer is as follows.

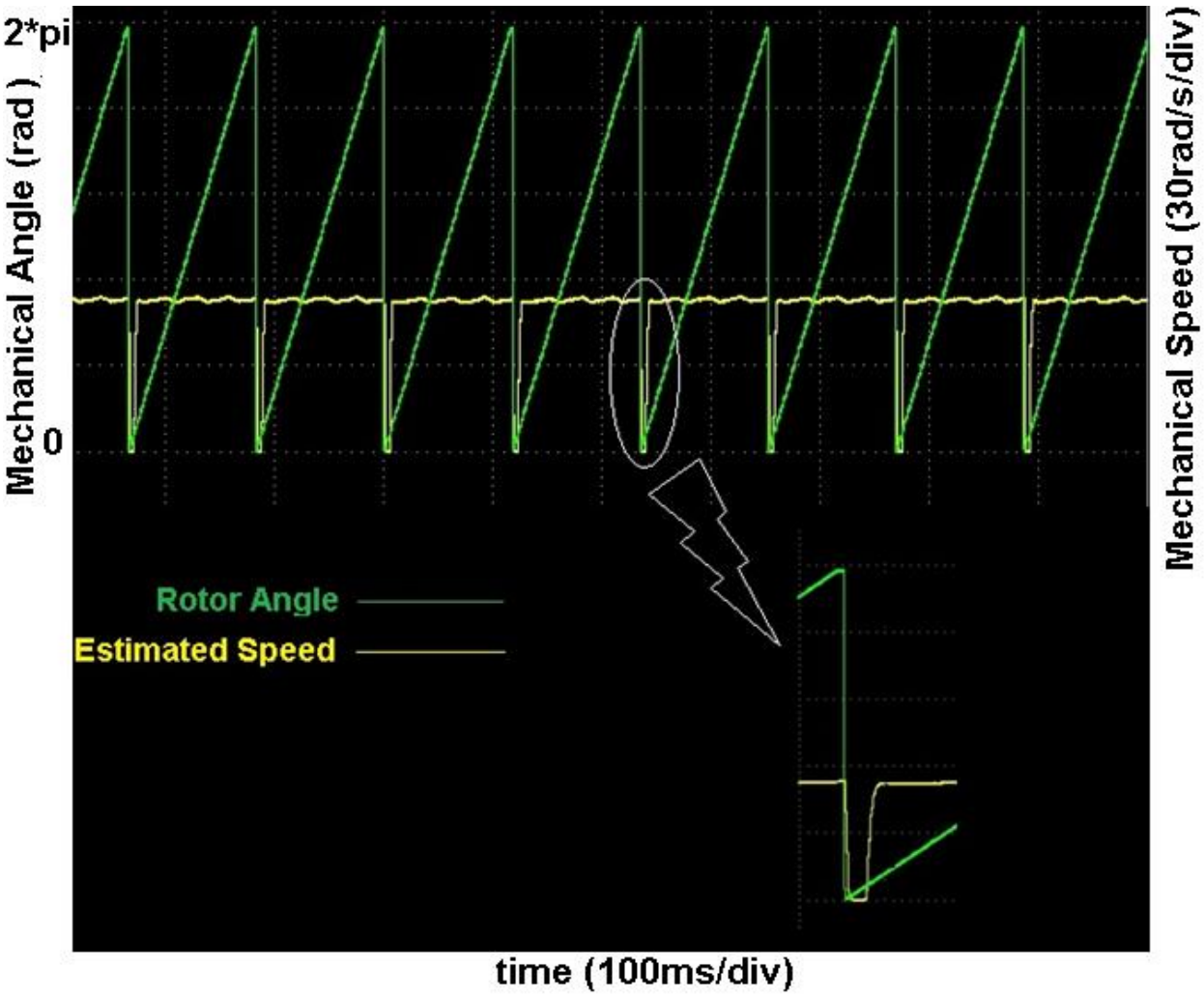

Figure 6.3.1.2: Speed Estimate from Luenberger Observer

It is important to mention here that speed seems to go from its average value to zero, it is not the case in real. Speed goes to very high negative value. Here it is saturated at 0 because DAC can plot values ranging from 0 to 5 only.

6.3.1.2 Speed Estimation from Vector Tracking Observer

In section 4.3, vector tracking observer was developed which apparently gives solution to this problem regarding speed estimate by luenberger observer. Result of speed estimate from VTO is shown in figure 6.3.1.3. It must be mentioned here that tuning for VTO is kept same as that of luenberger observer, when it is tracking position correctly. Only error calculation is made non-linear as discussed in section 4.2 and 4.3

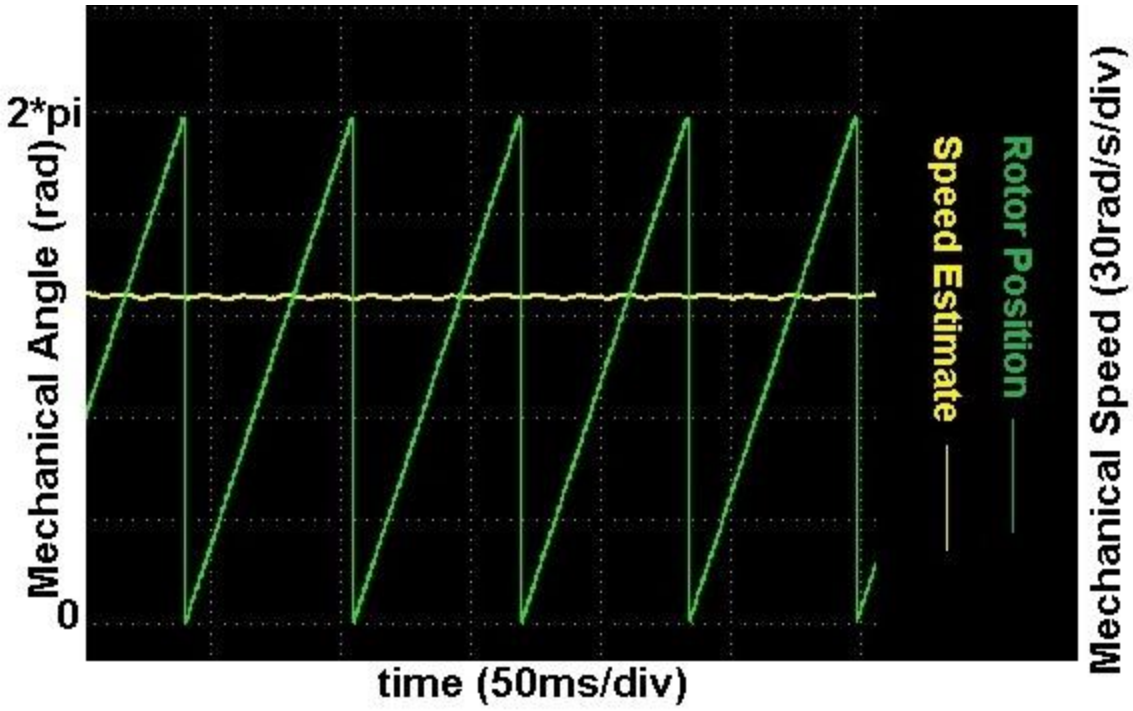

Figure 6.3.1.3: Speed Estimation from Vector Tracking Observer

So by forcing observer to track vector instead of scalar, unwanted speed bumps are eliminated

6.3.2 Dead-time Compensation

Once the controller is developed, either cross-coupling decoupling type or complex vector type, phase current waveform will not be sinusoidal as per expectations, as shown in figure 6.3.2.1.

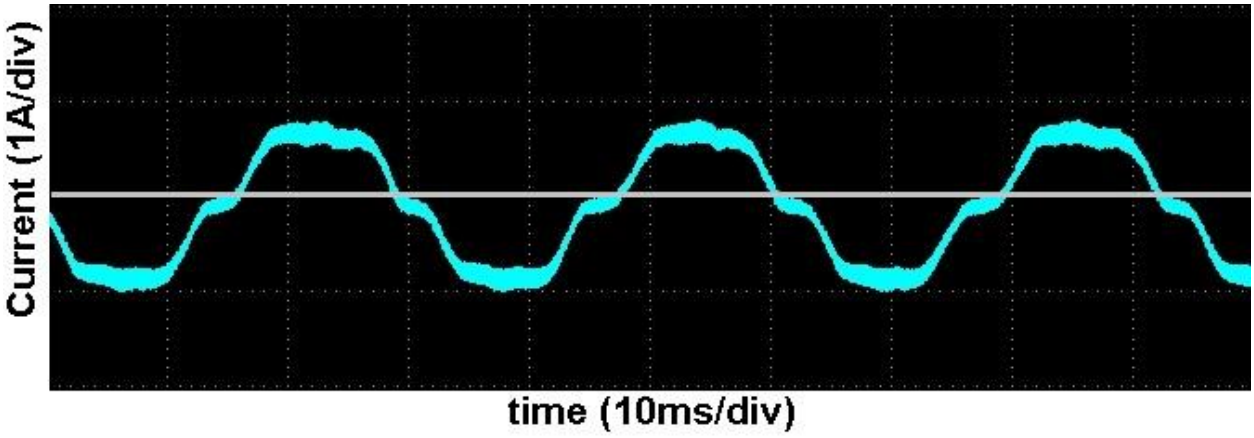

Figure 6.3.2.1: Phase-Current Waveform without Dead-time Compensation

Problem is arising because of dead-time associated with the gating signals of switches in the same leg of inverter. This phenomenon is discussed in section 3.3.2 in detail. For each phase dead-time compensation voltages are computed and compensated for in the control algorithm using equation 3.3.2.1. Resulting phase current waveform is shown in figure 6.3.2.2.

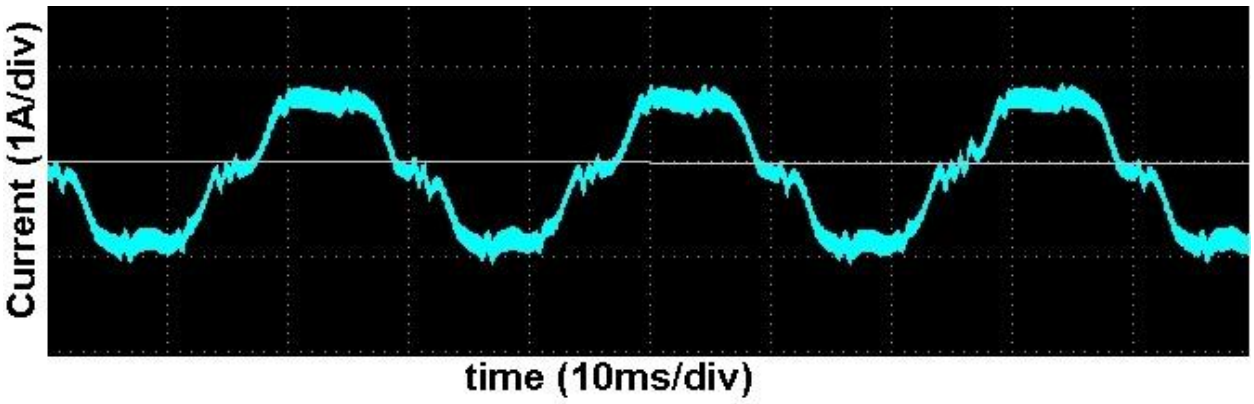

Figure 6.3.2.2: Phase Current Waveform with Dead-time Compensation Involving Sign of Phase Current

At zero-crossing of current, sign detection of phase current will cause uncertainty and current waveform is deteriorated even more.

This issue is resolved by using the other method in which technique is to detect sector of current vector at that instant and computing compensation voltages in stationary or synchronous reference frame as per equation 3.3.2.2 and 3.3.2.3.

Figure 6.3.2.3 shows dead-time compensation voltages in stationary reference frame and figure 6.3.2.4 in synchronous reference frame.

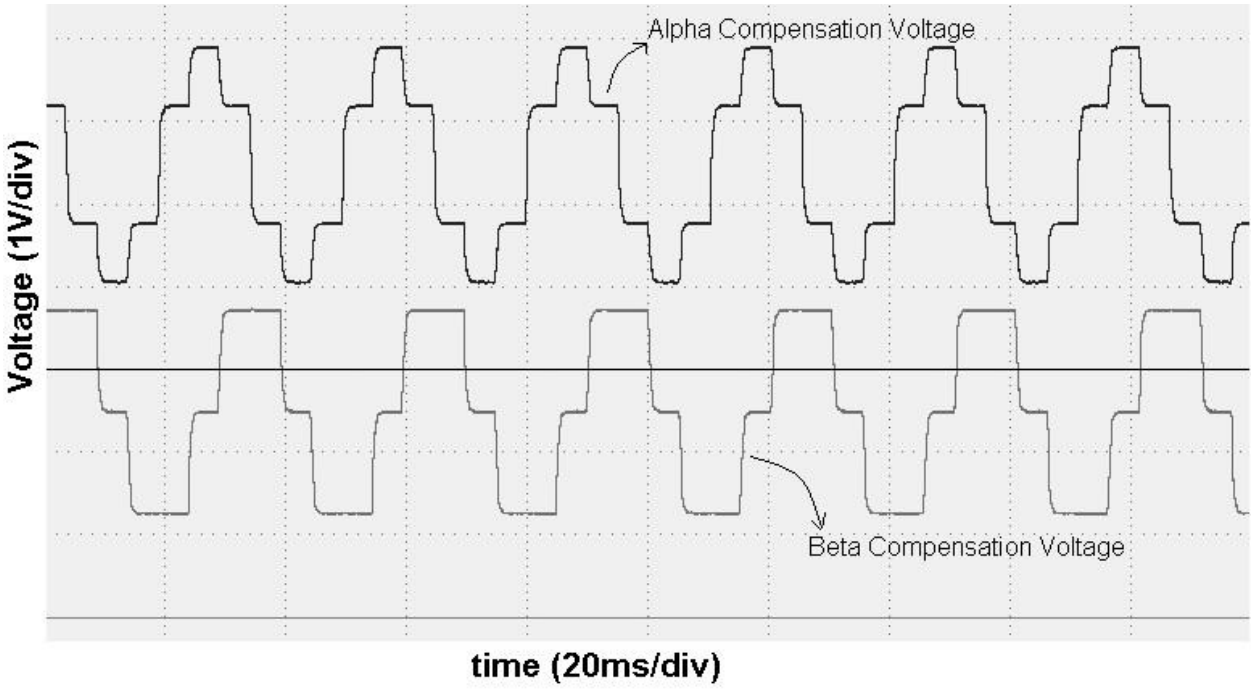

Figure 6.3.2.3: Dead-time Compensation Voltages in Stationary Reference Frame

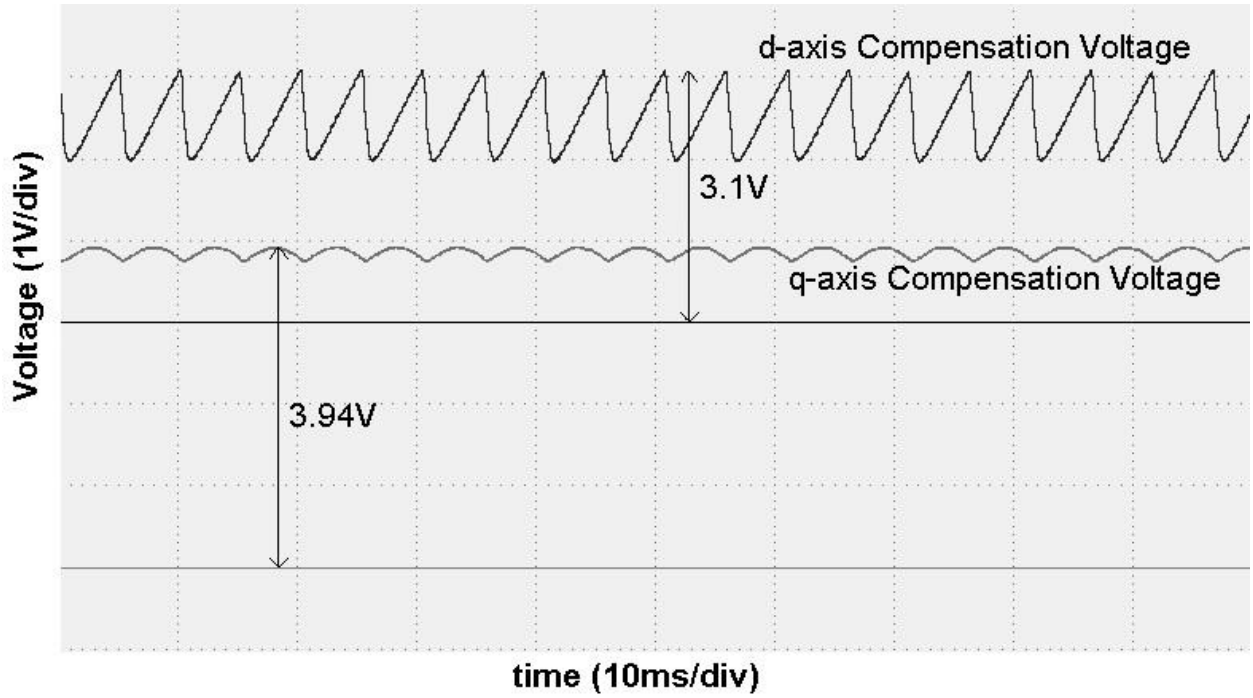

Figure 6.3.2.4: Dead-time Compensation Voltages in Synchronous Reference Frame

Dead-time compensation made using either of these voltages from figure 6.3.2.3 and figure 6.3.2.4 results same response in phase current wave. Improved current waveform is shown in figure 6.3.2.5.

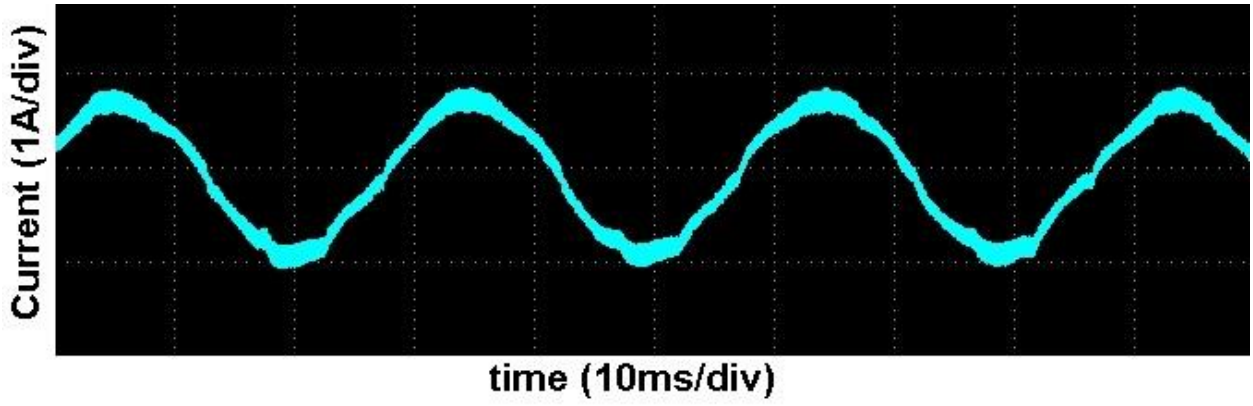

Figure 6.3.2.5: Phase Current Waveform with Dead-time Compensation

Comparing this figure with figure 6.3.2.1, it can be concluded that compensation is made well.

6.3.3 Step Current Response of Synchronous Frame PI Current Regulator with Cross-coupling Decoupling

Controller discussed in section 3.2.1 and its respective schematic developed in section 5.2.3.2, which includes cross-coupling decoupling, dead-time compensation, anti-windup algorithm and

synchronous frame PI regulators for both d and q axis currents is tested for current-step response. For this experiment, q-axis current is given 0.5A amplitude and d-axis current is forced at 0A. Bandwidth is set at 200Hz. To observe the dynamics of system clearly, rotor is blocked.

Response of the controller is shown in figure 6.3.3.1.

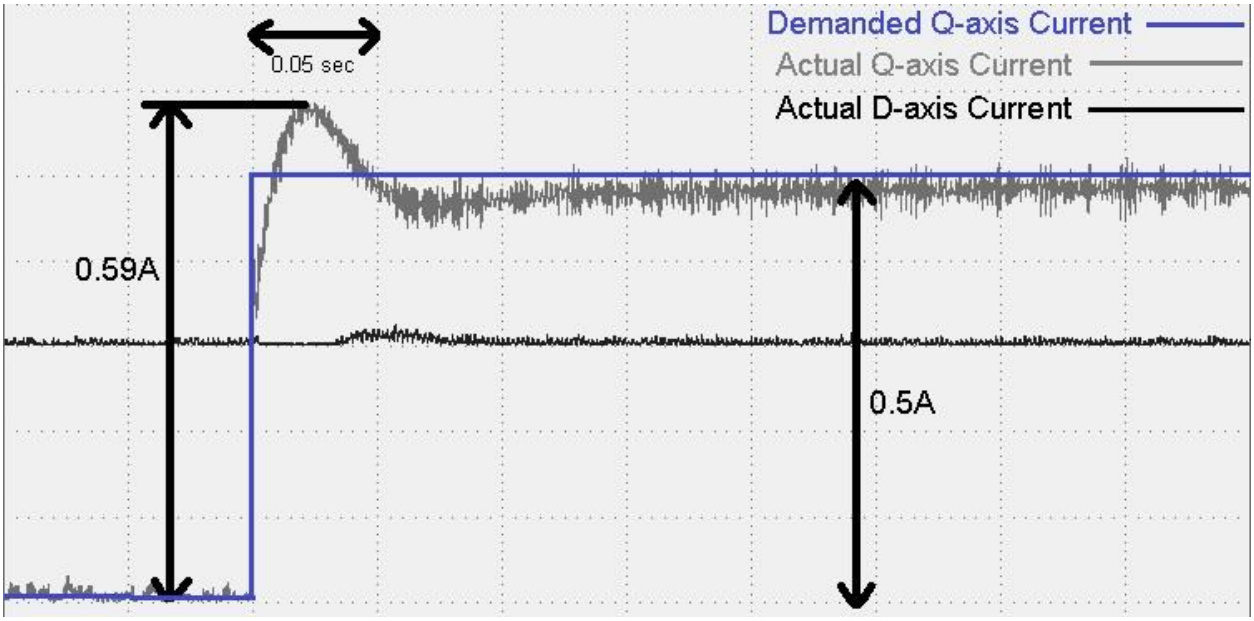

Figure 6.3.3.1: Commanded and Experimental Current Magnitude for Synchronous PI Current Regulator with Cross-coupling Decoupling

While tuning controller, it was assumed that controller zero will cancel plant pole exactly resulting in first order transfer function for closed loop. Current step response shows that zero and pole are not cancelled exactly so there is overshoot observed in transient state.

6.3.4 Step Current Response of Complex Vector Synchronous Frame PI Current Regulator

In section 3.2.2, design of complex vector synchronous frame PI current regulator is discussed. Respective schematic is also developed in section 5.2.3.3. This type of controller is less sensitive to motor parameters. For cross-coupling decoupling estimated motor parameters and rotor speed are used while for complex vector controller, controller zero is modified on the basis of speed only. Thus the dynamic state of step current response is expected to improve for same current demand and bandwidth. Figure 6.3.4.1 shows current step response for complex vector controller.

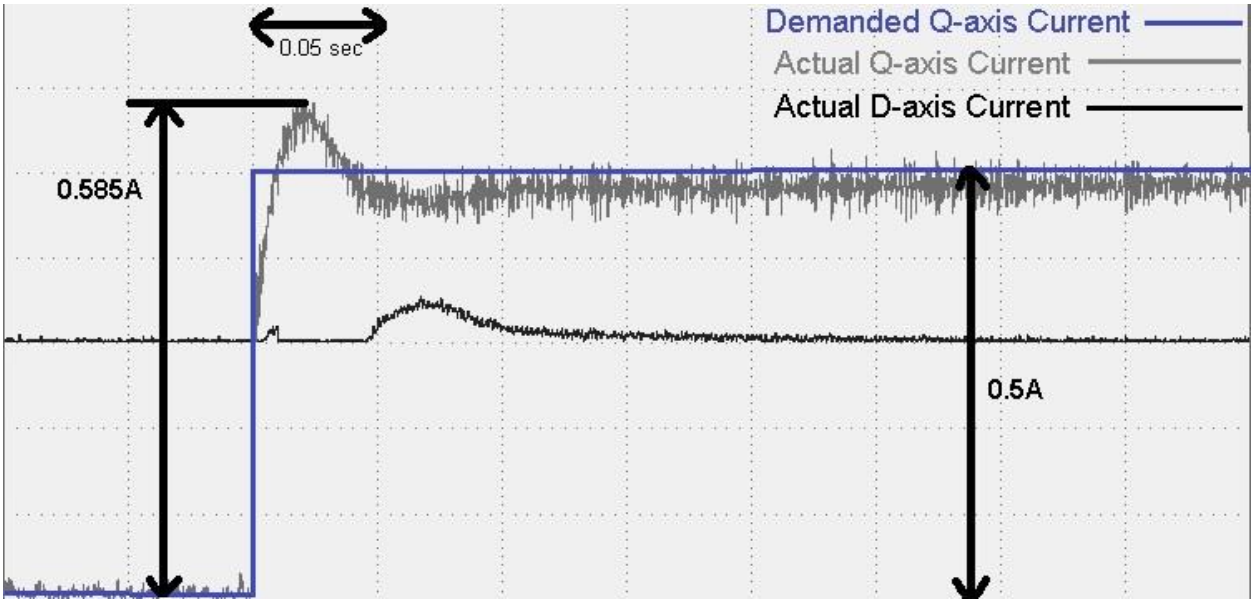

Figure 6.3.4.1: Commanded and Experimental Current Magnitude for Complex Vector Synchronous PI Current Regulator

Comparing figure 6.3.3.1 and 6.3.4.1, it can be concluded that transient state is improved for complex vector controller. Overshoot is decreased and steady-state is attained in relatively less time.

7. Conclusions and Future Work

This chapter summarizes what is being done in this thesis and what is concluded from all experiments. It also discusses future work that can be based upon this thesis work.

7.1 Conclusions

In chapter 1, discussion is made about the need of electrical machines for automotive application and IPMSM is proved to be a good candidate for high speed applications. Its detailed model is developed in chapter 2 in stationary as well as synchronous reference frame. Discussion is also made about validity of this model for all types of synchronous machines like surface permanent magnet machine and synchronous reluctance machine. The chapter also emphasizes on the need of development of synchronous reference frame model for controller development.

Chapter 3 discusses controller design and tuning in continuous and discrete time domain. Two type of controllers named synchronous frame PI current regulator with cross-coupling decoupling and complex vector synchronous frame PI current regulator are developed and it is shown that later shows better performance because it is less sensitive to electrical parameter variation. Experimental results validate this conclusion as shown in section 6.3.

To analyze steady state performance, effect of dead-time is discussed and different ways, to compensate for its effect, are mentioned. Improved results are also shown to approve the theoretical discussion.

For development of any type of controller, speed of the rotor was required. Speed estimation algorithms are developed in chapter4 for the purpose. Tuning of luenberger observer is done in continuous and discrete time domain. And it is shown that if observer will be tuned well, it will track input position with almost zero steady-state error and it is very robust regarding variation in mechanical model parameters. Noise rejection capability of this type of observer is very good. Later on, vector tracking observer is also discussed in detail and shown that it gives good estimate of speed for incremental encoder.

Power converter, being important component of drive control setup, is also studied in detail. Working pattern for SPWM and SVPWM is studied and it is shown that SVPWM is better technique with regard to DC-link voltage utilization and switching losses.

SimCoder is used for algorithm development, whole schematic is synchronized with available digital motor control kit. SimCoder being the very useful tool for drive control applications gives feasibility to use its readily-available tools as shown in chapter 5.

7.2 Future Work

Use of electric motor and its control is highly demanded in automotive as well as industrial applications. Position and speed control are required usually but current control loop being the innermost loop provides the basis for other control parameters. So this thesis work can be extended to design position and speed controllers. Drive control in different speed regions can be studied. Same algorithm can be modified to make it work for other type of synchronous machines also.

For this work incremental encoder is used for speed estimation. To reduce the price of drive, other types of observers can be studied to estimate speed. In other words, sensorless drive control algorithm can be developed on the basis of this work.

Once the concept of control is clear, other advanced controllers like deadbeat type controller can be developed. Which is capable of achieving higher bandwidths.

References

[1] Daniel Logue, Philip T. Krein, “Control of Induction Machine Drives”, University of Illinois at Urbana-Champaign, 2011.
[2] Fabio Giulii Capponi, Lecture slides-Dynamic Analysis and Control of AC Machines, La Sapienza University of Rome.
[3] K.Craig, Lecture slides- Actuators and Sensors in Mechatronics-Optical Encoders, Rensselaer Polytechnic Institute.
[4] Saurabh Kharjule, “Voltage Source Inverter”, International Conference on Energy Systems and Applications (ICESA), 2015.
[5] Debanjan Roy, Madhu Singh, “A Simplified Space Vector Pulse Width Modulation for three phase three-level diode clamped Inverter”, 2017
[6] Keliang Zhou and Danwei Wang, “Relationship between Space-Vector Modulation and Three-Phase Carrier-Based PWM: A Comprehensive Analysis Member”, IEEE TRANSACTIONS ON INDUSTRIAL ELECTRONICS, VOL. 49, NO. 1, FEBRUARY 2002.
[7] John W. Finch, *Senior Member IEEE*, and Damian Giaouris, *Member IEEE,* “Controlled AC Electrical Drives”, IEEE TRANSACTIONS ON INDUSTRIAL ELECTRONICS, VOL. 55, NO. 2, FEBRUARY 2008.
[8] Steve Petersen, “Variable Frequency Drive Control Methods”, Yaskawa America, Inc., Drives Technical Training.
[9] Fitzerald and kingsley’s , “Electric Machinery”, 7th edition
[10] N. Urasaki, T. Senjyu, T. Kinjo, T. Funabashi and H. Sekine, “Dead-time compensation strategy for permanent magnet synchronous motor drive taking zerocurrent clamp and parasitic capacitance effects into account”, IEE Proc.-Electr. Power Appl., Vol. 152, No. 4, July 2005.
[11] Alfredo R. Munoz, Member-IEEE, Thomas A. Lipo, Fellow-IEEE, “On-Line Dead-Time Compensation Technique for Open-Loop PWM-VSI Drives”, IEEE TRANSACTIONS ON POWER ELECTRONICS, VOL. 14, NO. 4, JULY 1999.
[12] Takashi Sukegawa, Member-IEEE, Keno Kamiyama, Senior Member-IEEE, Katsuhiro Mizuno, Takayuki Matsui-Member, IEEE, and Toshiaki Okuyama, “Fully Digital, Vector-Controlled PWM VSI-Fed ac Drives with an Inverter Dead-Time Compensation Strategy”, IEEE TRANSACTIONS ON INDUSTRY APPLICATIONS, VOL. 21, NO. 3, MAY/JUNE 1991.
[13] “High Voltage Motor Control and PFC (R1.1) Kit Hardware Reference Guide”, C2000 Systems and Applications Team, Texas Instruments.
[14] “SimCoder User’s Guide”, Powersim.
[15] Roberto PETRELLA, Marco TURSINI, Luca PERETTI, Mauro ZIGLIOTTO, “Speed Measurement Algorithms for Low-Resolution Incremental Encoder Equipped Drives: a Comparative Analysis”.
[16] Geza Kolumban, Lecture slides-Budapest University of Technology and Economics, Dept. of Measurement and Information Systems.
[17] Robert D. Lorenz, Keith W. Van Patten, “High-resolution velocity estimation for all-digital, ac servo drives”, IEEE TRANSACTIONS ON INDUSTRY APPLICATIONS, VOL. 21, NO. 4, JULY/AUGUST 1991.

[18] Zakariya M. Dalala, y. Cho, Jih-Sheng Lai, “Enhanced Vector Tracking Observer for Rotor Position Estimation for PMSM Drives with Low Resolution Hall-Effect Position Sensors”, IEEE, 2013.
[19] Assistant Professor Melik Dolen, Course Notes- ME 534: Computer Control of Machines, Department of Mechanical Engineering, Middle East Technical University, Ankara, Turkey.
[20] Fernando Briz, Michael W. Denger, Robert D. Lorenz, “Analysis and Design of Current Regulators using Complex Vectors”, IEEE TRANSACTIONS ON INDUSTRY APPLICATIONS, VOL. 36, NO. 3, MAY/JUNE 2000.
[21] Viktor Bobek, “PMSM Electrical Parameters Measurement”, NXP.
[22] Quang, Nguyen Phung, Dittrich, Jörg-Andreas, “Vector Control of AC Machines- System Development in practice”, Springer.
[23] Hyunjae Yoo, Yu-Seok Jeong, and Seung-Ki Sul, “Anti-windup for Complex Vector Synchronous Frame PI Current Controller”, 2004.